




# Nanomaterials with high solar reflectance as an emerging path towards energy-efficient envelope systems: a review

Rita Carvalho Veloso<sup>1,2,\*</sup> , Andrea Souza<sup>2</sup>, Joana Maia<sup>2</sup>, Nuno Manuel Monteiro Ramos<sup>2</sup>, and João Ventura<sup>1</sup>

<sup>1</sup>IFIMUP, Departamento de Física e Astronomia, Faculdade de Ciências da Universidade do Porto, Rua do Campo Alegre s/n, 4169-007 Porto, Portugal

<sup>2</sup>CONSTRUCT-LFC, Departamento de Engenharia Civil, Faculdade de Engenharia da Universidade do Porto, Rua Dr. Roberto Frias, 4200-465 Porto, Portugal

Received: 22 June 2021

Accepted: 23 September 2021

© The Author(s), under exclusive licence to Springer Science+Business Media, LLC, part of Springer Nature 2021

## ABSTRACT

The application of nanomaterials in the construction field is allowing the development of smart, green, durable and more efficient buildings. Among the most widely researched nanomaterials are nanosized cool pigments, which are being enforced to achieve thermal and energy-efficient façades, with the development of high reflectance and retro-reflectance coatings. Their peculiar optical and catalytic activity turns nanomaterials into suitable candidates to be used as dark coloured high solar reflectance without affecting aesthetic characteristics, thus improving the durability of coatings. The objective of this paper is to review the state-of-the-art on the benefits of using high reflectance nanopigments as coatings in building façades and their production and synthesis processes. It is thus divided into three main topics: (i) the benefits of using nanopigments on façades, (ii) the most important nanomaterials used as cool pigments and (iii) the main methods of synthesizing nanopigments. One expects that the study of near-infrared nanopigmentation synthesis processes will be able to promote and disseminate the use of nanotechnology in construction, assessing the production problems and limitation and thus helping to disseminate new products by reducing production costs and increase availability.

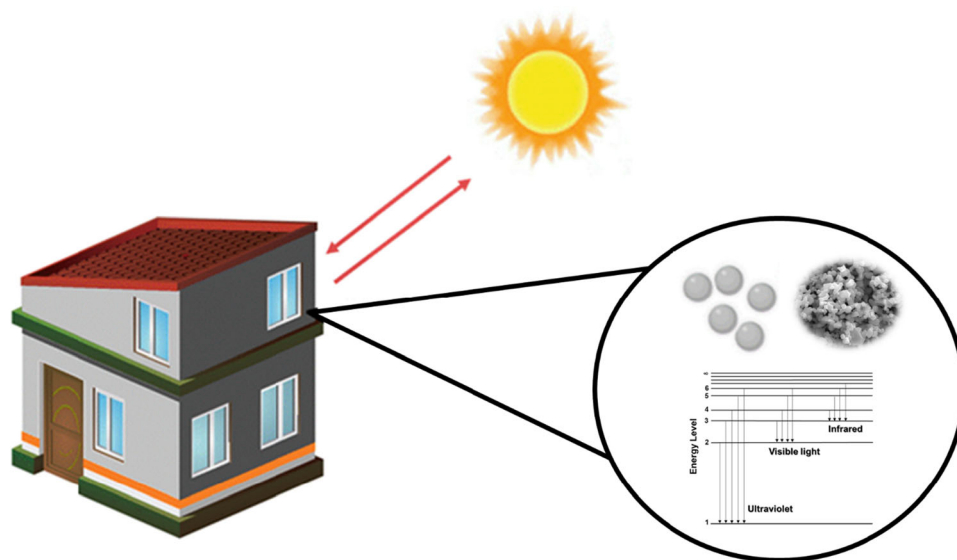
Handling Editor: Christopher Blanford.

Address correspondence to E-mail: up201001431@edu.fe.up.pt

<https://doi.org/10.1007/s10853-021-06560-3>

Published online: 12 October 2021

## GRAPHICAL ABSTRACT



## Introduction

Nanomaterials are gaining widespread importance due to their key characteristics and applications in diverse fields such as agriculture [1–3], energy [4, 5], electronics [6, 7], catalysis [8, 9], pharmaceuticals [10, 11], engineering [12, 13], technology [14, 15] or the food industry [16, 17]. The reduced size of nanomaterials affects their fundamental characteristics, altering the corresponding physical, chemical and biological behaviours. Research on nanomaterials then focuses on understanding and improving these properties, aiming novel effects and functional devices [18]. Among the many favourable characteristics often exhibited by nanomaterials, one just mentions their increased reactivity related with the enhanced surface area-to-volume-ratio, their high degree of crystallinity, chemical stability, high adsorption capacity or the possibility to tune their morphology [19, 20].

Among these unique characteristics, the optical and electronic properties of nanomaterials stand out. In particular, optical properties such as emission and adsorption (related with electronic transitions

between energy levels) are critically affected by dimensionality. Thus, as particle size decreases and the density of states becomes more quantized, the absorption spectra vary [18, 21]. Indeed, the mid-gap energy levels distribution leads to a wide range of absorption in nanoparticles, the crucial factor for their large optical and catalytic activity [22]. This opens the prospect of using nanoengineered materials to fine tune emission and adsorption for specific applications.

Nanotechnology is already starting to play an essential part in the development of new and improved construction materials [23]. As one moves towards nearly zero-energy buildings [24], there is the mandatory necessity to reduce the thermal gains in the urban environment. Around 40% of energy consumption and greenhouse gas emissions of European countries are attributed to buildings [25–28]. The assessment and enhancement of the sustainability of buildings is thus becoming a major necessity for the consolidated development of the construction sector worldwide, ultimately aiming to design new buildings with minimal energy requirements, reduced energy use and CO<sub>2</sub> emissions [29].

To achieve this goal, it is important to reduce the amount of solar radiation absorbed by buildings [30]. In fact, part of the sunlight that hits a surface is absorbed as heat [29] and the resulting temperature rise in buildings can lead to large refrigeration necessities to maintain the comfort of residents. The use of reflective coatings that reflect a large portion of solar radiation (the so-called cool pigments) is thus a decisive factor for the reduction of the thermal gains and overheating in buildings [31]. Even though sunlight intensity is larger in the visible region, invisible NIR radiation accounts for around half of all solar energy reaching us [32]. Thus, research in cool pigments focuses on NIR-reflecting materials that can be an economical, ecologically and passive method to help increase energy savings in buildings decreasing the energy required for cooling loads and enhancing indoor thermal comfort by reducing the surface and ambient temperatures [33]. Figure 1 shows the main thermal properties of cool materials.

This is where nanomaterials with tuned optical properties have a significant opportunity in the construction sector, as reviews in this manuscript. Several authors have already presented the progress and performance of reflective materials, as well as their implementation in buildings (roofs, pavements, ...) for a high cooling potential [34–41]. As Santamouris et al. [34] stated, recent research focus on the improvement of already available materials or the development of new cool materials. Rawat et al. [36], for instance, highlighted the energy-saving advantages using reflective materials in roofs structures, in different climatic zones. However, there is a limited number of literature reviews that focus on the actual reflective materials and their physical properties. Here, we will comprehensively assess the state-of-art of near-infrared (NIR) reflecting nanomaterials, emphasizing NIR reflective inorganic pigments and nanopigments applicable as cool materials in buildings, grouping them by crystalline class and physical properties. The inclusion and exclusion criteria for analysing the articles in this review were the synthesis process, crystalline class, spectral and solar reflectance studies, colour and the applicability in buildings surfaces, such as roofs and façades. For that, the manuscript is divided into three main sections. Section 2 will give an introduction to nanomaterials in the construction sector motivated by thermal comfort problems in buildings. Section 3 will detail the most important materials currently being

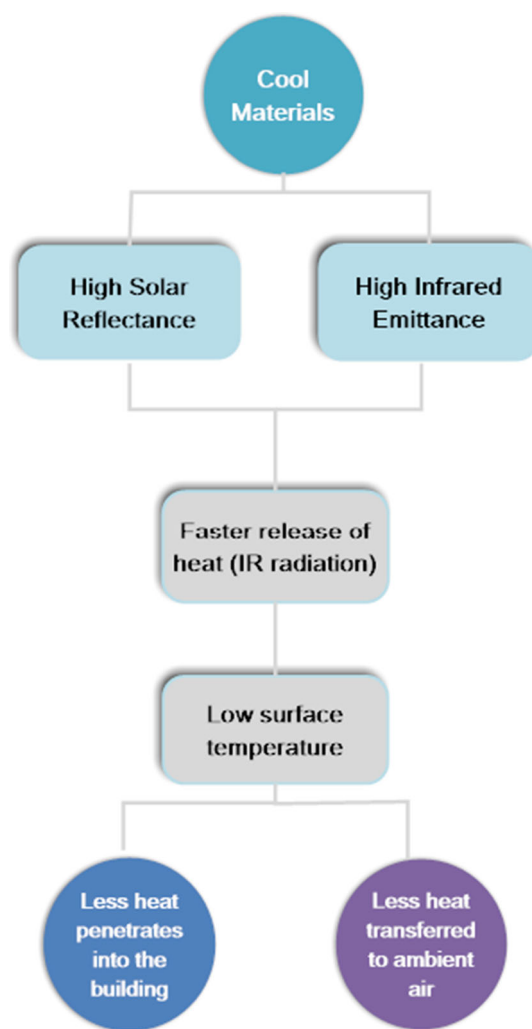


**Figure 1** Cool material properties. Reproduced with permission from ref [33], Copyright 2011, Elsevier.

researched for cool pigments, starting with near-infrared (NIR) reflecting inorganic nanopigments (including the most important metal oxide nanoparticles  $\text{TiO}_2$ ,  $\text{ZnO}$ ,  $\text{Cr}_2\text{O}_3$  and  $\text{ZrO}_2$ ), complex inorganic coloured pigments (particularly spinel-type oxides), perovskites-based, rare-earth-based pigments and core-shell structures. Section 4 will briefly present how nanoscience can provide new routes for the development of advanced adaptive structures in civil engineering and architectural design as smart building skins. Section 5 will summarize the main routes to obtain nanopigments, including solid-state, sol-gel, hydrothermal, molten salt and sonochemical synthesis and examples of relevant materials synthesized by each route. The final section will give a prospect for the future of cool nanopigments in construction.

## Nanomaterials in building envelopes

Nanotechnology can offer improved materials and applications for the construction sector. The main goal of the incorporation of novel construction technologies is to move towards green, smart and efficient buildings. As we have seen, the unique optical properties of nanomaterials offer the possibility to develop reflective nanopigments [42] for increasing thermal comfort and energy saving. Furthermore, besides their use as reflecting cool pigments, nanomaterials can bring additional value to construction materials. They can improve cementitious materials properties, increase composites durability, reduce weight, reduce heat transfer, promote energy efficiency and self-cleaning features [43, 44] or improved mechanical properties (including hardness, strain-to-failure or scratch resistance) in coatings [45, 46]. Novel construction materials play a crucial part in making buildings more sustainable by enabling the development of energy-efficient façades [47]. In this respect, enhancing the thermal performance of the envelope system is a critical way to decrease building energy consumption [48]. This may even involve cool coloured materials with high reflectivity in the NIR when the aesthetic of darker colours is favoured [49]. One of the most exciting technological applications is precisely to replace usual dark pigments that absorb NIR radiation, by cool materials with similar colours but with enhanced solar reflectance [50, 51]. Typically, cool materials have high solar reflectance and infrared emittance [52, 53]. By employing materials with tuned absorption and reflection of specific spectral wavelengths, the total energy absorbed by the surface where the cool pigment is applied is reduced [54–56]. According to Gobakis et al. [57], the definition of cool roofing materials depends on the specific Certification Program, but usually is required a minimum of 0.65 for solar reflectance and 0.85 for thermal emittance.

## Angular dependence of the solar reflectance

The solar reflectance of surfaces varies according to the angular distribution of the incident solar radiation, from a minimum value analogous to the normal incidence of a light beam to a maximum value corresponding to an incidence angle of 90°, depending

on the surface roughness [58]. According to Fresnel equations, reflections in smooth surfaces are strictly dependent on the angle of incidence and have high angular reflectance values, while reflections from rough surfaces are less affected by incident angle variations [59].

This issue is particularly pertinent in cool materials, since they can undergo treatments to become smoother and increase the solar reflectance. For instance, coatings for roof application usually present smooth surfaces. Thus, it is important to understand how the incident angle affects the solar reflectance in order to estimate the solar gains of building components [58]. Such estimation of solar gains of buildings should also include diffuse and specular reflections of the incident irradiation. Usually, solar gains can be determined using [58]:

$$Q_{SG} = I_b \cdot (1 - \rho) + I_d \cdot (1 - \rho) = (I_b + I_d) \cdot (1 - \rho) = I_g \cdot (1 - \rho) \quad (1)$$

where  $Q_{SG}$  is the solar gain heat power [ $W/m^2$ ],  $I_b$  the beam irradiance [ $W/m^2$ ],  $I_d$  the diffuse irradiance [ $W/m^2$ ],  $I_g$  the global irradiance [ $W/m^2$ ] and  $\rho$  the solar reflectance [–].

Building materials are commonly considered Lambertian due to their ability to reflect diffuse incident radiation on their surface. Such statement cannot be strictly valid since the reflectance of a material surface is the result of the combination of the incident (diffuse, hemispherical also called specular beam) and reflected (diffuse or specular) radiation geometries, associated with the contribution of the proper spectrum wavelength [Infrared (IR), visible, ultraviolet (UV)], as well as the incidence angle (Fig. 2). While the reflectance of a surface under specular reflection (such as in glass and metal coatings) depends on the incident angle, that of diffuse irradiation (as in most of the paint and

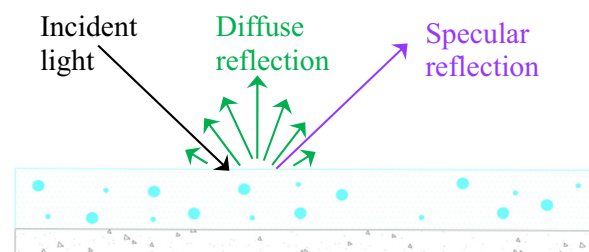


**Figure 2** Reflection properties of the incident light on an opaque façade.



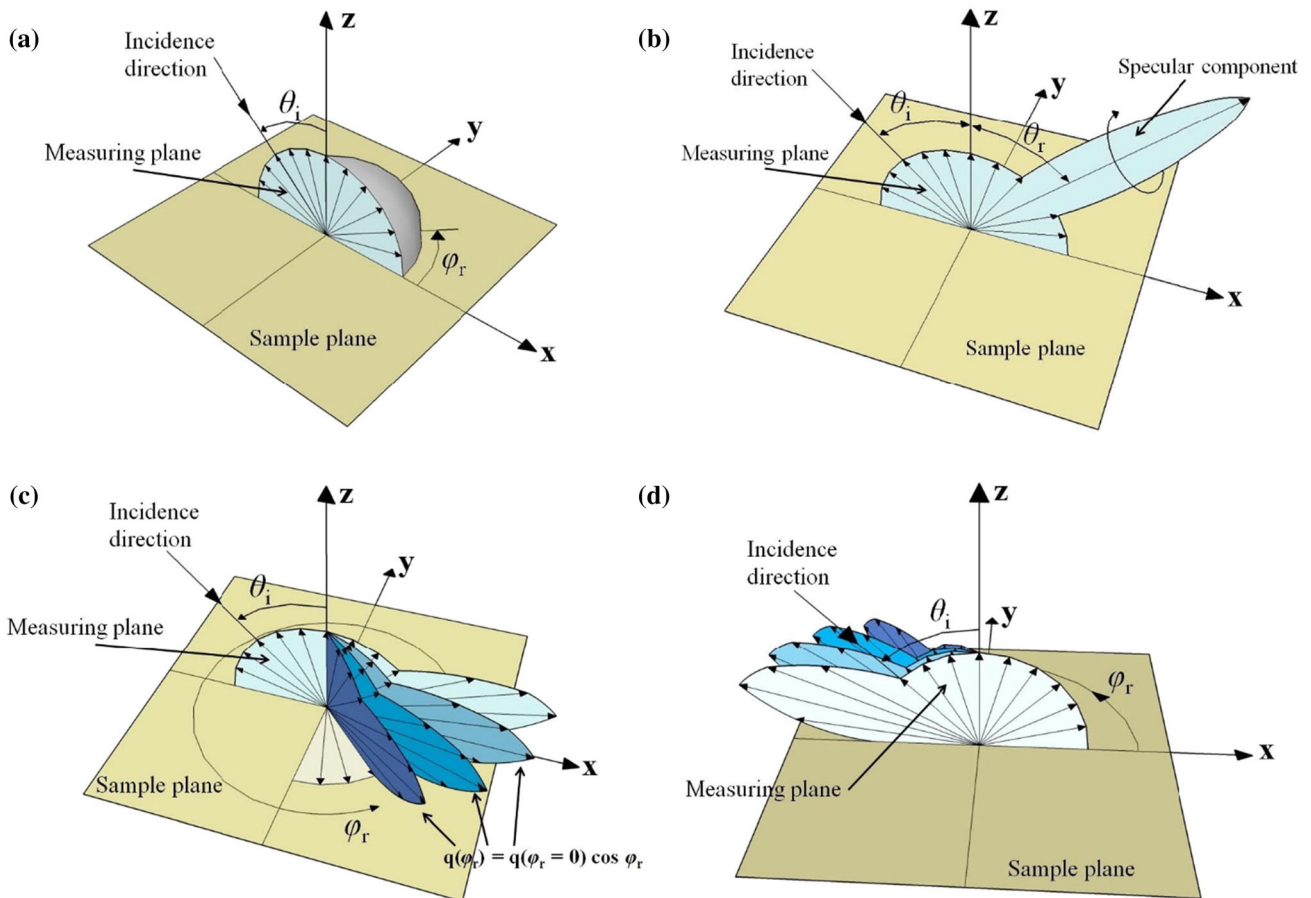


**Figure 3** 3D images of calculations of the directional-hemispherical reflectance of materials: **a** mainly Lambertian; **b** mainly specular; **c** mixed behaviour; **d** backscattering mixed. Reproduced with permission from Ref. [59], Copyright 2015, Elsevier.

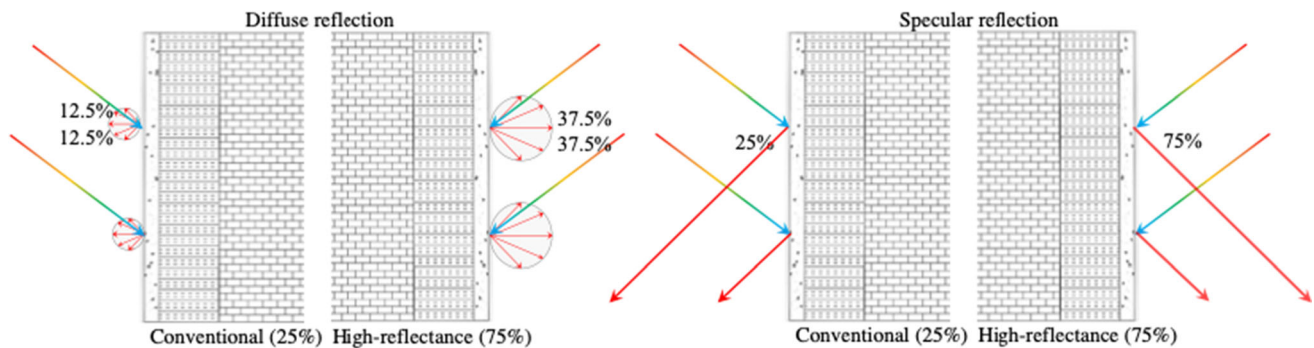


**Figure 4** Example of diffuse and specular reflections on the façades of a building. Reproduced with permission from ref. [60], Copyright 2016, Elsevier.

cementitious coatings) is constant regardless of the incidence angle, as mentioned before [59].

The main difference between conventional and cool coloured material products is that the latter can include paints, pigments, coatings and membranes to smooth the surface. This promotes a partly specular

surface and reduces the absorption due to surface roughness. On the contrary, traditional materials can comprise rough finishing and diffuse performance. However, many opaque construction materials frequently present a mixed behaviour, which includes specular and diffuse performances (Fig. 3).

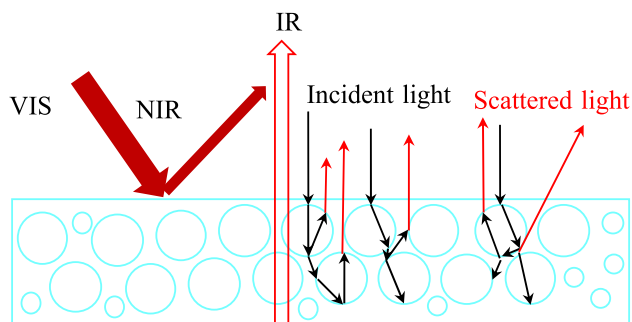


**Figure 5** Schematic of reflective nanopigment coating. Reproduced with permission from ref. [70], Copyright 2014, Elsevier.

As such, Carnielo et al. [58] considered two different reflectance components. The first is an angular component ( $\rho_\theta$ ) related with the variation of the solar beam irradiance with the incidence angle ( $\theta$ ) that can be calculated from the interpolation of experimental values obtained at various  $\theta$ -values. The second component is a constant reflectance ( $\rho_d$ ) related with the diffuse solar irradiance that uniformly hits a surface:

$$\rho_d = \int_0^{\pi/2} \rho(\theta) \cdot d\theta \quad (2)$$

The authors then proposed a method to calculate the dependence of solar gains on the incident angle using:

$$Q_{SG}(\theta) = I_b \cdot (1 - \rho_\theta) + I_d \cdot (1 - \rho_d) \quad (3)$$

Regarding the building envelope system, in Fig. 4, Takebayashi [60] identified that the reflection of solar radiation on diffuse conventional façades (e.g. concrete, paints or wood) results in 12.5% being reflected to the sky, 12.5% to the ground and 75% being absorbed by the building façade. However, the use of high reflectance cool coatings can reduce the thermal load to approximately 25%. If the façade has a high reflectance specular property, the reflection can even reach 75%. However, in this case, despite reducing the thermal absorption of the wall, the beam could cause pedestrian glare.

Although the application of materials with high solar reflectance seems relatively easy with plenty space to implement this strategy in hot climates, there are still urgent difficulties that must be taken into account. For example, surfaces with high reflectance can cause glare problems leading to hazards and discomfort [61]. Another potential problem is the

limited range of colours/hues to be applied to buildings. However, these problems can be avoided by providing materials with a broad range of colour palette (for aesthetic reasons) but controlled near-infrared reflectance to achieve the desired effects [62].

### Near-infrared reflecting inorganic pigments and nanopigment

Typically, cool pigments are chosen from materials displaying the highest reflectances, with complex metal oxides being the main source of NIR reflective inorganic pigments, selectively reflecting radiation in the visible and infrared regions. In particular, white materials, such as titanium dioxide, present the best heat reflection performance with a solar reflectance of around 87% [63] and are thus the most used cool materials. Such high reflectance leads to a lower sunlight absorption from exterior surfaces, such as roofs, decreasing the cooling necessities of the building. Low light absorbance and high dispersion of radiation in the visible regions are other relevant properties of white pigments (400–800 nm). Nevertheless, conventional dark tones (such as black pigments; highly absorbing and reflecting only  $\approx 5\%$  of the total solar irradiation) are still abundantly used on exteriors, either because of aesthetic reasons or to conceal soiling.

The reflectivity and absorptivity of a pigment are independent, opening the possibility to design coloured NIR reflective coatings [64], with the corresponding heat reflection being strongly related with the pigment colour. Furthermore, reflective nanopigments can be designed in order to selectively reflect visible and infrared radiation (Fig. 5). To design a NIR-reflecting pigment, it is required to maximize the total reflectance and emissivity and, withal, minimize the possible contamination by infrared absorbing materials white pigments [65]. Another key parameter to design a cool pigment is the used particle size, which allows engineering the scattering power [66].

The optical properties of a coating depend on (i) the refractive indices of the pigment and binder; (ii) the thickness of the film; and (iii) the size, shape and concentration of the pigment particles [67, 68]. Painted coatings are considered thin films, so that their optical properties can be classified in three broad cases: (a) transparent films that allow most

light to pass but can absorb some of it; (b) translucent films in which light is scattered in both directions; and (c) opaque films where the concentration of colorant or pigment particles is high and a portion of light is absorbed and the other is scattered back to the top [69].

Light scattering by particles can be modelled by Maxwell's equations but exact solutions can only be found for specific particle geometries (e.g. spherical). Concerning the influence of the size of a scattering particle, one can define a size parameter ( $\kappa$ ) given by (in which  $r$  is the particle radius  $r$  and  $\lambda$  the wavelength of the incident radiation):

$$\kappa = \frac{2\pi r}{\lambda} \quad (4)$$

Two cases then follow: if the size parameter is small ( $\kappa \leq 0.3$ ) the particles are classified as small and light scattering is defined by Rayleigh theory; on the other hand, if the size parameter is between  $0.3 \leq \kappa \leq 0.5$ , the particles are considered large and scattering is treated by Mie theory [71], which is a complete analytical solution of Maxwell's equations used to characterize the scattering from any spherical particle with an arbitrary size.

The multiple-scattering phenomena that arises in the scattering of light from surfaces is fundamental in nature and several models are described in the literature [72, 73]. The simplest model to predict and explain the optical properties of colorant layers is the Kubelka–Munk (KM) theory [74, 75]. This two-flux model is widely applied in the pigment industry and translucent/opaque films [68]. For the latter, the effective scattering coefficient  $S$  is particularly high because of the high concentration of the pigment and light is completely scattered [69], giving origin to the Kubelka–Munk equation:

$$\frac{K}{S} = \frac{(1 - R_\infty)^2}{2R_\infty}, \quad (5)$$

where  $K$  is the absorption coefficient and  $R_\infty$  is the reflectance at an infinite thickness.

However, the use of the KM model is limiting since it assumes that the light passes through the film only in a diffuse mode and refractive index changes are not considered. On the other hand, the Sauderson correction [76] adjusts the coating's reflectance by considering the refractive index gap that can possibly exist between the layer coating and air. In real films, there is a scattering effect, with the light propagating

in any direction. The KM model contemplates two fluxes with diffused light in both directions (upwards and downwards). Applying the Sauderson correction on the classical KM theory actually estimates the difference of the refractive indexes and gives a better approach on the reflectance values.

## Metal oxides nanoparticles

Inorganic pigments are commonly used in different applications, including paints and coatings [77]. Table 1 shows the most common metal oxide compounds used as cool pigments. As readily seen, the largest solar radiation reflections are obtained using white coatings, from which the most typical is titanium dioxide ( $\text{TiO}_2$ ). Nevertheless, other oxides or their synthetic analogues can be used as pigments after suitable modifications.

$\text{TiO}_2$  is the most used pigment in coatings formulation, improving the quality and coverage power, durability and brightness of the coating [83, 84]. Besides that, there are other metal oxides nanomaterials such as  $\text{ZrO}_2$ ,  $\text{ZnO}$  or  $\text{Cr}_2\text{O}_3$ , that have been used as key-enabling technologies for the production of control functional coatings to minimize energy usage in buildings [85]. However, the use of heavy metals is beginning to be worrying and alarming [81, 86] and an ideal approach is the use of naturally occurring oxides or the production of their analogues with appropriate modifications that make them suitable to be used as pigments.

## Titanium dioxide ( $\text{TiO}_2$ )

Titanium dioxide ( $\text{TiO}_2$ ) is a white colour pigment widely used for eco-friendly applications, including in construction materials (tiles, concrete, coatings or glasses), because of its unique properties (low cost, non-toxicity, optical transparency, large refractive index, chemical stability or good thermal performance) [87, 88]. In these applications, the behaviour of  $\text{TiO}_2$  nanomaterials is largely influenced by their electronic and optical properties, particle size, morphology and crystalline structure [89]. Anatase (tetragonal), brookite (orthorhombic) and rutile (tetragonal) are the three main crystalline phases of  $\text{TiO}_2$  [90]. The most stable modification is the rutile phase, while anatase irreversibly transforms into

**Table 1** Common pigments used as cool material and their relevant properties

Compound	Crystal structure	Colour	Particle size	Form	% NIR reflectance	Reference
TiO <sub>2</sub>	Tetragonal, Rutile	White	Micrometres	Powder	~ 87	[63]
ZnO	Hexagonal, Wurtzite	White	Nanometres	Powder	~ 85	[78, 79]
ZrO <sub>2</sub>	Monoclinic, baddeleyite	White	Micrometres	NA	NA	[80]
Cr <sub>2</sub> O <sub>3</sub>	Sesquioxide	Green	Nanometres	Powder	50–57	[81, 82]

rutile during heating at a transformation temperature that depends on the synthesis process, annealing atmosphere, crystallinity degree and impurity content [91, 92].

### Relevant properties

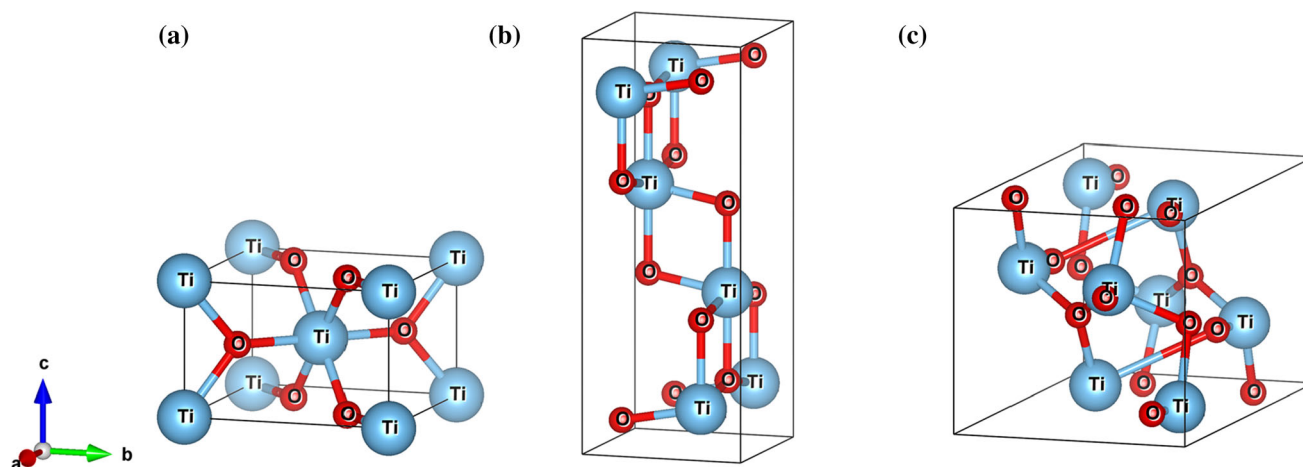
From the TiO<sub>2</sub> phases, rutile {crystal system: tetragonal (4/mmm), space group: P4<sub>2</sub>/mmn–D<sub>14</sub><sup>4h</sup>}, anatase {tetragonal (4/mmm), I4<sub>1</sub>/amd–D<sub>19</sub><sup>4h</sup>} and brookite {orthorhombic (mmm), Pbca–D<sub>15</sub><sup>2h</sup>}, only the first two have an important role in industrial applications. Brookite has a much smaller significance due to the drawback in fabricate pure-phase crystal, when compared to rutile and anatase TiO<sub>2</sub> (Fig. 6) [90, 93].

Being a large bandgap (> 3 eV) *n*-type semiconductor, most of the practical applications of TiO<sub>2</sub> use its light adsorption capacity, particularly photocatalysis and photovoltaics. However, its large band gap and the fast recombination of photoexcited carries limit its light adsorption properties to UV light that constitutes only ≈5% of the total solar radiation [94, 95]. Table 2 summarizes the main properties of the anatase and rutile phases of TiO<sub>2</sub>.

### Applications in the coating industry

TiO<sub>2</sub> has been extensively used in building materials and in the coating industry due to a diversified set of properties. Compared with other metal oxide materials, it provides high photocatalytic activity and is highly effective under weak solar irradiation. Furthermore, TiO<sub>2</sub> can be incorporated in traditional construction materials without degrading the original performance [97].

With the development of the coating industry, several studies have been directed to take advantage of the characteristics and properties of TiO<sub>2</sub>. It has already been reported that TiO<sub>2</sub> is the most effective UV protector [98] and improves the solar reflectance of coatings. For instance, Godnjavec et al. [99] modified the surface characteristics of TiO<sub>2</sub> nanomaterials to be used as additives in clear acrylic coatings. Looking at the results, it appears that TiO<sub>2</sub> improved the dispersion in the acrylic coating, as well as UV protection. In general, particle size influences a large variety of properties of materials [100]. Consequently, it will determine the appearance (colour and brightness), as well as the reflectance of coatings. In the coatings industry, commercial rutile TiO<sub>2</sub> generally

**Figure 6** Planar building-block representation of TiO<sub>2</sub> in the **a** rutile **b** anatase and **c** brookite phases.



**Table 2** Structural and physical characteristics of TiO<sub>2</sub> (anatase and rutile). Adapted from ref. [95, 96]

Property	Anatase	Rutile
Molecular weight (g/mol)	79.88	79.88
Melting point (°C)	1825	1825
Boiling point (°C)	2500–3000	2500–3000
Light absorption (nm)	< 390	< 415
Mohr's hardness	5.5	6.5–7.0
Refractive index	2.55	2.75
Dielectric constant	31	114
Crystal structure	Tetragonal	Tetragonal
Lattice constant (Å)	a = 3.7842 b = 3.7842 c = 9.5146	a = 4.5937 b = 4.5937 c = 2.9581
Density (g/cm <sup>3</sup> )	3.79	4.13
Ti–O bond length (Å)	1.94 (4) 1.97 (2)	1.95 (4) 1.98 (2)
Bandgap energy (eV)	3.20	3.0

has a particle size in the order of nanometres (200–300 nm) and efficiently reflects radiation with a wavelength between 400 and 1700 nm. However, larger sized titanium dioxide particles ( $\approx 10 \mu\text{m}$ ) reflect better radiation in the 800 and 2300 nm range, but is less effective in the 400–800 nm range. Song et al. [101] studied how the particle size distributions of commercial TiO<sub>2</sub> pigments [TiO<sub>2</sub> Pure (280 nm), Altiris 550 (360 nm) and Altiris 800 (410 nm)] influences the corresponding optical properties. They showed that the sunlight reflectance decreases with increasing pigment particle size (Fig. 7).

Another study, conducted by Piri et al. [102], aimed to characterize the reflectance, transmittance and absorption of different surfaces coated with TiO<sub>2</sub> particles of different size (35, 120 and 250 nm) and concentration (0.1, 0.5, 1.0, 5.0, 10% wt) (Fig. 8). This study confirmed that the optical properties of the coatings are strongly dependent on particle size and corresponding concentration. It was shown that the TiO<sub>2</sub> nanoparticles strongly absorb light in the UV region, but reflect most of VIS and NIR radiation.

Shen et al. [88] studied how the concentration and particle size of TiO<sub>2</sub> nanoparticles affect the thermal and mechanical properties of coatings applied in thermal insulation. The solar reflectance with different gradations was also tested, with the results indicating an improvement of the solar reflectance and

thermal insulation of the coating with increasing nanosized particles content.

### Modifications on TiO<sub>2</sub>

The higher cost of nanosized TiO<sub>2</sub> when compared with regular TiO<sub>2</sub> will necessarily result in the increase of a production costs. Moreover, two other major characteristics limit the use of nanosized TiO<sub>2</sub>. First, the small particle size and enhanced surface area of nano-TiO<sub>2</sub> typically lead to an incompatibility with the polymeric matrix and thus to agglomeration and to a decrease of the overall UV protection efficiency which is determined by the dispersion of the TiO<sub>2</sub> nanoparticles. Second, it is necessary to avert the formation of free radicals, which can occur due to the photochemical reactivity of TiO<sub>2</sub> [99, 103]. To overcome these challenges, several physical and chemical routes are used to modify the TiO<sub>2</sub> structure. One of the solutions is the modification of the surface of the nanoparticles with inorganic oxides that can further decrease the difference in the refractive index of the coating.

Narrowing the bandgap in order to improve TiO<sub>2</sub> photostability and reactivity under solar radiation is one of the motives to research modifications in TiO<sub>2</sub>. The main goal in doping TiO<sub>2</sub> is to cause interstitial or substitutional defects or create vacancies in order to change colour, magnetic and optical properties, reactivity or conductivity of the original oxides used [96]. Much effort has been made to enhance the optical properties of TiO<sub>2</sub> by bandgap engineering including metal, non-metal and self-doping.

A very efficient methodology for narrow the bandgap of semiconductors is, for example, the incorporation of non-metallic compounds. In order to achieve photoactivity in visible light, dopants such as nitrogen, carbon, fluorine, boron or phosphorous are added to the structures of titanium dioxide [104]. Likewise, metallic elements such as, lithium (Li), aluminium (Al) and potassium (K) are also used to improve the reflectance of the particles of TiO<sub>2</sub>. Usually, commercial TiO<sub>2</sub> rutile is doped with Al<sub>2</sub>O<sub>3</sub> to improve its photochemical stability. Kumar et al. [105] applied Al-doped TiO<sub>2</sub> nanoparticles on plastic substrate coatings to develop light reflectors. These reflectors showed a diffuse reflectance of over 98% for a coating thickness of 0.25 mm (Fig. 9) due to defects in the rutile lattice created by the Al doping,



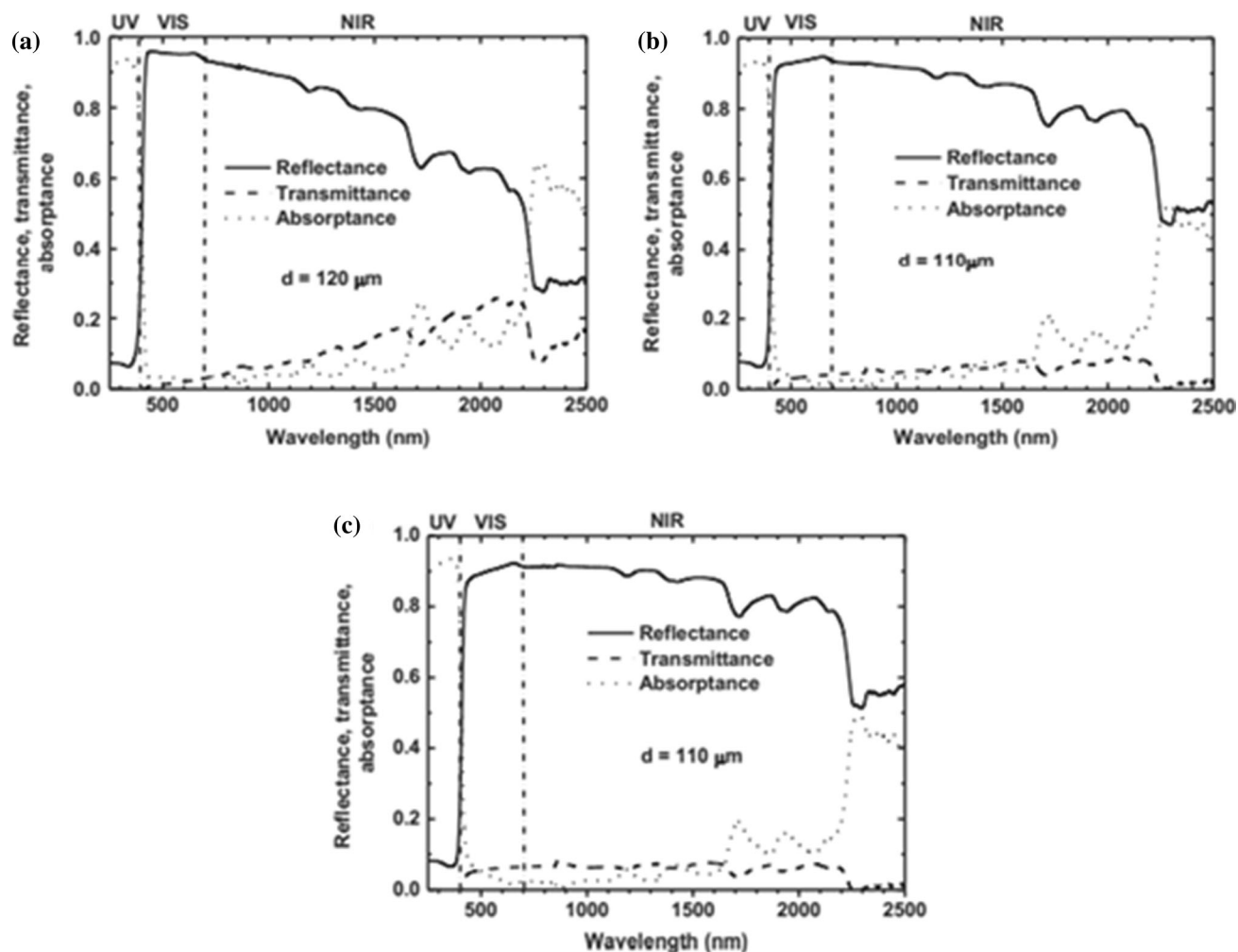


**Figure 7** Optical properties of paint coatings with **a** rutile TiO<sub>2</sub> (280 nm), **b** Altiris 550 (360 nm) and **c** Altiris 800 (410 nm) pigments (28 wt%). Reproduced with permission from ref. [101], Copyright 2014, Elsevier.

acting as traps for the photogenerated charges [64, 106].

Such procedures give rise to impurity states in the TiO<sub>2</sub> bandgap that improve visible-light harvesting. Nevertheless, doping leaching, thermal instability, or less efficient recombination of charges induced by additions and/or traps, still presents some limitations, raising environmental issues [107, 108]. The largest problem with doped TiO<sub>2</sub> at present may be the loss of photoactivity during recycling and long-term storage [108]. Therefore, major areas of future research should include the development of new nanodopants, a new method of nanodopant incorporation into the TiO<sub>2</sub> structure as well as new applications for coating technologies.

## Zinc oxide (ZnO)

In the last few years, one of the most promising metal oxides is zinc oxide due to its wide range of radiation absorption, high chemical and mechanical stability, good catalytic activity, electrochemical coupling coefficient and low toxicity [109]. Zinc oxide can be applied in the most diverse areas such as cosmetics, pharmacy, paints and coatings, floor coverings, plastics and rubber products, storage batteries, detergents or soaps, textiles and also electrical equipment [79].

## Relevant properties

Due to its stability in harsh processing conditions, it is considered an excellent antibacterial agent, as well

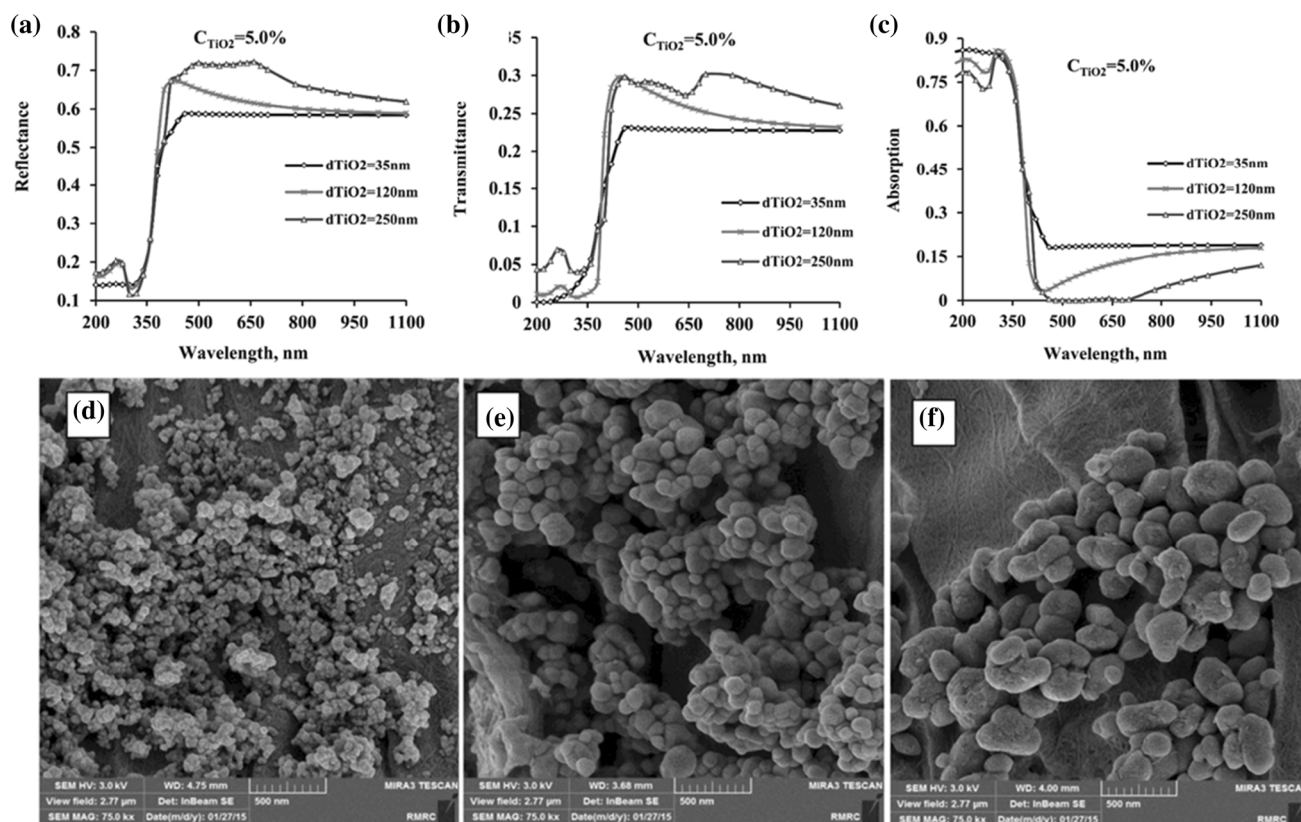


**Figure 8** Effect of the diameter of  $\text{TiO}_2$  nanopigments on the corresponding reflectance, transmittance and absorption (a, b and c); SEM (Scanning Electron Microscopy) images of  $\text{TiO}_2$  with

diameters of 35 nm (d), 120 nm (e) and 250 nm (f). Reproduced with permission from ref. [102], Copyright 2017, Elsevier.

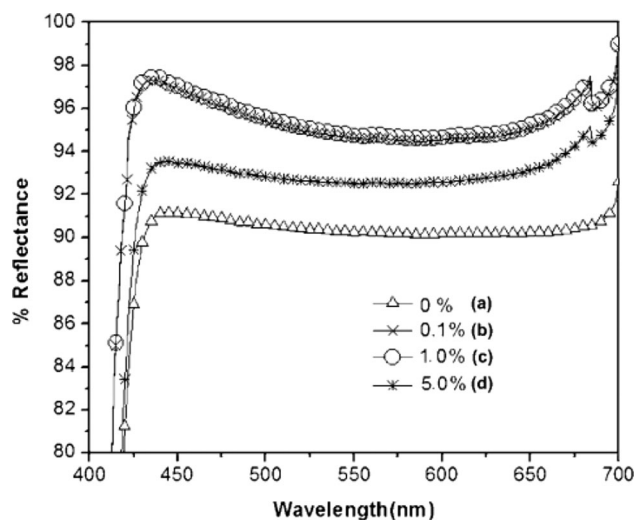


**Figure 9** Diffuse reflectance of Al-doped  $\text{TiO}_2$  nanoparticles exposed to light radiation with 0% (a), 0.1% (b), 1.0% (c) and 5.0% (d). Reproduced with permission from ref. [105], Copyright 2013, Cambridge University Press.

as its use is considered safe for animals and humans [110]. It belongs to the group II-IV of the semiconductors with a wide range of direct bandgap at room temperature of 3.37 eV [111], belonging to the hexagonal crystalline system (Fig. 10) a much simpler crystal growth technology that turns manufacturing costs ZnO-based pigments potentially lower. Such structure develops a crystal lattice of a Wurtzite type since the Zn–O tetrahedra join at a common zinc atom forming a nucleus for additional tetrahedra [112].

### Applications in the coating industry

Together with titanium dioxide, ZnO is a widely used white pigment, found both in decorative and artistic paints, even though it cannot compete with the hiding power (a particle's ability to scatter light) of  $\text{TiO}_2$  rutile ( $n = 2.75$ ), due to its low refractive index,  $n = 2.02$  [64, 113]. Mixtures of ZnO with barium sulphate, lead white or titanium dioxide are often found in oil paints to enhance the hiding power [114].

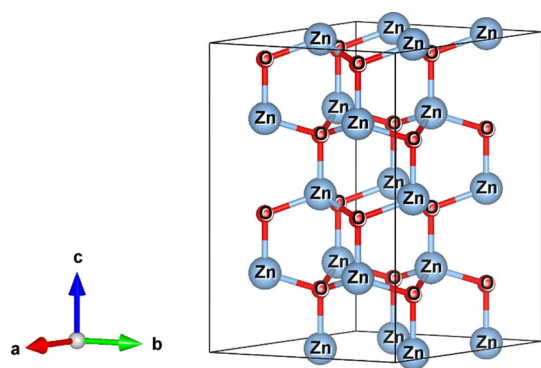


**Figure 10** Crystalline structure of polyhedral zinc oxide (wurtzite).

It is expected that pigments optimized in size and morphology will achieve optimum diffuse solar reflectance for smaller film thicknesses, which contributes to improving the durability of the system as the volume of pigment required is reduced. Kiomarsipour et al. [79] developed a novel ZnO pigment morphology to increase its scattering ability. They synthesized five different morphologies of ZnO pigments (nanoparticle-decorated, nanorods, micro-rods, submicrorods and scale-like) by a simple hydrothermal procedure and studied the effects of the ZnO morphology on the spectral reflectance (Fig. 11). As shown in Fig. 11 for  $\text{TiO}_2$ , the decorated surface with ZnO nanoparticles showed increased light scattering.

Nevertheless, ZnO is no longer used as a principal pigment, but instead as an additive in exterior paint for wood preservation. It improves the durability and resistance of coatings from mildew and can absorb UV radiation [115]. However, ZnO pigments (as  $\text{TiO}_2$ ; see Table 1) are also active photocatalysts so that the absorption of UV light can result in the degradation of the organic binders and thus in coatings with decreased lifetime [116].

To improve their properties, it is possible to engineering the bandgap of ZnO. This technology allows the fabrication of energy-saving windows by alloying, for example, with MgO, which increases the bandgap, or with CdO, which decreases the bandgap. Doping with compounds such as aluminium (Al) or gallium (Ga) turns ZnO into a modest electrical conductor with the ability to reflect NIR light. As such, it was proposed as a piece of a multi-layered coating system for windows with the capability of energy-saving or heat-rejecting. In this realization, the coating is transparent to visible light, while

reflecting infrared radiation into the outside (rejecting radiant heat in hot weather) or back into the room (lowering heating necessities in cold weather). [66].

### Zirconium dioxide ( $\text{ZrO}_2$ )

Zirconium dioxide (zirconia) occurs naturally as the mineral baddeleyite and is fabricated by calcining other zirconium compounds. Bulk  $\text{ZrO}_2$  is a wide bandgap ( $\sim 5$  eV) insulating material.  $\text{ZrO}_2$  has three stable phases at normal conditions: cubic above 2370 °C, tetragonal between 1170 and 2370 °C and monoclinic below 1170 °C [117] (Fig. 12). Contrarily to  $\text{TiO}_2$ , in which all phases have six-coordinate Ti, monoclinic zirconia presents seven-coordinate Zr centres due to the larger size of the Zr atom. [118].

Zirconia is particularly interesting for coatings in the near-UV to IR ranges due to its good refractive index and low absorption properties. It can be used in exterior service paint as a coating for the surface of titanium oxide pigment particles. Such coating reduces UV excitation of titanium dioxide, minimizing the interaction with organic paint binder and extend the service life. Zirconia has also been used in white camouflage paints for use in snow environments as a substitute of  $\text{TiO}_2$  pigments since it more closely simulates snow in microwave and infrared spectra. [80]. Besides, aqueous solution zirconium compounds can have the ability to crosslink carboxylates resins, which can be used in both water-based inks and paints to improve both heat and scrub resistances [119].

### Chromium oxide ( $\text{Cr}_2\text{O}_3$ )

In spite of their excellent performance as reflective materials, white pigments present several disadvantages such as light pollution, poor stain resistance or monochrome. Thus, with the increasing necessity for additional functions and attractiveness, cool pigments are still unsatisfactory for society [81]. There is a large necessity to substitute conventional coloured pigments with reflective pigments which, although absorbing smaller amounts of NIR radiation, offer coatings with analogous coloration to conventional buildings materials but with enhanced solar reflectance. [120].

$\text{Cr}_2\text{O}_3$  is the only solid chromium oxide phase stable above 773 K. Below this temperature, different oxygen-rich phases can occur in the  $\text{Cr}_2\text{O}_3$ – $\text{CrO}_3$

**Figure 11** UV/VIS/NIR spectral reflectance of different morphology ZnO pigments. Reproduced with permission from ref. [79], Copyright 2013, Elsevier.

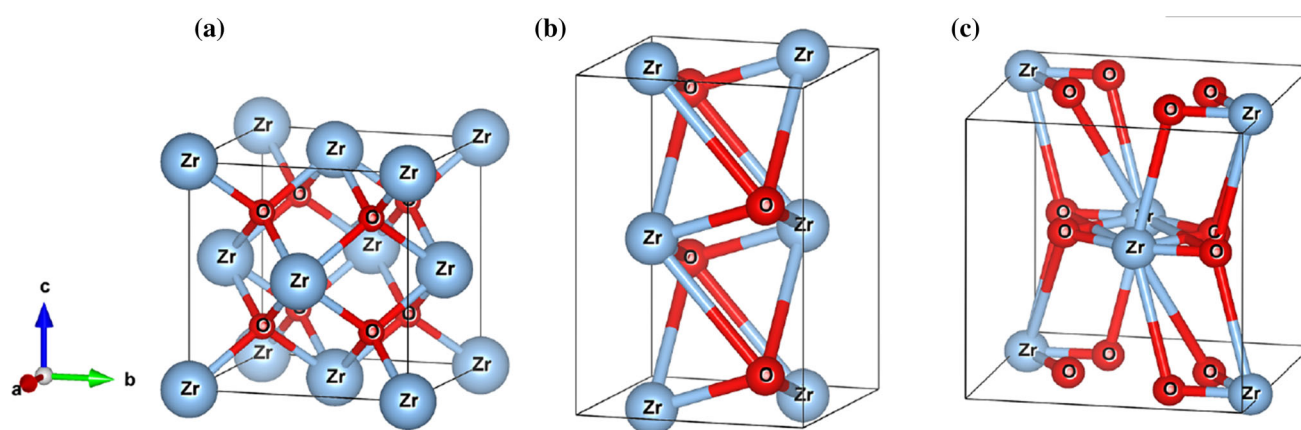
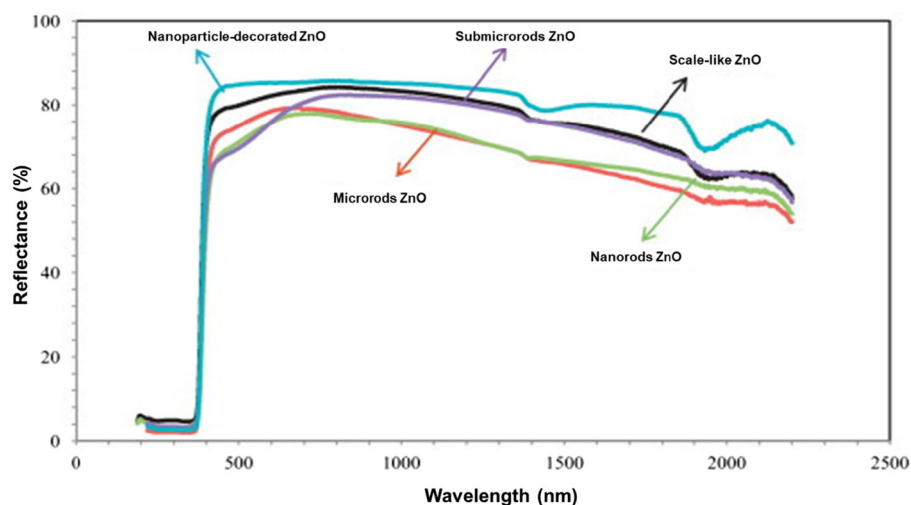


**Figure 12** Crystal structures of  $\text{ZrO}_2$ : cubic (a), tetragonal (b), and monoclinic (c).

composition range [121]. Chromium (III) oxide is a highly stable sesquioxide (Fig. 13) and is isomorphous with corundum [122],  $\alpha\text{-Al}_2\text{O}_3$ , in which oxygen is positioned in an approximate hexagonal close packing lattice, with  $\text{Cr}^{3+}$  occupying 2/3 of the octahedral interstices. Like corundum,  $\text{Cr}_2\text{O}_3$  is a hard, brittle and antiferromagnetic material [123].

$\text{Cr}_2\text{O}_3$  has a high melting temperature of approximately 2435 K, which makes chromium sesquioxide an important refractory compound. For this reason, it is a proper material for coatings due to their wear resistance and thermal protection. By employing nanosized chromium (III) oxide, it is possible to obtain newer or enhanced applications in surface coatings [124].

In the past, chromium oxide has already been used by military in camouflage coatings to avoid objects detection. Green pigments, such as  $\text{Cr}_2\text{O}_3$ , have medium-high NIR solar reflectance, between 50 and

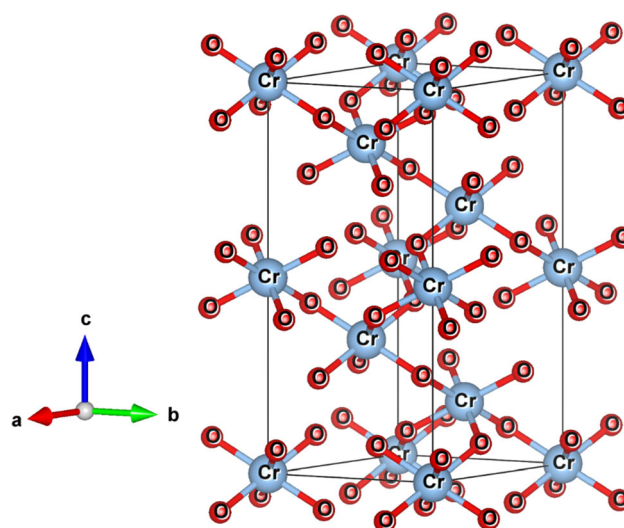


**Figure 13** Unit cell of chromium (III) sesquioxide.



57% [81], being used as roofing material that efficiently reduce their surface temperature and simultaneously improves the appearance of the roof [82, 125].

Due to the dark green tone, different efforts are being performed to obtain a brighter green. For example, Liang et al. [82] prepared pure  $\text{Cr}_2\text{O}_3$  from the thermal decomposition of  $\text{CrOOH}$ , obtaining both high NIR reflectance and good colour performance (Fig. 14).

Based on the  $\text{Cr}_2\text{O}_3$  composition, a large variety of colour pigment systems have been developed with enhanced NIR reflectance [126, 127]. In order to obtain high NIR reflectance (70–82%), small amounts of metal ions such as aluminium, [128, 129], titanium (Fig. 15) [82], vanadium, cobalt or bismuth are normally introduced into  $\text{Cr}_2\text{O}_3$ . Other reports have shown that doping with rare-earth elements (La, Pr) can lead to the production of environmental benign, high reflective (> 85%) nanopigments based on  $\text{Cr}_2\text{O}_3$  [130].

Nonetheless, the chromatic properties of the final products are still undesirable, acquiring a dark green hue. Besides, rarely is reported the phenomenon or principle why doping with such elements changes the NIR reflectance of  $\text{Cr}_2\text{O}_3$  host. [82].

However, usual  $\text{Cr}_2\text{O}_3$  fabrication processes cause several problems, including the high cost of production and environmental pollution from dust containing hexavalent chromium (Cr-VI) which is highly toxic and a human carcinogenic. Recently, several procedures have been developed to prepare high-quality green chromic oxide nanoparticles taking into account health safety and environmental protection [131]. Thus, there is an assertive motivation to

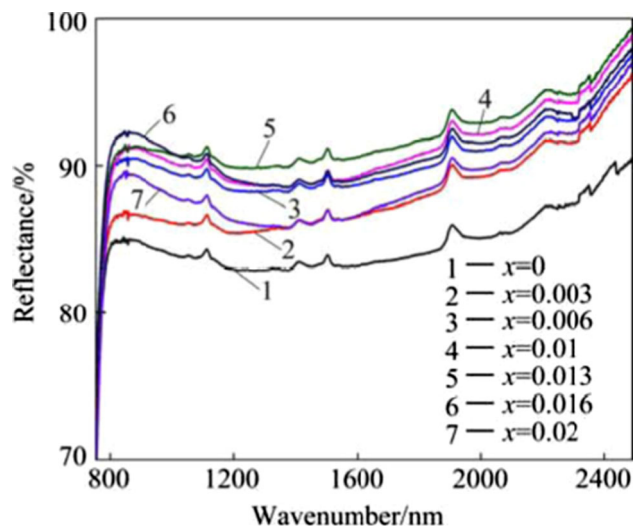


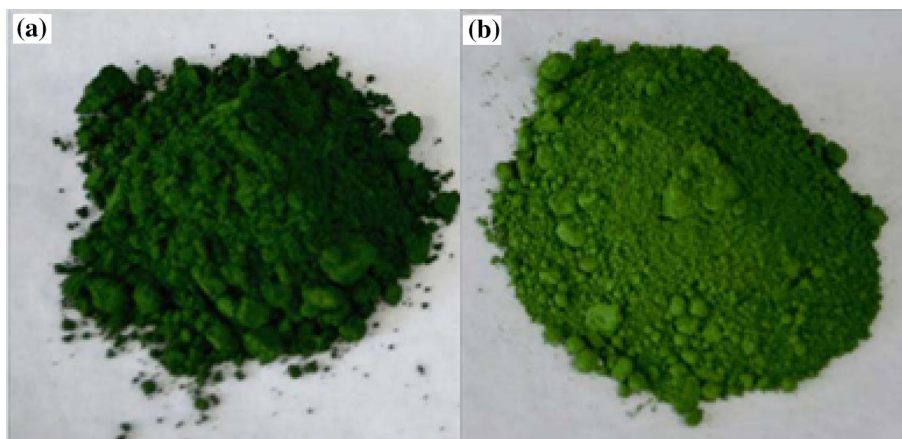
**Figure 15** The reflectance spectra of  $\text{Cr}_{2-x}\text{Ti}_x\text{O}_{3+\delta}$  pigments in the near-infrared region. Reproduced with permission from ref. [82], Copyright 2015, Elsevier.

develop coloured cool pigments through green processes and materials that are less harmful to the environment.

### Mixed metal oxides or complex inorganic coloured pigments

Mixed metal oxides or complex inorganic coloured pigments (CICPs) are the primary variety of inorganic NIR reflective pigments [42, 130], with a large number of patents being reported on these pigments. This shows their broad and significant interest, which comprises two main areas: (i) reduce heat build-up and (ii) visual camouflage. In particular, nanomixed metal oxides are attracting large interest for their

**Figure 14** Photographs of **a** regular dark green  $\text{Cr}_2\text{O}_3$  pigments and **b** yellowish-green  $\text{Cr}_2\text{O}_3$  prepared by calcination. Reproduced with permission from ref. [82], Copyright 2015, Elsevier.





potential as pigments, further offering exceptional resistance to acid, bases and organic solvents [132]. Nanocrystalline metal oxides possess some significant optical applications, which include anti-reflective properties in optical coatings, better photonic bandgap materials and improved optical limiting materials for eye protection [42]. Examples of such compounds are listed in Table 3.

Among these systems, spinel-type oxides (Fig. 16) with the general formula  $AB_2O_4$  or, depending on the cations distribution on the crystalline structure, the inverse formula  $B(AB)O_4$ , are attracting large attention due to their thermal and chemical stability [45, 133–135].

Cobalt aluminate ( $CoAl_2O_4$ ) an important intense blue pigment is an example of a compound with a normal spinel structure (Fig. 17a) [137] and is extensively used as a colouring agent in several applications due to its inherent properties (colour performance, chemical and thermal stability, high refractive index) [148] (Fig. 17b). Ali et al. [136] prepared, via a combustion method, nanopigment  $CoAl_2O_4$  exhibiting a blue colour (in the visible region) and a high solar reflectance ( $\sim 51.8\%$ ).

However, the manufacturing cost for cobalt-based product is high, since cobalt is scarce. Therefore, Bao et al. [146] modified  $CoAl_2O_4$  with  $Mg^{2+}$  for  $Co^{2+}$  ions by a sol–gel route. On the other hand, due to the capability of spinel-type materials to accommodate

different cations, the authors also doped with  $Fe^{3+}$  for  $Al^{3+}$  in  $Co_{0.5}Mg_{0.5}Al_2O_4$  to obtain various colours and tonalities with a particle size in the 40–100 nm range (Fig. 18a). Through this study, it was possible to achieve a vast range of colours by incorporating in the  $Co_{0.5}Mg_{0.5}Al_{2-x}Fe_xO_4$  matrix appropriated  $Fe^{3+}$  ions through bandgap engineering. Most prominently, these engineered pigments exhibited various colour tonalities in the visible range and high NIR solar reflectance ( $> 43\%$ ) (Fig. 18b and c).

Another notable spinel-type pigment is zinc aluminate ( $ZnAl_2O_4$ ). Such compound possesses a wide bandgap and appears as a white pigment in the visible region, which has potential on optical coating applications.  $ZnAl_2O_4$  and  $ZnAl_2O_4$ -based pigments synthesized by different techniques are being widely reported because of the simple fabrication process and low cost. Yang et al. [138] fabricated, by a sol–gel synthesis, a variety of coloured pigments of Mn-doped  $ZnAl_2O_4$  and Mn/N co-doped  $ZnAl_2O_4$  (Fig. 19a). The particle range of such materials was around 27–31 nm with results of NIR solar reflectance (Fig. 19b and c) in the 85% ( $x = 0.0$ ) to 50% ( $x = 0.5$ ) range, indicating that co-doped samples are suitable candidates for cool materials.

An important commercially CICPs widely used as a pigment is cobalt chromite ( $CoCr_2O_4$ ), which acts as an intense bluish-green hue [149]. Since chromium and cobalt are harmful and rare, it is mandatory to

**Table 3** Examples of mixed metal oxides used as NIR-reflecting pigments

Compound	Crystal structure	Colour	Particle Size	% NIR reflectance	Reference
$CoAl_2O_4$	Spinel	Intense blue	Nanometres	51–79%	[136, 137]
$ZnAl_2O_4$	Spinel	White	Nanometres	85%	[138]
$CoCr_2O_4$	Spinel	Blue greenish	Nanometres	43%	[139]
$ZnCr_2O_4$	Spinel	Grey	Nanometres	$\sim 60\%$	[139]
$NiAl_2O_4$	Spinel	Blue greenish	Nanometres	24–53%	[140]
$NaZnPO_4$ - based	Monoclinic	Intense blue	Micrometres	32–52%	[141]
$BiVO_4$	Monoclinic	Bright yellow	Nanometres	$\sim 50\%$	[142]
$BiPO_4$	Monoclinic	White	Micrometres	80%	[143]
$Ta^{5+}$ doped $BiVO_4$	Monoclinic	Bright yellow	Nanometres	$\sim 85\%$	[144]
$P^{5+}$ doped $BiVO_4$	Monoclinic	Bright yellow	Nanometres	$\sim 90\%$	[144]
$V^{5+}$ doped $BiPO_4$	Monoclinic	Bright yellow	Micrometres	$\sim 90\%$	[143]
Mn and Mn/N doped- $ZnAl_2O_4$	Spinel type	White to brown	Nanometres	15–50%	[138]
$Zn_{0.9}Co_{0.1}Al_2O_4$	Spinel type	Intense blue	Nanometres	63%	[145]
$Co_{0.25}Zn_{0.75}Cr_2O_4$	Spinel type	Light blue	Nanometres	52%	[139]
$Co_{0.5}Mg_{0.5}Al_2O_4$	Spinel type	Blue	Nanometres	54.2%	[146]
$Co_{0.5}Mg_{0.5}Al_{2-x}Fe_xO_4$	Spinel type	Dark blue to black	Nanometres	45.7–54.2%	[146]
$CoCr_{0.5}Al_{1.5}O_4$	Spinel type	Blue	Nanometres	43%	[139]
Ce and Fe doped $ZnAl_2O_4$	Spinel type	Reddish yellow	Nanometres	65–86%	[147]

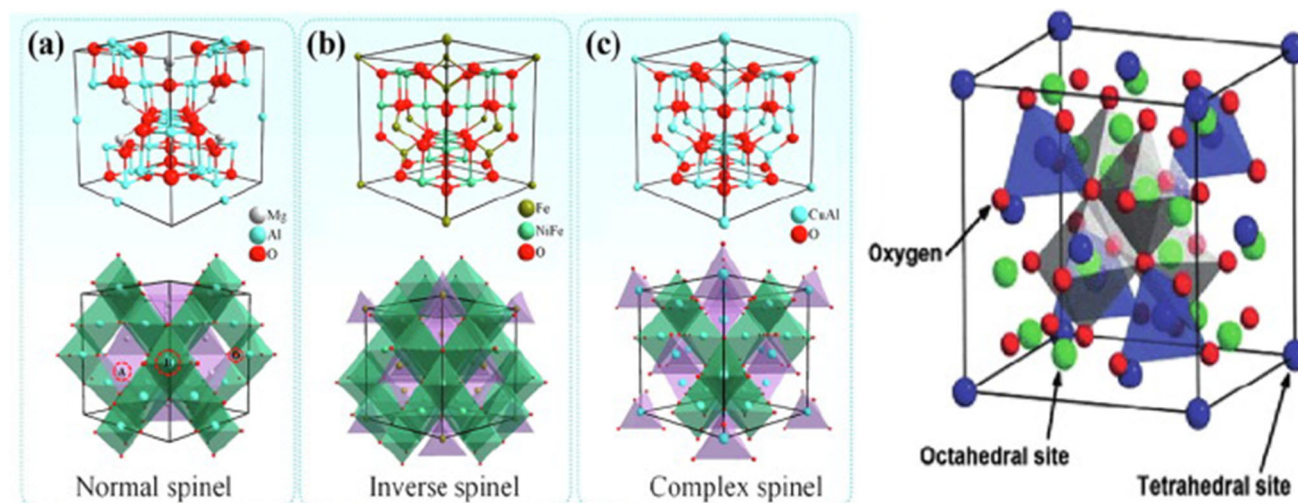


**Figure 16** Examples of typical spinel structures. Reproduced with permission from ref. [134], Copyright 2017, Elsevier.

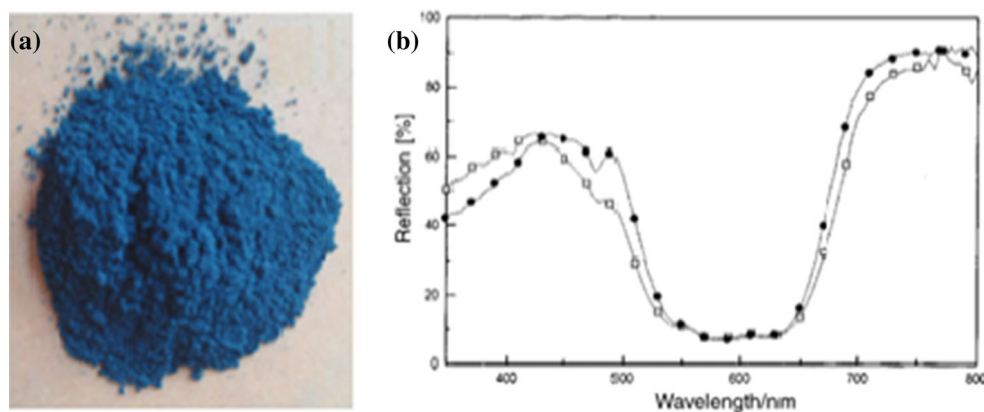


**Figure 17** **a** Photograph of  $\text{CoAl}_2\text{O}_4$  nanopigment obtained via self-propagation combustion method. Reproduced with permission from ref. [137], Copyright 2017, Hindawi; **b** Diffuse reflectance of

$\text{CoAl}_2\text{O}_4$  after 15 min at 600 °C (squares) and standard  $\text{CoAl}_2\text{O}_4$  pigment (circles). Reproduced with permission from ref. [148], Copyright 2000, Royal Society of Chemistry.

incorporate low cost and less toxic elements to  $\text{CoCr}_2\text{O}_4$ , thus reducing environmental damages and fabrication costs. However, the optical properties of such pigment have not been often reported. Hedayati et al. [139] modified  $\text{CoCr}_2\text{O}_4$  with  $\text{Al}^{3+}$  and  $\text{Zn}^{2+}$ , via a sol-gel route obtaining particles with sizes between 100 and 250 nm. Their results showed that the NIR solar reflectance was enhanced by increasing the  $\text{Zn}^{2+}$  and  $\text{Al}^{3+}$  concentrations (Fig. 20), demonstrating their potential use as cool pigments.

### **$\text{ABO}_3$ -type perovskite-based pigments**

$\text{ABO}_3$ -type oxides are extremely interesting, particularly due to their optoelectronic properties. Generally, these compounds can exhibit diverse crystal structures, such as perovskite and ilmenite [150], but the majority of  $\text{ABO}_3$ -type oxides crystallize in the simple mineral perovskite ( $\text{CaTiO}_3$ ) structure or similar. These oxides exist in varied range of A and B cations [151–153] (with A larger than B). In ideal perovskite structures, A occupies the eight corner positions, while B (which can be 3d, 4d or 5d transition metal ions) occupies the body centre position.

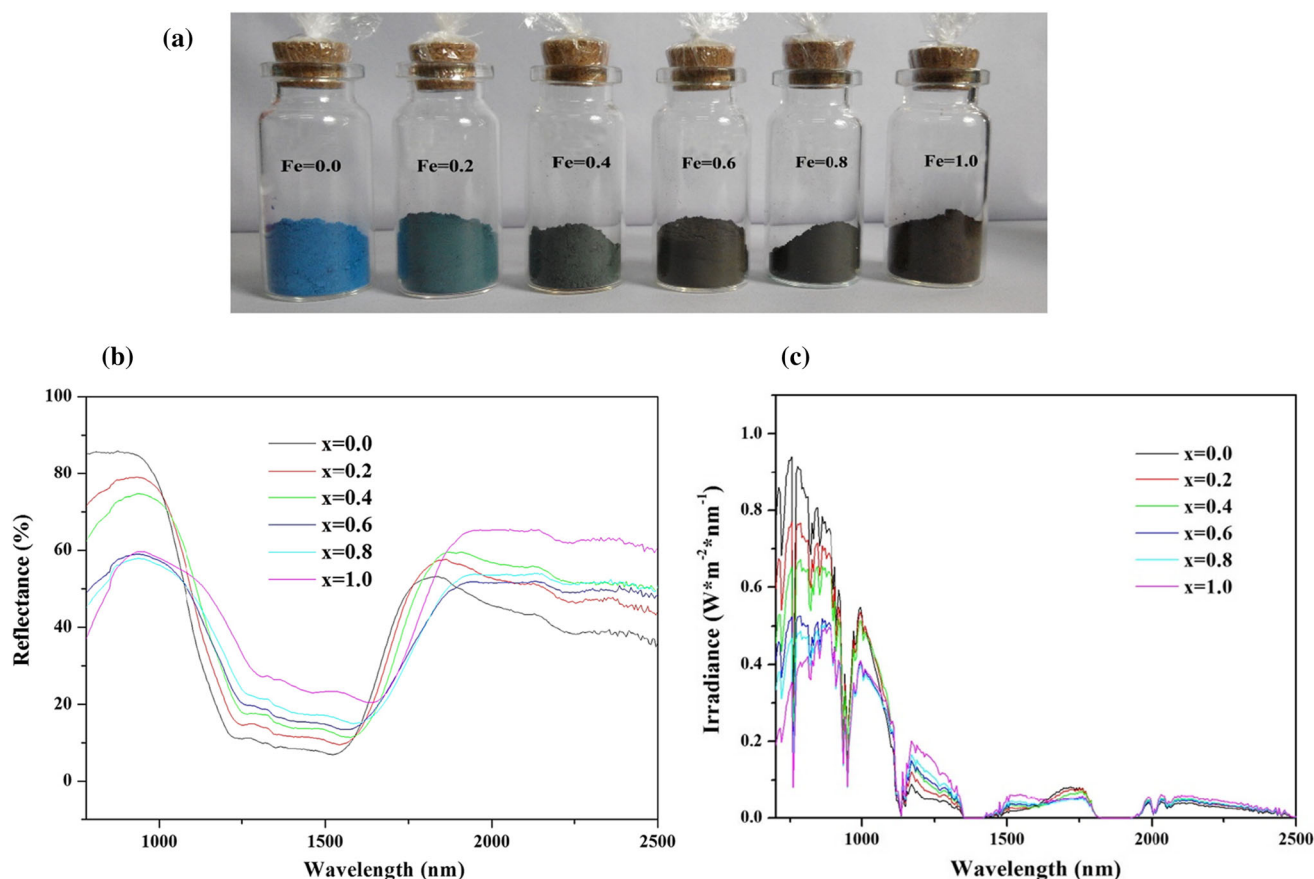


**Figure 18** **a** Photographs of  $\text{Co}_{0.5}\text{Mg}_{0.5}\text{Al}_{2-x}\text{Fe}_x\text{O}_4$  ( $x = 0, 0.2, 0.4, 0.6, 0.8$ , and  $1.0$ ) powdered pigments; **b** NIR reflectance and **c** NIR irradiance of  $\text{Co}_{0.5}\text{Mg}_{0.5}\text{Al}_{2-x}\text{Fe}_x\text{O}_4$  powdered samples. Reproduced with permission from ref [146], Copyright 2016, Elsevier.

The O ions are located at the centres of the six faces (Fig. 21) [154].

Several  $\text{ABO}_3$ -type complex or doped oxides can be used as near-infrared pigments (Table 4). For example, Meenakshi et al. [155] synthesized pale yellow perovskite-like bismuth titanate ( $\text{Bi}_4\text{Ti}_3\text{O}_{12}$ ) using a simple hydrothermal method. Their results (Fig. 22) showed that such nanopigment (around 250–500 nm) acts as a better near-infrared reflective pigment and has superior cooling property than the  $\text{TiO}_2$  conventional white pigment.

Another promising candidate to be used as a cool pigment is zinc titanate. Since there is restricted literature about the cooling effects of  $\text{ZnTiO}_3$ , Lv et al. [116] studied the possibility to synthesize, by a simple solid-state technique, such pigment, which turns out to be a challenge due to the delicate phase equilibria of the  $\text{ZnO}$ – $\text{TiO}_2$  system. They successfully produced hexagonal  $\text{ZnTiO}_3$ , with a distribution range between 100 and 1  $\mu\text{m}$ , which has an optical bandgap as high

as 3.75 eV and has superior near-infrared reflectance (about 95%) and cooling properties when compared to conventional white pigments (Fig. 23). In the interest of avoiding degradation of organic binders of paint by high-energy UV light, there is a blue shift of the absorption edge from 380 (ZnO) to 320 nm, overcoming the challenge of using white pigment such as  $\text{TiO}_2$  and ZnO.

Although light colours are important in the pigments industry, there is a necessity to expand the range of colours to darker ones. As we have seen, the interest is to introduce pigments that possess colour due to visible-light absorption while at the same time providing a cooling effect by reflecting NIR. To increase the colour range, Yuan et al. [63] doped perovskite  $\text{BiFeO}_3$  with rare-earth elements ( $\text{La}^{3+}$ ) to adjust the colour performance by controlling energy gaps and displacement phenomenon in the valence and conduction bands. Interestingly, although the  $\text{BiFeO}_3$  NIR reflectance can be enhanced to around

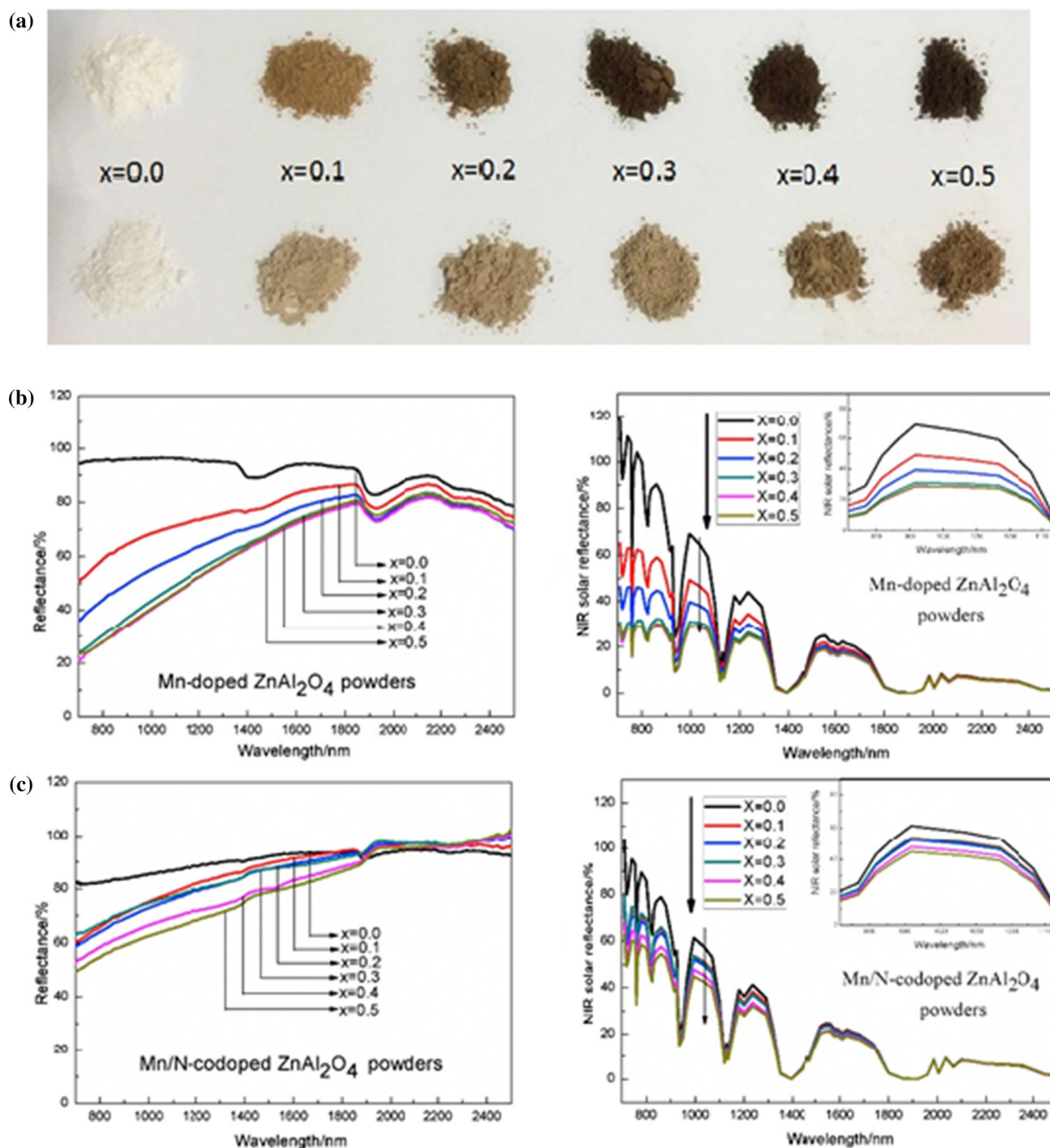


**Figure 19** a Photographs of Mn-doped  $\text{ZnAl}_2\text{O}_4$  and Mn/N co-doped  $\text{ZnAl}_2\text{O}_4$  compounds ( $x = 0.0, 0.1, 0.2, 0.3, 0.4, \text{ and } 0.5$ ); NIR reflectance and NIR solar reflectance of b Mn-doped  $\text{ZnAl}_2\text{O}_4$

powders and c Mn/N co-doped  $\text{ZnAl}_2\text{O}_4$  powders. Reproduced with permission from ref. [138], Copyright 2017, Elsevier.

72% by doping with  $\text{La}^{3+}$ , the visible colour becomes lighter (Fig. 24).

Former reports on Cr-doped perovskites showed that these pigments have darker tones and a high

absorption in the visible region. As no NIR reflectance results had been presented, Zou et al. [163] synthesized such pigments by the calcination of  $\text{CaCO}_3$  and the Cr-dopant at the surface of  $\text{TiO}_2$



**Figure 20** Diffuse reflectance spectra of  $\text{CoCr}_{2-y}\text{Al}_y\text{O}_4$  ( $y = 0, 0.5, 1, 1.5$  and  $2$ ) pigments. Reproduced with permission from ref. [139], Copyright 2015, Elsevier.

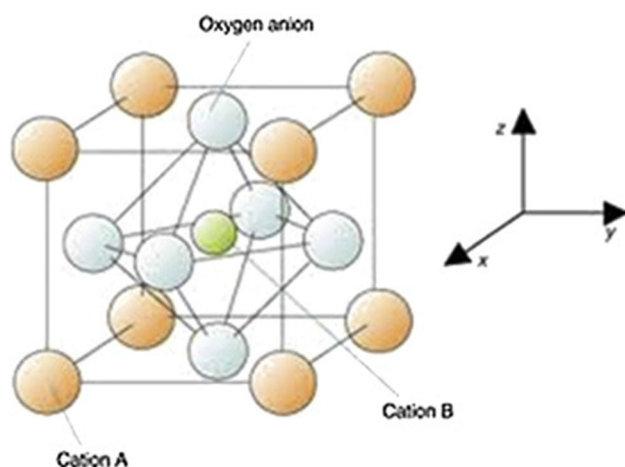
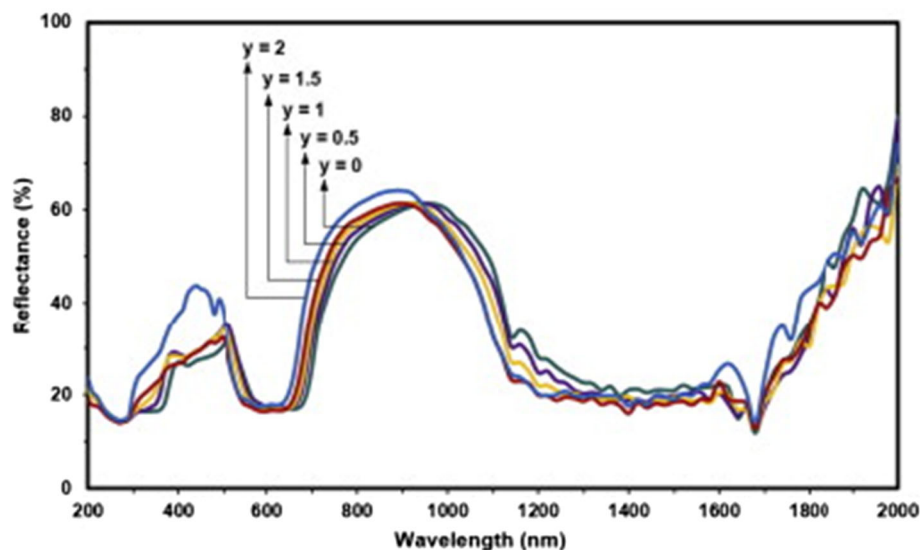


**Figure 21** An example of a typical  $\text{ABO}_3$  perovskite-type unit cell structure. Reproduced with permission from ref. [154], Copyright 2014, Elsevier.

particles and achieved dark colours with only 1% Cr-doped  $\text{CaTiO}_3$  having a size distribution between 0.5 and 2  $\mu\text{m}$ , with around 80% near-infrared reflectance (Fig. 25).

Other attracting pigments are doped compounds  $[(\text{In}_{2x-1}\text{Cu}_x\text{Ti}_x), (\text{In}_{1-x}\text{Fe}_x), (\text{In}_{1-x}\text{Mn}_x)]$  and  $(\text{In}_{1-x-2y}\text{Mn}_x\text{Ti}_y\text{Zn}_y)]$  based on  $\text{YInO}_3$  structure with intense bright colours. They have higher stability, improved NIR reflectance and they are environmentally friendly. Li et al. [170] were able to build a multi-coloured pattern through rational design by a simple solid-state method based on the  $\text{YInO}_3$  perovskite

structure (Fig. 26a). In addition to their bright colour, these pigments were able to reflect NIR. For instance, the purple samples reflect around 90% of NIR radiation (Fig. 26b) [170], this led to the development of low-cost, eco-friendly and extremely stable inorganic  $\text{ABO}_3$ -type oxide near-infrared reflecting pigments.

### Pigments based on rare-earth elements

Traditional inorganic pigments generally contain heavy metals, which cannot satisfy society needs for environmental protection and energy-saving. As a result, many researchers have employed rare-earth metals to modify pigments to improve their NIR reflectivity and colour. The industrial utilization of rare-earth elements has been increasing quickly because of their non-toxic nature, stability and intense shades. Therefore, a huge variety of NIR-reflecting materials based on rare-earths are being studied as substitutes for conventional cool pigments, favouring the use of lanthanide oxides [174]. The most representative pigments based on rare-earth element are listed in Table 5.

Transition metal ions are typically integrated as chromophores into  $\text{A}_2\text{B}_2\text{O}_7$  stoichiometry materials to obtain coloured materials [175]. Because of the toxicity of some of these ions (Cr, Ni, Co ...), the use of different, harmless elements will be decisive in the future. With their ideal properties, lanthanides oxides are perfect candidates to substitute the harmful ions



**Table 4** Examples of ABO<sub>3</sub> type-based oxides used as NIR-reflecting pigments

Compound	Crystal structure	Colour	Particle size	% NIR reflectance	Reference
MgTiO <sub>3</sub>	Ilmenite	White	Nanometres	60–75%	[156, 157]
NiTiO <sub>3</sub>	Ilmenite	Yellow	Nanometres	60–80%	[158, 159]
CoTiO <sub>3</sub>	Ilmenite	Green	Nanometres	~ 50%	[160]
ZnTiO <sub>3</sub>	Perovskite	White	Nanometres	95%	[116]
SrTiO <sub>3</sub>	Perovskite	White to grey	Nanometres	85%	[161, 162]
CaTiO <sub>3</sub>	Perovskite	Yellow	Micrometres	90%	[163]
YMnO <sub>3</sub>	Perovskite	Blue greenish	Nanometres	53.4%	[164, 165]
BiFeO <sub>3</sub>	Perovskite	Dark brown	Nanometres	53%	[63]
Bi <sub>4</sub> Ti <sub>3</sub> O <sub>12</sub>	Perovskite	Pale yellow	Nanometres	95%	[155]
CaCu <sub>3</sub> Ti <sub>4</sub> O <sub>12</sub>	Perovskite	Pale brown	Nanometres	57%	[166]
Ca <sub>2</sub> Mn <sub>0.85</sub> Ti <sub>0.15</sub> O <sub>4</sub>	Perovskite-like	Black	Micrometres	66.2%	[167]
SrSn <sub>0.075</sub> Cr <sub>0.025</sub> O <sub>3-δ</sub>	Perovskite-like	Pink	Nanometres	~ 60%	[168]
Bi <sub>0.6</sub> La <sub>0.4</sub> O <sub>3</sub>	Perovskite-like	Reddish brown	Nanometres	72%	[63]
Cr <sup>3+</sup> doped CaTiO <sub>3</sub>	Perovskite-like	Dark brown	Nanometres	~ 80%	[163]
Cr <sup>3+</sup> doped BaTiO <sub>3</sub>	Perovskite-like	Yellow greenish	Nanometres	68–79%	[169]
Y (In,Mn) O <sub>3</sub> - based	Perovskite-like	Ochre to deep blue	Nanometres	63–90%	[170–172]
Fe <sup>3+</sup> doped YMnO <sub>3</sub>	Perovskite-like	Nearly black	Micrometres	~ 80%	[173]
Mg <sup>2+</sup> doped CaCu <sub>3</sub> Ti <sub>4</sub> O <sub>12</sub>	Perovskite-like	Light brown	Nanometres	~ 62%	[166]

in the A<sub>2</sub>B<sub>2</sub>O<sub>7</sub> structure towards environmentally friendly materials [174, 176, 177].

Amongst the lanthanide oxides, materials based on cerium oxide (CeO<sub>2</sub>) are being studied for cool pigment applications due to their opacity and low toxicity [194]. Bi<sub>2</sub>Ce<sub>2</sub>O<sub>7</sub> has a low bandgap of 2.3 eV that allows its easy fine-tuning to produce various colours [181]. To analyse the effect of substitutions on the structure and colour characteristics of Bi<sub>2</sub>Ce<sub>2</sub>O<sub>7</sub>, Raj et al. [176] synthesized a cerium oxide-based material with Bi<sup>3+</sup> being substituted by yttrium and Ce<sup>4+</sup> substituted for terbium, by a solid-state path to produce Bi<sub>2-x</sub>Y<sub>x</sub>Ce<sub>2</sub>O<sub>7</sub> and Bi<sub>2</sub>Ce<sub>2-x</sub>Tb<sub>x</sub>O<sub>7</sub> (x = 0.25, 0.50, 0, 75, 1.0, 1.25 and 1.50) materials. With such substitution, it was possible to achieve novel series of red and yellow, low toxicity cool pigments with high NIR reflectance at a particle size of 1–3 µm (Fig. 27a). As shown in Fig. 27b, the Bi<sub>2-x</sub>Y<sub>x</sub>Ce<sub>2</sub>O<sub>7</sub> and Bi<sub>2</sub>Ce<sub>2-x</sub>Tb<sub>x</sub>O<sub>7</sub> spectra display an extraordinary reflectance in the range of 70–88% and 90–94% for the red and yellow pigments making them suitable to be used as NIR-reflecting coatings [176].

Due to the excellent chemical and thermal stabilities of the rare-earth oxides, a lanthanum and cerium mixed oxide (La<sub>2</sub>Ce<sub>2</sub>O<sub>7</sub>), with low thermal conductivity, has been used as a turbine blade coating [186]. Huang et al. [186] then focused their study on

exploring the influence of doping La<sub>2</sub>Ce<sub>2</sub>O<sub>7</sub> with Pr<sup>4+</sup> and Tb<sup>4+</sup> on the colour shade and NIR reflectance. A series of new pigments with the formula La<sub>2</sub>Ce<sub>2-x</sub>M<sub>x</sub>O<sub>7</sub> (M = Pr, Tb) were fabricated via a sol-gel route with a particle size around 500 nm. Doping Tb<sup>4+</sup> for Ce<sup>4+</sup> in La<sub>2</sub>Ce<sub>2</sub>O<sub>7</sub> caused a decrease of the bandgap from 3.34 to 2.24 eV with increasing dopant (up to 0.5%). Hence, the colours of the fabricated pigments were varied from yellow to dark orange, an evolution analogous to that of Pr-doped pigments (Fig. 28a). To study the thermal properties of the synthesized pigments, La<sub>2</sub>Ce<sub>2-x</sub>Pr<sub>x</sub>O<sub>7</sub> and La<sub>2</sub>Ce<sub>2-x</sub>Tb<sub>x</sub>O<sub>7</sub> pigments were chosen as coating of a metal sheet of roof surface. The results showed that these coatings significantly improve the NIR and solar reflectances, confirming that the synthesized materials possess potential as new cool pigments (Fig. 28b) [186].

Cheng et al. [190] developed, also using a sol-gel route, a series of non-toxic yellow-orange NIR-reflecting pigments based on La<sub>2</sub>Ce<sub>2</sub>O<sub>7</sub>. The W<sup>6+</sup> and Fe<sup>3+</sup> co-doping contributed to enhancing the solar reflectance since the samples possessed high NIR reflectance (Fig. 29a) to test the suitability of the La<sub>2</sub>Ce<sub>1.7</sub>W<sub>0.15</sub>Fe<sub>0.15</sub>O<sub>7+δ</sub> pigment, a galvanized sheet was used, demonstrating an increase of the NIR solar reflectance from 19 to 71% with the application of the coating (Fig. 29b). Thus, the synthesized pigments

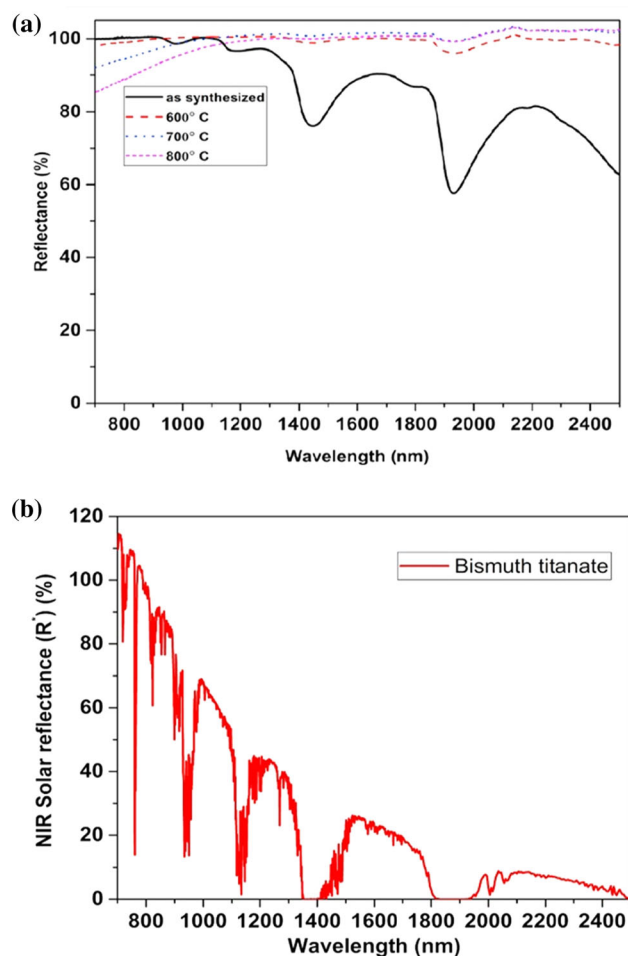


**Figure 22** **a** Reflectance spectra of Bi<sub>4</sub>Ti<sub>3</sub>O<sub>12</sub> (BTO) for different calcination temperatures. **b** BTO NIR solar reflectance. Reproduced with permission from ref. [155], Copyright 2018, Elsevier.

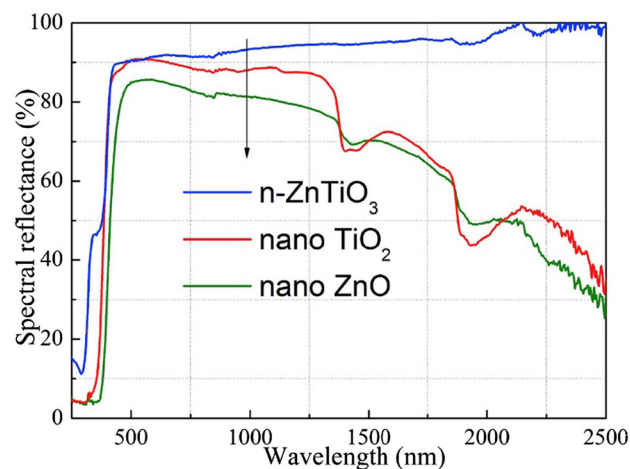


**Figure 23** Diffuse reflectance spectra of nanosized ZnO, nanosized TiO<sub>2</sub> and nanosized ZnTiO<sub>3</sub> samples. Reproduced with permission from ref. [116], Copyright 2019, Elsevier.

can be considered potential candidates for energy-saving coatings in building façades to reduce the interior temperature [190].

Y<sub>2</sub>Ce<sub>2</sub>O<sub>7</sub>, with a bandgap of 3.11 eV, was recently synthesized from a CeO<sub>2</sub>-based host lattice with substituted terbium for Ce<sup>4+</sup>. Raj et al. [189] successfully prepared, by a typical solid-state approach, a novel series of red pigments based on Y<sub>2</sub>Ce<sub>2-x</sub>Tb<sub>x</sub>O<sub>7</sub>. These powder samples with a size of approximately 100 nm demonstrated a very high solar reflectance after tested onto various building substrates (Fig. 30).

A similar research was conducted by Vishnu et al. [185] that developed a new range of environmentally friendly NIR-reflecting inorganic pigments (with a particle size of around 10 μm) based on yttrium cerate doped with Mo<sup>6+</sup> and Pr<sup>4+</sup> metal ions using a solid-state reaction. The Mo<sup>6+</sup>-doped pigments denoted an intense yellow tone with a high NIR solar reflectance in the 700–2500 nm range. On the other hand, the praseodymium-doped pigments exhibited a variety of colours, from red to dark brown. These results confirm that, by bandgap engineering, it is possible to achieve various colour shades in the visible region while simultaneously achieving high NIR solar reflectance (80.5% for yellow and 57.5% for reddish brown).

Although rare-metal-based pigments are being studied to potentially replace traditional pigments because of their low toxicity and high reflectivity, the higher cost of some rare-earth metals is a key limiting factor still preventing their widespread use as pigments [195].

## Core-shell structures

A good approach for producing high-performance multifunctional materials is the core-shell structures, with an outer shell encapsulating the inner core. Such structures not only enhance the physical-chemical properties of pigments, but also successfully prevent the inner core from interacting with the environment [196]. Compared with pigments mixtures, core-shell structures can enhance the darkness of colours and the solar reflectivity [195].

The materials morphology and structure are crucial factors for the application of core-shell particles (Table 6). As noticed before, the morphology and particle size affect the optical properties of cool

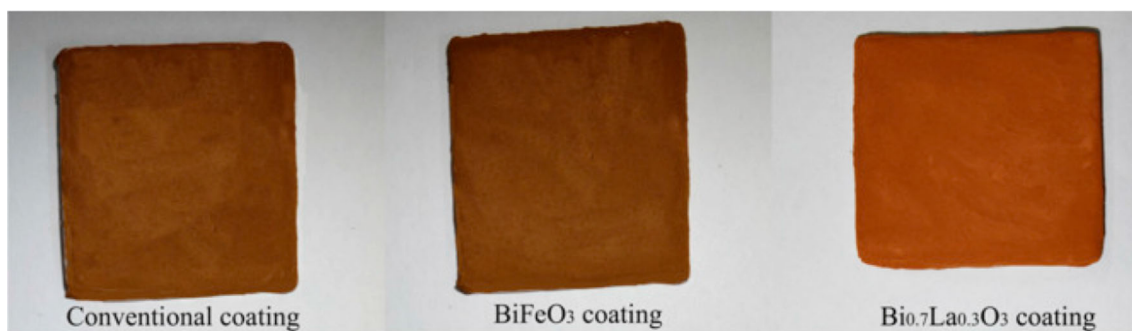


**Figure 24** Concrete cement substrates coated with different pigments. Reproduced with permission from ref. [63], Copyright 2018, Elsevier.

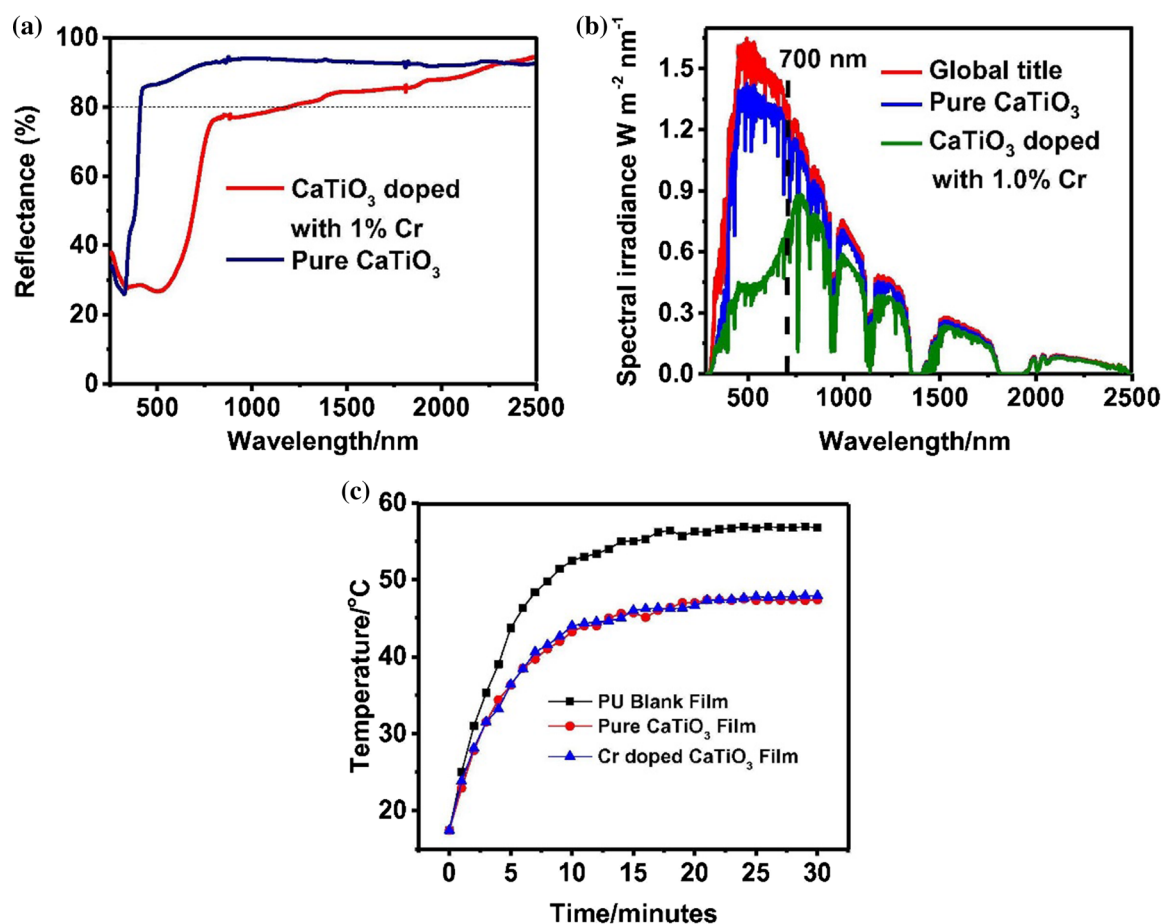
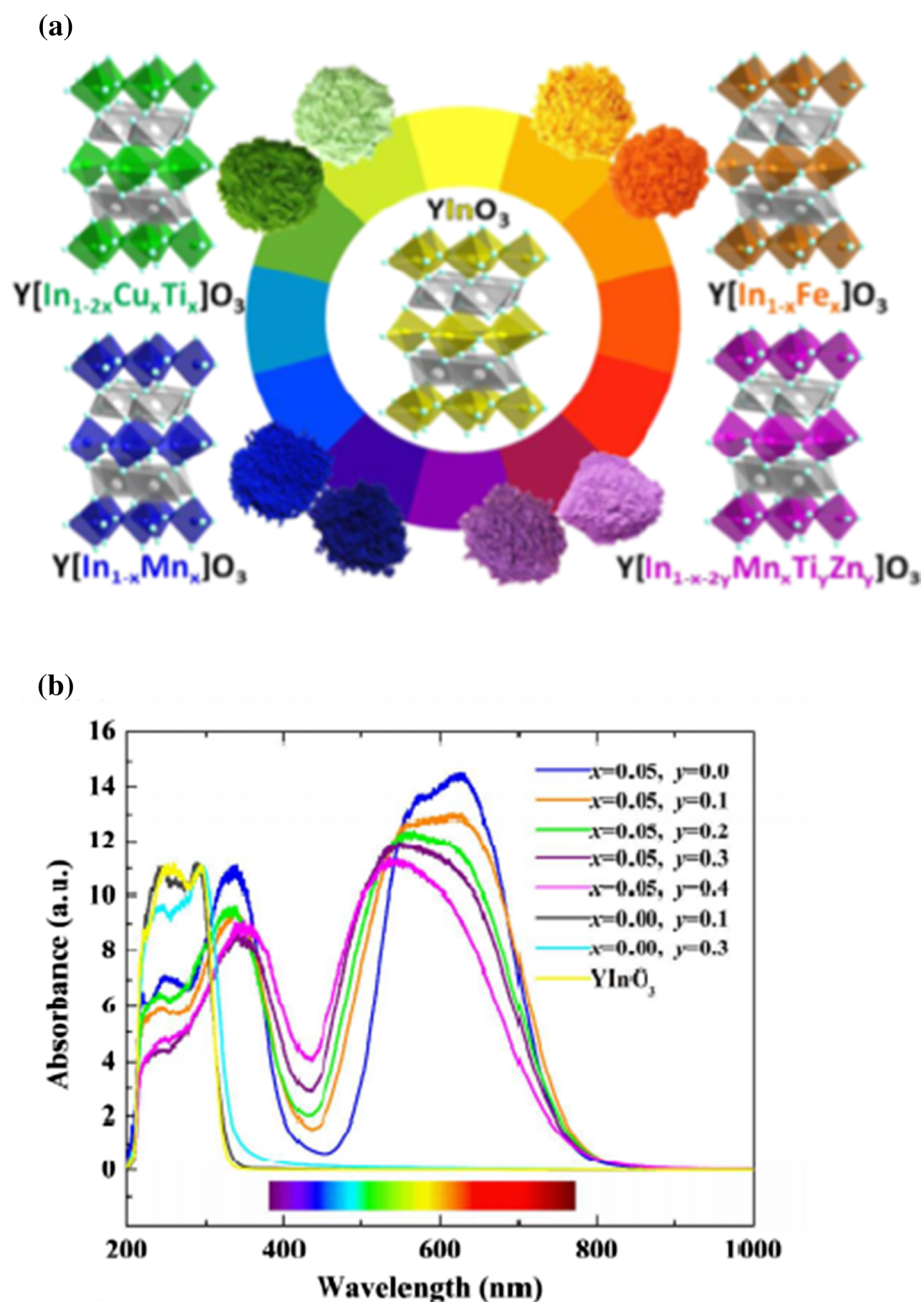


**Figure 25** **a** Graphs of the UV–VIS–NIR diffuse and **b** solar irradiance reflection curves. **c** Variation of the surface temperatures of ceramic tiles of undoped and 1% Cr-doped  $\text{CaTiO}_3$  pigments. Reproduced with permission from ref. [163], Copyright 2019, Elsevier.

**Figure 26** **a** Range of colours created by doping  $\text{YInO}_3$ ; **b** diffuse reflectance curve of purple pigments  $\text{Y}[\text{In}_{1-x}\text{Mn}_x\text{Ti}_y\text{Zn}_y]\text{O}_3$  ( $x = 0.05$ ,  $y = 0.1 \sim 0.4$ ). The blue  $\text{YIn}_{0.95}\text{Mn}_{0.05}\text{O}_3$ ,  $\text{YInO}_3$  and compositions without Mn chromophore ( $x = 0.00$ ,  $y = 0.1$  and  $0.3$ ) are also shown. Reproduced with permission from ref. [170], Copyright 2016, American Chemical Society Publications.



pigments [197]. When mixed with  $\text{TiO}_2$  pigments that have higher NIR reflectance, the NIR reflectance of colour materials is also improved. Nevertheless, the colour intensity is also reduced. This clearly shows that there is still the need to enhance the NIR reflectance of colour pigments while at the same time improving their colour intensity [196, 197].

Yao et al. [195] prepared composite inorganic pigments with  $\text{TiO}_2@\text{CuO}$  core-shell structure (Fig. 31a) by a co-precipitation method, which had a dark colour and high NIR reflectivity. Copper oxide is a

common black metal oxide used in the industry and can exhibit NIR reflectance with dark colours in a certain composition range (Fig. 31e–f). When used as a blending pigment, rutile  $\text{TiO}_2$  further enhances the NIR reflectivity (from around 61 to 96%) (Fig. 31g, e, h). Therefore, this blended pigment might be a promising candidate for inexpensive, environmentally friendly cool pigments [195].

Nickel titanate ( $\text{NiTiO}_3$ ), a standard yellow pigment, also displays enhanced solar reflectance [158, 159]. Incorporating  $\text{NiTiO}_3$  in  $\text{TiO}_2$  structure can

**Table 5** Pigments based on rare-earth elements used as NIR-reflecting materials

Compound	Crystal structure	Colour	Particle size	% NIR reflectance	Reference
CeO <sub>2</sub>	Face-centered cubic	Pale yellow white	Nanometres	~ 80%	[176, 178]
Y <sub>2</sub> Cu <sub>2</sub> O <sub>5</sub>	Orthorhombic	Green blue	Nanometres	~ 40%	[179]
Y <sub>2</sub> BaCuO <sub>5</sub>	Orthorhombic	Green	Nanometres	61%	[180]
Bi <sub>2</sub> Ce <sub>2</sub> O <sub>7</sub>	Monoclinic	Yellow	Micrometres	~ 90%	[181]
LaYO <sub>3</sub>	Fluorite type	White	Nanometres	92%	[182]
LaFeO <sub>3</sub>	Orthorhombic	Dark orange	Nanometres	65.4%	[183]
Y <sub>2</sub> Ce <sub>2</sub> O <sub>7</sub>	Cubic fluorite	Ivory white	Nanometres	~ 90%	[184, 185]
La <sub>2</sub> Ce <sub>2</sub> O <sub>7</sub>	Fluorite type	White	Nanometres	95.95%	[186]
Sm <sub>2</sub> Ce <sub>2</sub> O <sub>7</sub>	Cubic fluorite	Yellow cream	Micrometres	~ 80%	[187]
GdCeO <sub>3.5</sub>	Cubic fluorite	Yellow	Nanometres	91%	[188]
Bi <sub>2-x</sub> Y <sub>x</sub> Ce <sub>2</sub> O <sub>7</sub>	Cubic fluorite	Yellow	Micrometres	93%	[176]
Bi <sub>2</sub> Ce <sub>2-x</sub> Tb <sub>x</sub> O <sub>7</sub>	Cubic fluorite	Red	Micrometres	88%	[176]
Fe <sup>3+</sup> doped Y <sub>2</sub> Ce <sub>2</sub> O <sub>7</sub>	Cubic fluorite	Light yellow	Nanometres	~ 80%	[184]
Mo <sup>6+</sup> doped Y <sub>2</sub> Ce <sub>2</sub> O <sub>7</sub>	Cubic fluorite	Yellow	Micrometres	80.5%	[185]
Pr <sup>4+</sup> doped Y <sub>2</sub> Ce <sub>2</sub> O <sub>7</sub>	Cubic fluorite	Red	Micrometres	57.5%	[185]
Tb <sup>4+</sup> doped Y <sub>2</sub> Ce <sub>2</sub> O <sub>7</sub>	Cubic C-type	Red	Micrometres	55.1–86.9%	[189]
W <sup>6+</sup> /Fe <sup>3+</sup> doped La <sub>2</sub> Ce <sub>2</sub> O <sub>7</sub>	Fluorite type	Yellow to orange	Nanometres	83.27–89.55%	[190]
Tb <sup>4+</sup> /Pr <sup>4+</sup> + doped La <sub>2</sub> Ce <sub>2</sub> O <sub>7</sub>	Fluorite type	Soft orange to Dark orange	Nanometres	~ 90%	[186]
Bi <sup>3+</sup> doped LaYO <sub>3</sub>	Cubic bixbyite type	Light yellow to bright yellow	Nanometres	~ 91%	[182]
Bi <sup>3+</sup> /Tb <sup>4+</sup> co-doped LaYO <sub>3</sub>	Cubic bixbyite type	Soft orange to Dark orange	Nanometres	84.13–92.41%	[182]
Al <sup>3+</sup> doped LaFeO <sub>3</sub>	Orthorhombic	Orange to Yellow	Nanometres	53.7–56.7%	[183]
Bi <sub>3</sub> YO <sub>6</sub> doped with Fe <sub>2</sub> O <sub>3</sub>	Fluorite type	Bright yellow to ochre red	Nanometres	88.64–99.58%	[191]
V doped LaPO <sub>4</sub>	Monoclinic	White to greyish yellow	Nanometres	62.14–87.86%	[192]
Fe doped Pr <sub>2</sub> Zr <sub>2</sub> O <sub>7</sub>	Fluorite type with pyrochlore	Reddish orange	Micrometres	~ 70%	[193]

help to further improve their NIR reflectance. He et al. [196] produced by a sol–gel route core–shell NiTiO<sub>3</sub>@TiO<sub>2</sub> yellow particles, with around 850 nm diameters.

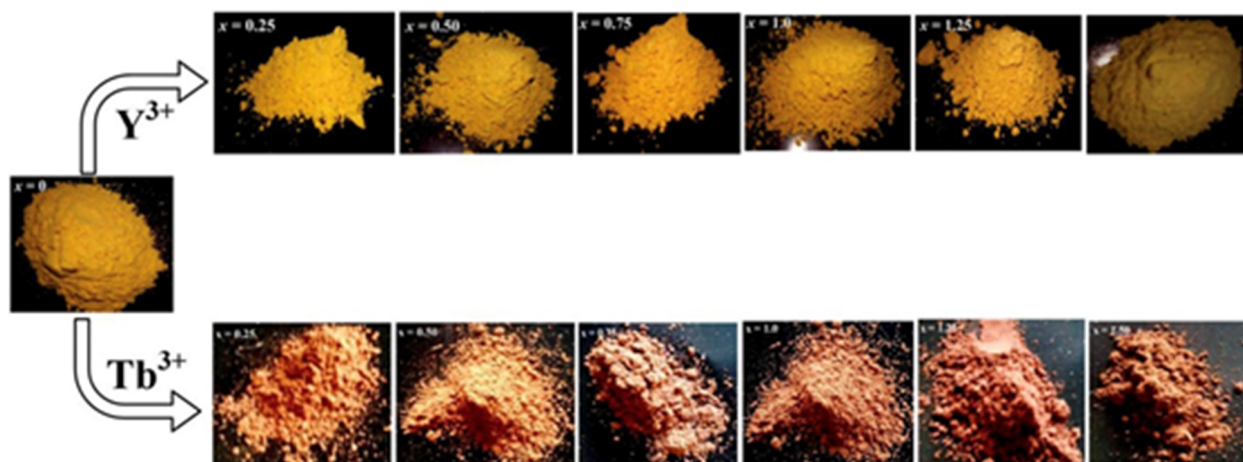
Furthermore, a reduced amount of NiTiO<sub>3</sub> particles would result in the decrease of the NIR absorption, while the incorporation of rutile TiO<sub>2</sub> (with a superior NIR reflectance) stimulates the NIR reflection of the core–shell structure. Nevertheless, the NiTiO<sub>3</sub> and TiO<sub>2</sub> mixture was able to reflect light and prevent the NiTiO<sub>3</sub> from absorbing part of the visible light [196]. Consequently, the mixed pigment exhibits a faded hue. Thus, the unique core–shell structure of the NiTiO<sub>3</sub>@TiO<sub>2</sub> pigment showed improved NIR reflectance and bright yellow colours.

Niaraki et al. [199] prepared two different NIR-reflecting nanocomposites based on Fe, Cr and Ti oxides. The first consisted on (Fe,Cr)<sub>2</sub>O<sub>3</sub>@TiO<sub>2</sub> core–shell particles, using mixing and co-precipitation methods;

the second was a physical mixture of Fe–Cr–Ti oxides materials. The effects of the thermal treatment (500 °C and 1000 °C) and of the preparation method were investigated. In both cases, it was noticed that the average particle sizes were ≈30 nm, and that, by increasing the treatment temperature to 1000 °C, the NIR reflectance increased for both cases (core–shell and mixture) (Fig. 32a and b). However, the core–shell structure reveals much higher NIR reflectance (57.8%) than that of the mixture composed by the mixed oxides (47.8%). The enhanced rate of the NIR reflectance of the (Fe,Cr)<sub>2</sub>O<sub>3</sub>@TiO<sub>2</sub> calcinated at 1000 °C was attributed to the improved refractive index of the core–shell structure. A simple schematic of the reflectance mechanism of the two pigments is shown in Fig. 32e [199].



(a)



(b)

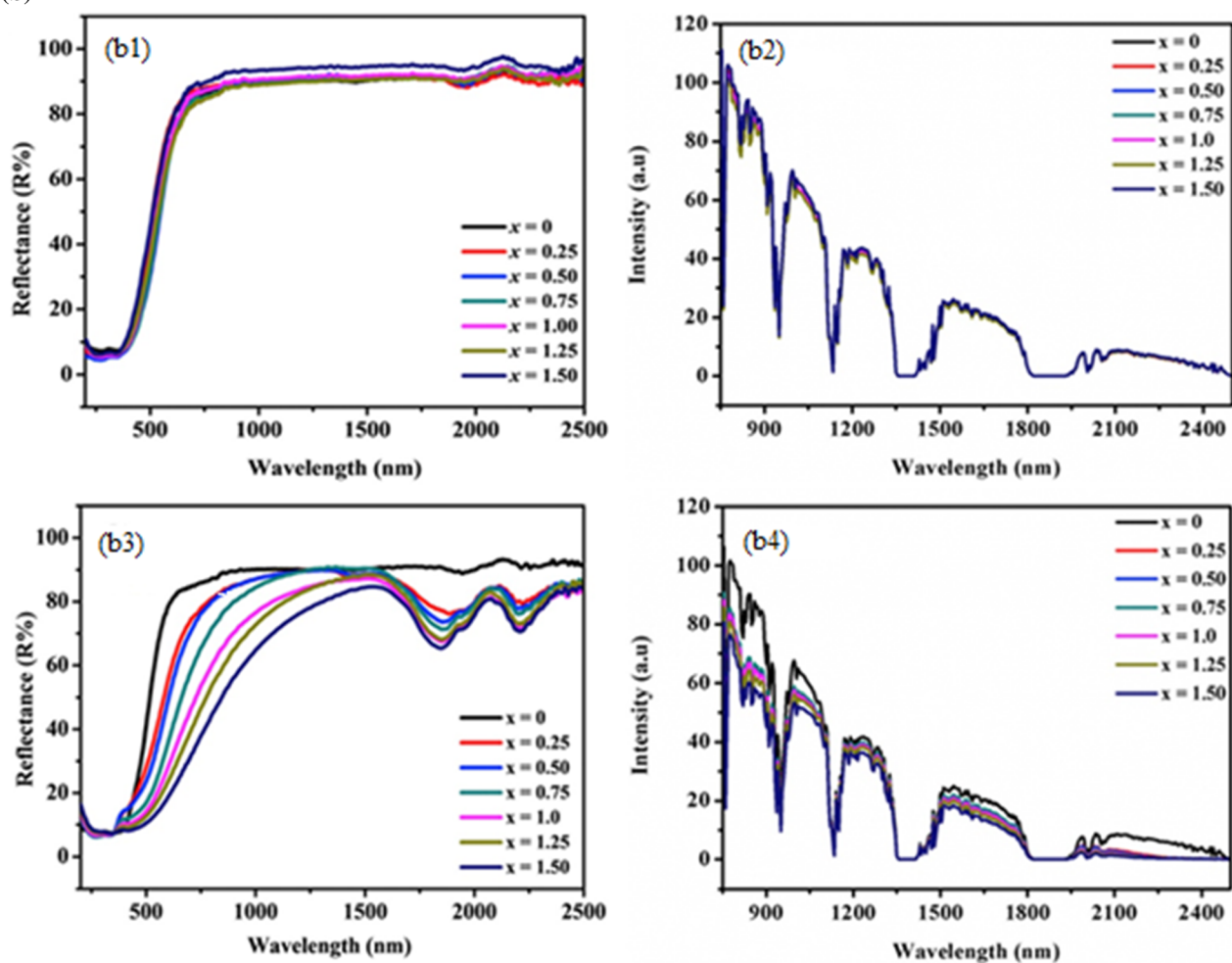
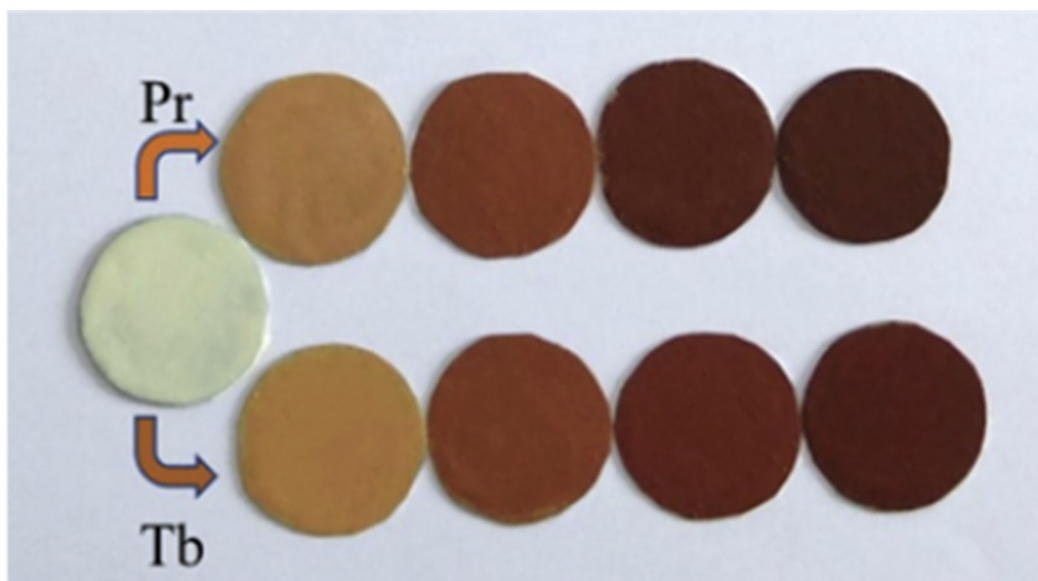


**Figure 27** **a** Photographs of  $\text{Bi}_{2-x}\text{Y}_x\text{Ce}_2\text{O}_7$  and  $\text{Bi}_2\text{Ce}_{2-x}\text{Tb}_x\text{O}_7$  ( $x = 0, 0.25, 0.5, 0.75, 1.0, 1.25$  and  $1.50$ ) pigments. **b** NIR reflectance spectra of **b1**  $\text{Bi}_{2-x}\text{Y}_x\text{Ce}_2\text{O}_7$  and **b2**  $\text{Bi}_2\text{Ce}_{2-x}\text{Tb}_x\text{O}_7$  ( $x = 0, 0.25, 0.50, 0.75, 1.0, 1.25$  and  $1.50$ ) pigments and solar

NIR reflectance spectra of **b3**  $\text{Bi}_{2-x}\text{Y}_x\text{Ce}_2\text{O}_7$  and **b4**  $\text{Bi}_2\text{Ce}_{2-x}\text{Tb}_x\text{O}_7$  ( $x = 0, 0.25, 0.50, 0.75, 1.0, 1.25$  and  $1.50$ ) pigments. Reproduced with permission from ref. [176], Copyright 2019, Elsevier.

(a)



(b)

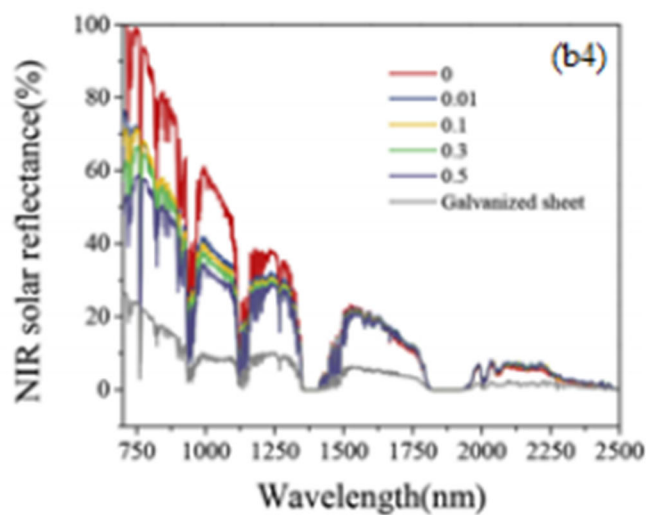
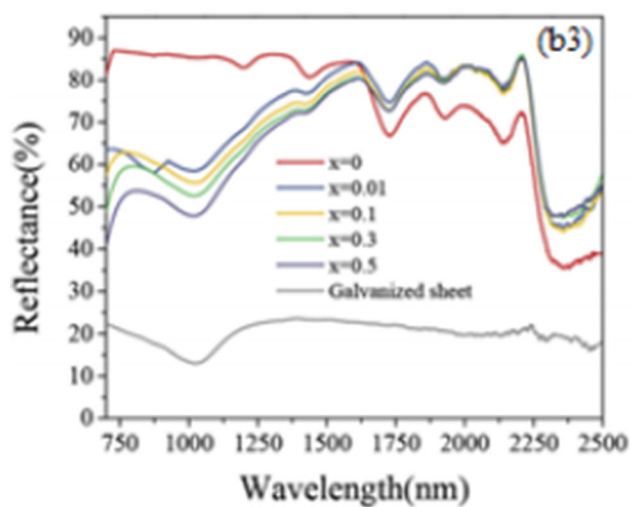
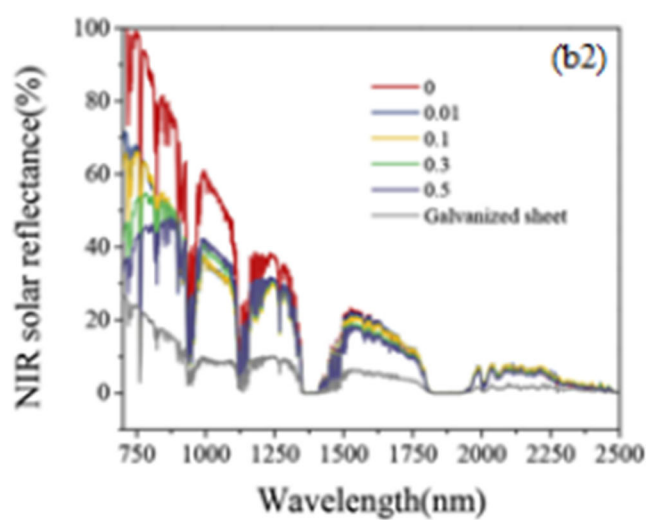
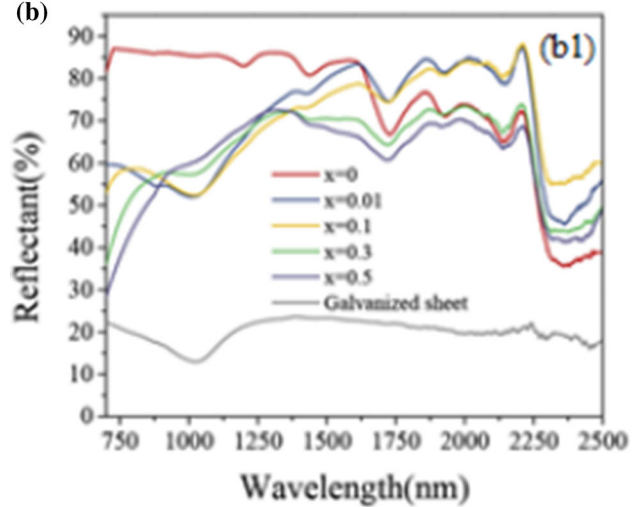


**Figure 28** **a** Photograph of the coatings coloured with  $\text{La}_2\text{Ce}_{2-x}\text{Pr}_x\text{O}_7$  and  $\text{La}_2\text{Ce}_{2-x}\text{Tb}_x\text{O}_7$  ( $x = 0, 0.01, 0.1, 0.3, 0.5$ ) pigments. **b** NIR reflectance and solar reflectance curves of the coloured coatings with **(b1, b2)**  $\text{La}_2\text{Ce}_{2-x}\text{Pr}_x\text{O}_7$  and **(b3, b4)**  $\text{La}_2\text{Ce}_{2-x}\text{Tb}_x\text{O}_7$  ( $x = 0, 0.01, 0.1, 0.3, 0.5$ ). Reproduced with permission from ref. [186], Copyright 2017, Elsevier.

## Building façade's smart and adaptive nanomaterials

Smart and adaptive façades are gaining more interest besides just the use of cool pigments due to their ability to interact with and adjust to the environment, adapting their behaviour and functionality (Fig. 33) [207]. Such envelope systems are capable to modify their properties and regulate the indoor characteristics and heat transfer in response to load variations or

to changes in indoor or outdoor parameters, to improve comfort [208].

One of the most critical issues is to select the best material to incorporate in the building's façade since different properties, such as durability, insulation, quality, cost, aesthetics and strength, must be considered [209]. Table 7 shows the typical and function of several smart and adaptive materials used in building façades, from which we highlight a few in the following.

The disadvantage of the intermittent nature of solar energy can be overcome through a transferal system between the energy supply and demand sectors based on Phase Change Materials technology (see e.g. [239]). Some studies have found that PCMs integrated into buildings can mitigate energy by 10–87% for cooling purposes. As a result, PCMs have been

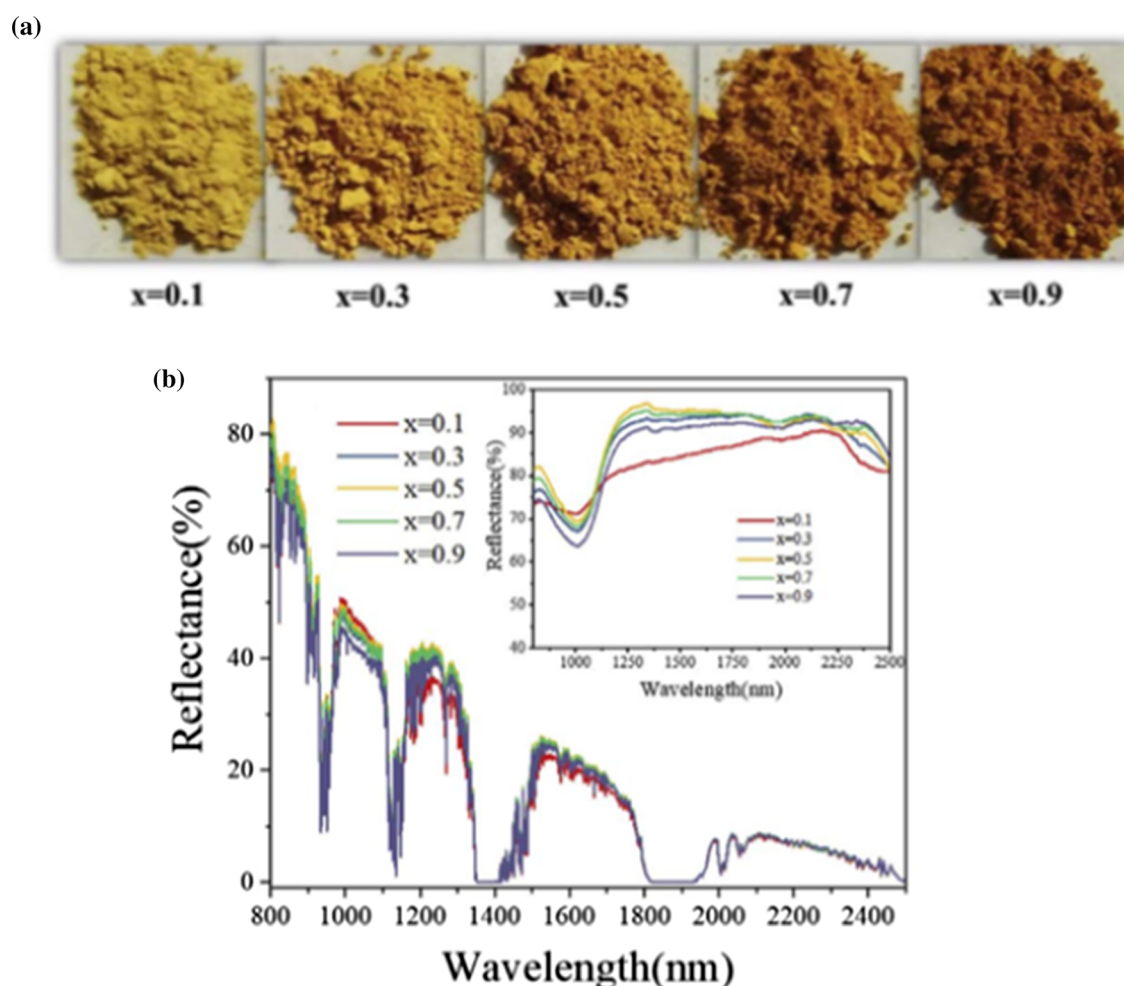


**Figure 29** **a** Photographs and **b** NIR solar reflectance spectra of  $\text{La}_2\text{Ce}_{2-x}\text{W}_{0.5x}\text{Fe}_{0.5x}\text{O}_{7+\delta}$  ( $x = 0.1, 0.3, 0.5, 0.7, 0.9$ ) pigments. Reproduced with permission from ref. [190], Copyright 2018, Elsevier.

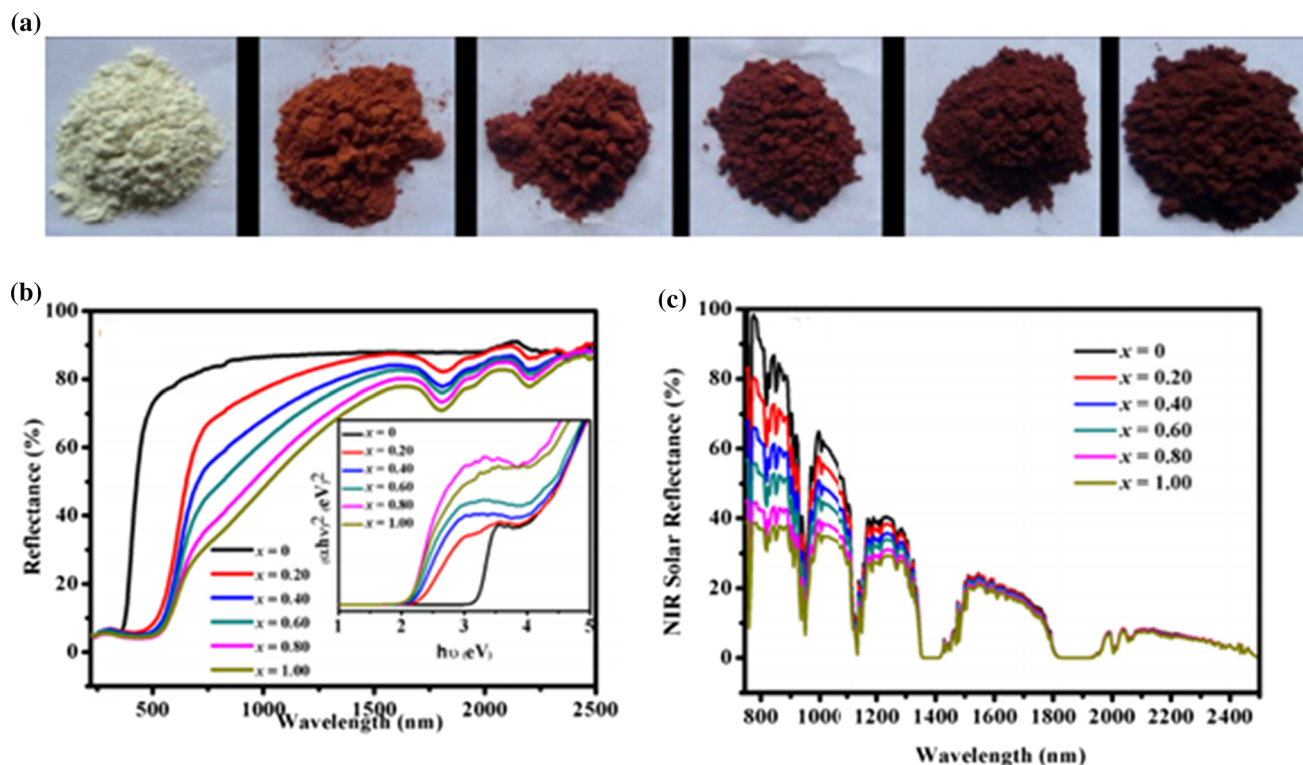


**Figure 30** **a** Photographs of  $\text{Y}_2\text{Ce}_{2-x}\text{Tb}_x\text{O}_7$  ( $x = 0, 0.2, 0.4, 0.6, 0.8$ , and  $1.0$ ) red pigments. **b** Reflectance spectra and **c** solar reflectance of  $\text{Y}_2\text{Ce}_{2-x}\text{Tb}_x\text{O}_7$  ( $x = 0, 0.2, 0.4, 0.6, 0.8$ , and  $1.0$ ) red

pigments (Tauc plots in the inset). Reproduced with permission from ref. [189], Copyright 2015, Elsevier.

**Table 6** Examples of core-shell structures used as NIR-reflecting pigments. (HGM: Hollow Glass Microspheres)

Compound	Colour	Particle size	% NIR reflectance	Reference
$\text{TiO}_2@\text{CuO}$	Grey to dark grey	Nanometres	61–96.1%	[195]
$\text{NiTiO}_3@\text{TiO}_2$	Bright yellow	Nanometres	~ 70%	[196]
$\text{TiO}_2@\text{CoTiO}_3$	Green	Nanometres	~ 60%	[160]
$\text{TiO}_2@\text{NiTiO}_3$	Yellow	Nanometres	~ 70%	[198]
$(\text{Fe}, \text{Cr})_2\text{O}_3@\text{TiO}_2$	Brown	Nanometres	57.8%	[199]
$\text{Fe}_2\text{O}_3@\text{SiO}_2@\text{TiO}_2$	Reddish brown	Nanometres	~ 68%	[200]
$\text{Fe}_2\text{O}_3@\text{SiO}_2$	Brown	Nanometres	~ 45%	[201]
$(\text{HGMs})@\text{ZnS}_x\text{Se}_{1-x}$	Light yellow	Micrometres	~ 85%	[202]
$(\text{HGMs})@\text{ZnS}_x\text{Se}_{1-x}:\text{Cu/In}$	Bright red	Micrometres	~ 75%	[202]
$(\text{HGMs})@\text{ZnO}$	White	Nanometres	~ 95.7%	[203]
$(\text{HGM})@\text{BiOCl}_{1-x}\text{I}_x$	Yellow to light Orange	Micrometres	92.6–94.7%	[204]
Mica-titania	White	Nanometres	~ 97.4%	[205]
$\text{BiFe}_{1-x}\text{Al}_x\text{O}_3@\text{mica-titania}$	Brown to orange	Nanometres	63.5–73.6%	[206]

recognized as one of the most progressive materials to enhance energy efficiency and sustainability in buildings especially for heating and cooling [231]. However, the performance enhancement of buildings using PCMs is a complex research and optimized situation, as there are many variables and significant

uncertainties involved in building physics. Chromogenic devices (e.g. gaso-, thermo-, electro- and photochromic) are also a technology used to vary the amount of solar energy through windows (or other substrates) in buildings. Such materials experience a change in their optical properties in the visible and/



or infrared region, due to the application of a specific external stimulus [240]. As an example, Piccolo et al. showed that cooling energy saving can increase by 38% when using electrochromic coatings in glass when compared to a clear glass [241]. Therefore, combining NIR reflective nanopigments with other smart or adaptive materials could be a powerful tool in designing net zero-energy buildings.

## Methods to synthesize pigments/nanopigments

Different approaches can be used for the production of inorganic pigments, including solid-state method [35, 242], sol-gel [243–245], hydrothermal processes [246, 247], molten salts routes [248, 249] or the sonochemical approach [250–252]. The properties of the synthesized products depend critically on the particle size and the method adopted to fabricate the pigments is crucial for the obtained optical properties [35].

### Solid-state route

In a typical solid-state reaction, nanoparticles preparation necessitates high-temperature treatments above 1000 °C for long periods until the disappearance of the intermediary phases (Fig. 34). The precursor oxides are mixed in a stoichiometric ratio and homogenized by wet milling in an agate mortar, using solvents such as ethanol, water or acetone. The residual solvent is, therefore, evaporated and the resultant powders calcinated in the furnace. However, problems have arisen with this method, such as poor sintering behaviour, heterogeneous and imprecise control of stoichiometry. This process can also lead to bulky, robust powder agglomerates, unwanted phases, irregular grain growth and poor reproducibility [242].

As an example, Oka e Masui [167] synthesized  $\text{Ca}_2\text{Mn}_{1-x}\text{Ti}_x\text{O}_4$  using the conventional solid-state procedure to identify whether such a compound could be the right candidate for a novel NIR reflective black pigment. A part of  $\text{Mn}^{4+}$  was substituted by  $\text{Ti}^{4+}$  to improve the reflectance of the pigment. Stoichiometric amounts of  $\text{CaCO}_3$ ,  $\text{MnO}_2$  and  $\text{TiO}_2$  were mixed and the powder has heated in air at 1200 °C for 6 h. The composition  $\text{Ca}_2\text{Mn}_{0.85}\text{Ti}_{0.15}\text{O}_4$  was

optimized to satisfy both enough blackness and high NIR reflectance compared to conventional black pigments (< 50%) (Fig. 35).

### Sol-gel

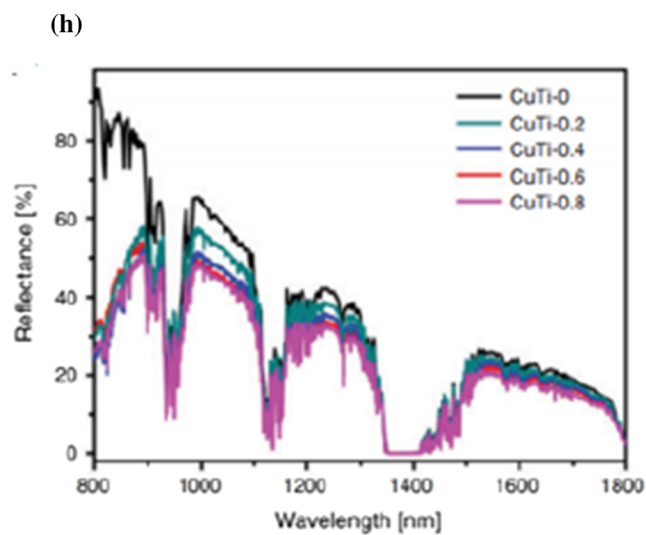
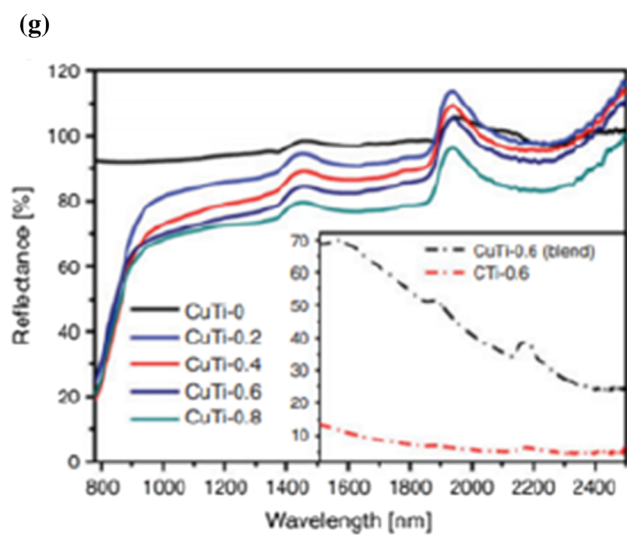
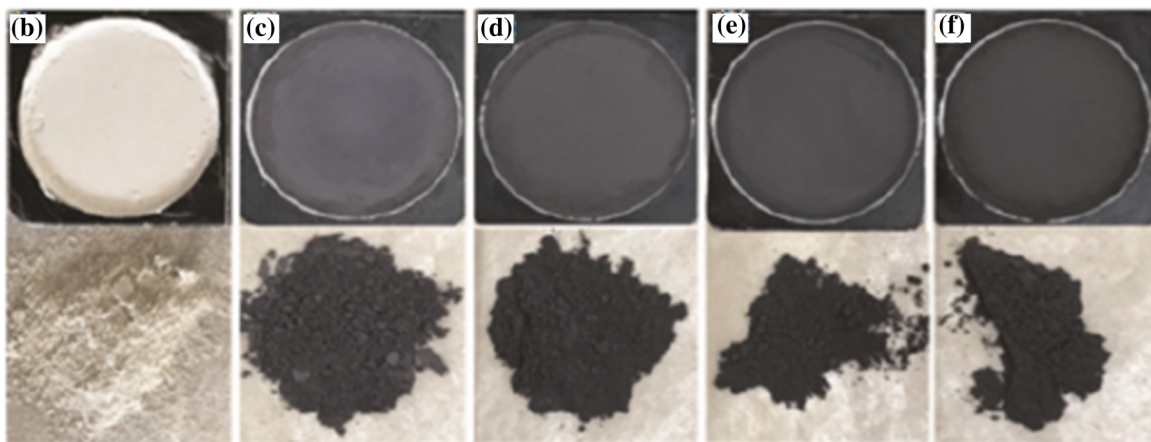
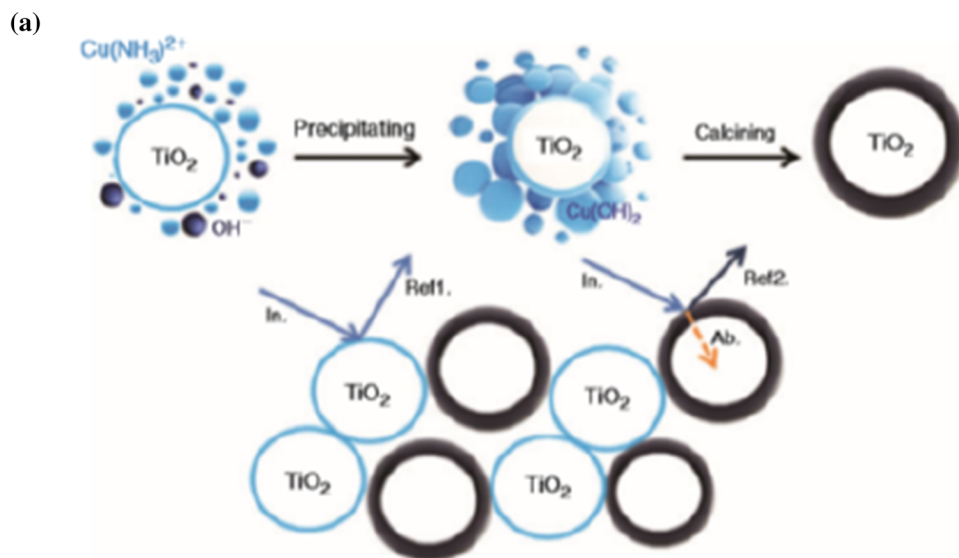
Sol-gel is a wet-chemical process that includes the development of an inorganic system by the formation of a colloidal suspension (sol) and the gelation of the sol forming a continuous liquid phase gel; (Fig. 36). Compared with other conventional routes, sol-gel offers several advantages: low temperature, high purity control, controlled composition, microstructure and textural properties since there is an intimate mixing of the components, which ultimately ensures the homogeneity of the final product [243–245].

Radhika et al. [188] were able to control the morphology of gadolinium-doped cerium oxide powders using a facile synthesis process mixing traditional citrate gel and calcination methods, resulting in highly dispersed mixed oxides (Fig. 37).

### Hydrothermal method

The hydrothermal procedure (Fig. 38) has great prospect to produce materials that would normally be obtained by conventional high-temperature routes of solid-state chemistry. In hydrothermal methods, a solvent allows the quick mixture of many chemical compounds, leading to homogenous products, offering the possibility to control crystal growth and particle morphologies. This method represents a large opportunity to produce multivalued oxides with two or more metals, where the fast mixing of the constituent elements provides a large synthesis advantage [246]. Wet-chemical routes, like hydrothermal synthesis, offer the opportunity for synthesize high purity, highly crystallized, homogenous, ultrafine, well-dispersed nanopowders [247].

Ding et al. [143] prepared a series of  $\text{V}^{5+}$ -doped  $\text{BiPO}_4$  pigments (Fig. 39) exhibiting high NIR reflectance using a simple hydrothermal method. Stoichiometric amounts of bulk materials were added to 80 mL of glycerol/distilled water solvent to obtain  $\text{BiP}_{1-x}\text{V}_x\text{O}_4$  ( $x = 0, 0.01, 0.05, 0.08, 0.10, 0.15$ ). To dissolve the mixture fastly, the authors used an ultrasonic cleaner. Lastly, the mixture was transferred into an autoclave at 160 °C for 24 h.



◀ **Figure 31** **a** Scheme of the formation of CuO@TiO<sub>2</sub> particles and corresponding light/pigment interaction. Photographs of composite pigments: **b** Cu@Ti 0%, **c** Cu@Ti 0.2%, **d** Cu@Ti 0.4%, **e** Cu@Ti 0.6% (**f**) and Cu@Ti 0.8%; **g** NIR reflectance and **h** NIR solar reflectance curves of Cu@Ti composite pigments. Reproduced with permission from ref. [195], Copyright 2018, CSIRO Publishing.

## Molten salt synthesis

Sol–gel and hydrothermal processes are wet-chemical materials fabrication methods that still present several disadvantages, such as being difficult and expensive routes. Thus, one still needs alternative routes to synthesize nanopowders having precise diameters and morphology. Recently, a large range of oxide nanopowders was synthesized using molten salt synthesis (MSS) (Fig. 40) [249]. Molten salts can form a liquid above the melting point of the selected salts, acting as a solvent for reactant dissolution, diffusion and precipitation. This route permits the melt-solid to react much quicker due to the small diffusion distances and large mobility of the melted oxides, resulting in complete reactions in moderately short times. Compared to other synthetic methods, MSS offers a low processing temperature and control of the nanopowders morphology [248].

King et al. [249] used a molten salt-assisted synthesis to prepare pure ZnTiO<sub>3</sub> powders from standard ZnO and TiO<sub>2</sub> oxides in sodium/potassium chlorides (the melting point of 670 °C at the eutectic composition).

## Green synthesis: sonochemical approach

Sonochemistry (Fig. 41) has proven to be an important tool in the preparation of metal oxides. The interesting characteristic of power ultrasounds arises from the fact that it provides a form of energy for the modification of chemical reactivity. It is well known that ultrasonic irradiation promotes cavitation in an aqueous medium where the formation, growth, and collapse of microbubbles occurs. Cavitation can form

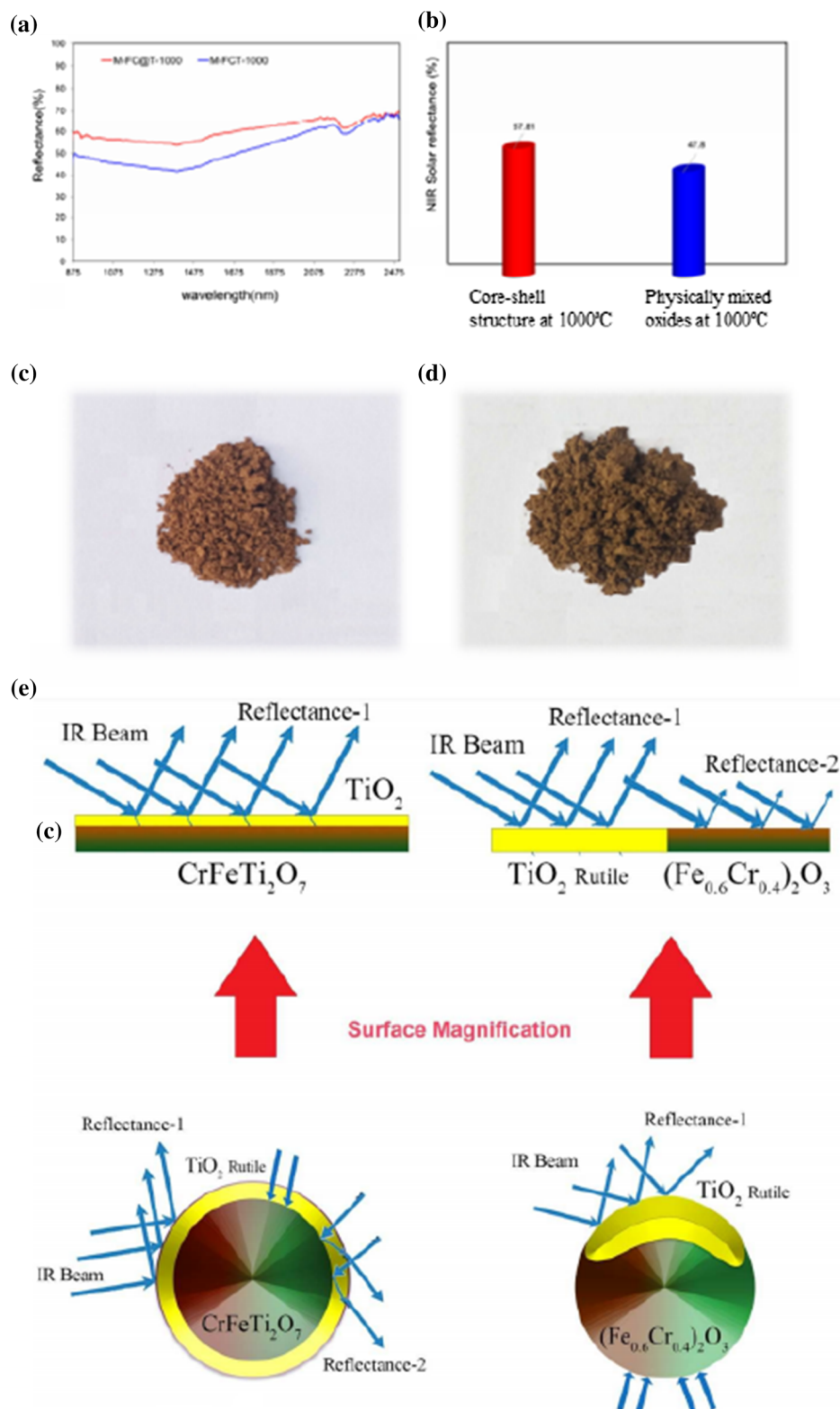
at high temperatures and pressures ( $\approx 5000$  °C and above 1800 kPa), thus allowing the occurrence of uncommon chemical reactions. In many cases, thermally induced procedures offer crystalline nanoparticles [251].

For example, Pholnak et al. [250] successfully used a commercial ultrasonic homogenizer to obtain single-phase spheroidal ZnO nanomaterials using the sonochemical synthesis. Compared with conventional techniques, the synthesis that uses ultrasounds can often be initiated without the need for additives and sonochemistry, making use of cruder reagents. Thus, the reactions may be accelerated or performed under less forcing conditions when sonication is applied [252].

## Summary and outlook

In this review, we presented the state-of-the-art of near-infrared reflective nanomaterials. This paper aimed to classify such nanomaterials according to their crystal structure, identifying the best routes to a successful production and to demonstrate their current importance. In the literature, there is a large number of reported reflective inorganic pigments, which reveals their great importance when applied in buildings. As seen, there is a large interest in obtaining novel NIR reflective nanomaterials that are more ecological and resilient, less dangerous and that can replace conventional toxic and heavy metal materials. The use of adaptive materials to reduce the quantity of absorbed solar energy in buildings can indeed be a promising solution to soften the urban heat island effect. By reducing the amount of absorbed radiation, the incorporation of near-infrared reflecting pigments in coatings can be a strategy to help decrease the cooling load demand. Its combination with other technologies will enable achieving improved energy performance in buildings. The current barriers for the implementation of such nanomaterials are the relatively high initial cost that could be solved by their widespread uptake in the building industry in the future.

**Figure 32** **a** NIR reflectance spectrum and **b** solar NIR reflectance value; photographs of: **c** core-shell structure ( $\text{Fe, Cr}_2\text{O}_3/\text{TiO}_2$ ) and **d** physically mixed  $\text{Fe-Cr-Ti}$  oxides (at  $1000^\circ\text{C}$ ); **e** reflectance mechanism in core-shell structure and physically mixed samples. Reproduced with permission from ref. [199], Copyright 2019, Elsevier.





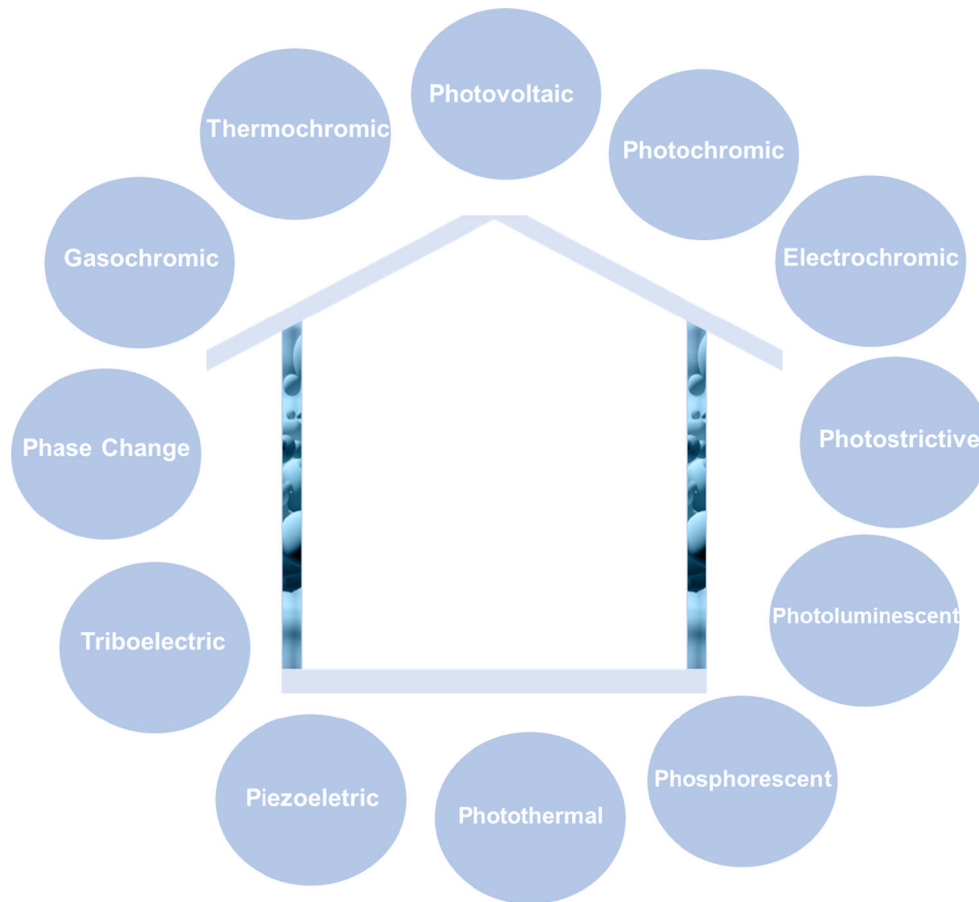


**Figure 33** Selection of building façade's smart and adaptive materials.

Further research should also focus on the life cycle assessment of these new and functional reflective nanopigments to be applied on building envelope systems, since their low environmental impact are strictly related with their durability. Moreover, such

studies should assess the long-term durability on coatings (using full-size prototypes), analyse the impact of surface reflectivity on the overall energy consumption and thermal comfort in both air-conditioned and non-air-conditioned buildings.

**Table 7** Identification of building façade's smart and adaptive materials. Adapted from ref. [209]

Materials	Function	Typical material	Reference
Thermochromic	Reversibly change of colour (related with a change in the crystalline phase and structure) due to a temperature variation	$\text{In}_2\text{O}_3$ , $\text{VO}_2$	[210] [211] [212] [213]
Photovoltaic	Convert solar radiation into electrical energy	$\text{TiO}_2$ , $\text{ZnO}$ , $\text{SnO}_2$ , $\text{Nb}_2\text{O}_5$ , $\text{SiO}_2$ , CNT's	[214]
Photochromic	Exhibit changes in the optical properties in reaction to light	$\text{TiO}_2$ quantum dots, $\text{NiO/Ni}_2\text{O}_3$ , $\text{MoO}_3$ -azobenzenes	[215] [216] [217]
Phosphorescent	Convert ultraviolet into white light	$\text{SrAl}_2\text{O}_4$ : $\text{Eu}^{2+}$ , $\text{Dy}^{3+}$ ; $\text{Sr}_4\text{Al}_4\text{O}_{25}$ : $\text{Eu}^{2+}$ , $\text{Dy}^{3+}$ , $\text{B}^{3+}$ ;	[218]
Photostrictive	Exhibit changes in shape in reaction to light	Liquid crystalline polymer	[219]
Photoluminescent	When excited by light, the transition from the excited state back into the ground state is accompanied by delayed or simultaneous light emission according to the material's nature	$\text{CaAl}_2\text{O}_4$ : $\text{Eu}^{+2}$ , $\text{Nd}^{+3}$ , $\text{La}^{+3}$ ; $\text{Sr}_2\text{MgSi}_2\text{O}_7$ : $\text{Eu}$ , $\text{Dy}$	[220] [221]
Photothermal	Generate thermal energy when photoexcited	Aluminium-doped zinc oxide (AZO), $\text{ZnO}$ thin layers, $\text{TiO}_2/\text{Ag}/\text{TiO}_2$ , fluorine-doped tin oxide (FTO)	[222] [223] [224]
Piezoelectric	Generate an electric potential in response to pressure	$\text{Pb}[\text{Zr}_x\text{Ti}_{1-x}]\text{O}_3$ ; $\text{NaNbO}_3$	[225] [226] [227]
Triboelectric	Type of contact electrification in which certain materials become electrically charged after coming in contact with a different material	Liquid crystals, indium tin oxide (ITO)	[228] [229] [230]
Phase change (PCM)	Release/absorb energy at the phase transition to provide useful heat/cooling	Paraffins, fatty acids, salt hydrates, metallic	[231] [232] [233] [234]
Electrochromic	Colour or opacity of a material changes when a voltage is applied	$\text{WO}_3$ , $\text{IrO}_2$ , $\text{MoO}_3$ , $\text{In}_2\text{O}_3$ :Sn,	[235] [236] [237]
Gasochromic	Reversibly switches its optical transmittance when exposed to diluted hydrogen and oxygen gases	Pt- $\text{WO}_3$ thin film	[238]

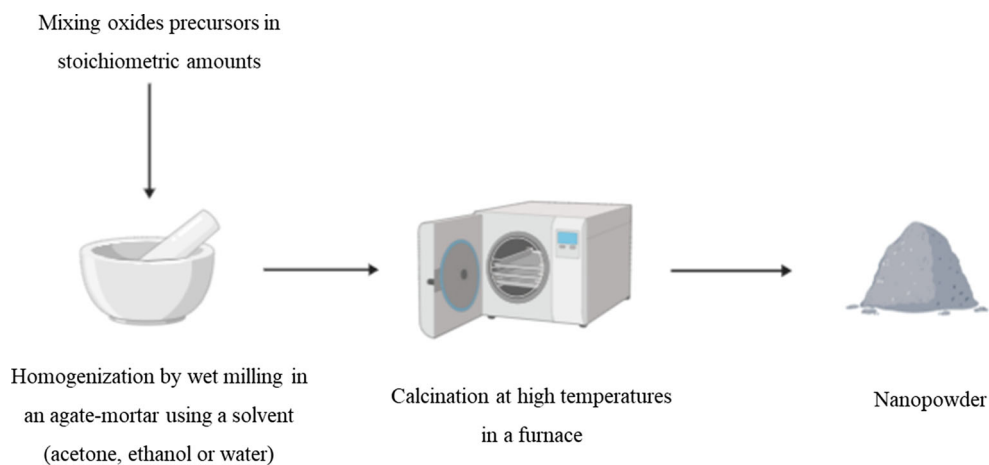


**Figure 34** Schematic representation of a solid-state synthesis procedure.

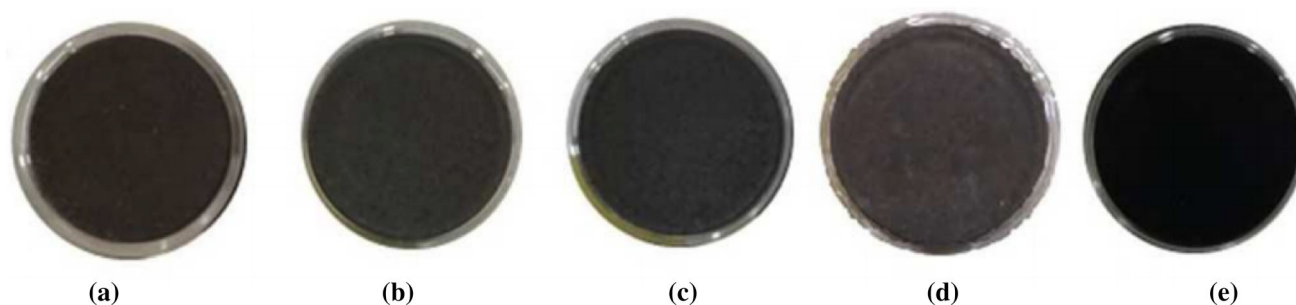


**Figure 35 a** Photographs of  $\text{Ca}_2\text{Mn}_{0.85}\text{Ti}_{0.15}\text{O}_4$  synthesized by conventional solid-state route **(a)**, **b** Black 6350 (iron and chromium oxide), **c** Black 6301 (manganese and bismuth oxide),

**d** MPT-370 (calcium, manganese, and  $\text{TiO}_2$ ) and **e** carbon black. Reproduced with permission from ref. [167], Copyright 2016, Elsevier.

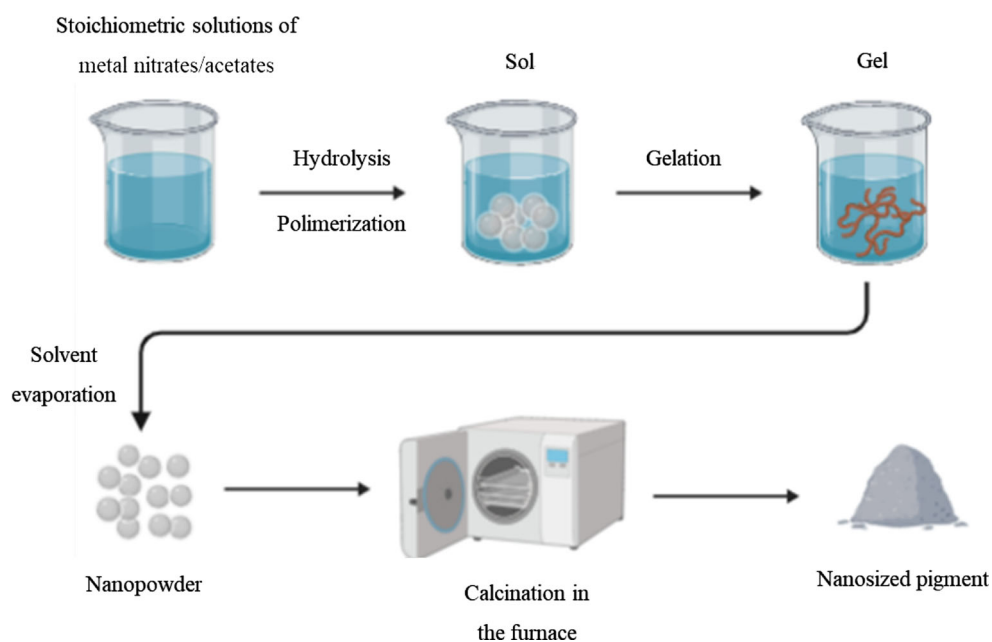


**Figure 36** Representation scheme of a sol-gel route.



**Figure 37** Photographs of Gd:Ce:Mo oxides prepared by a sol-gel method: **a** 1:1:0; **b** 1:0.95:0.05; **c** 1:0.9:0.1; **d** 1:0.85:0.15; **e** 1:0.8:0.20; **f** 1:0.75:0.25; **g** 1:0.65:0.35. Reproduced with

permission from ref. [188], Copyright 2014, American Chemical Society Publications.

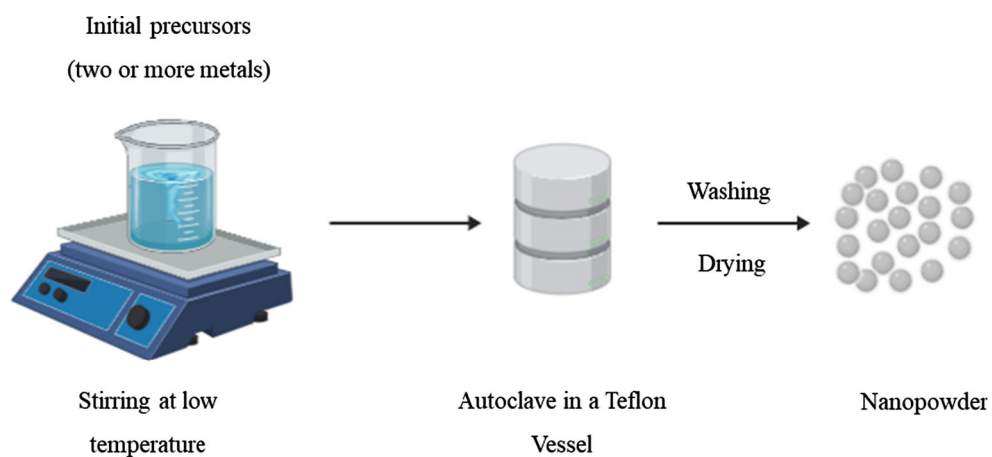


**Figure 38** General representation of a hydrothermal synthesis method.



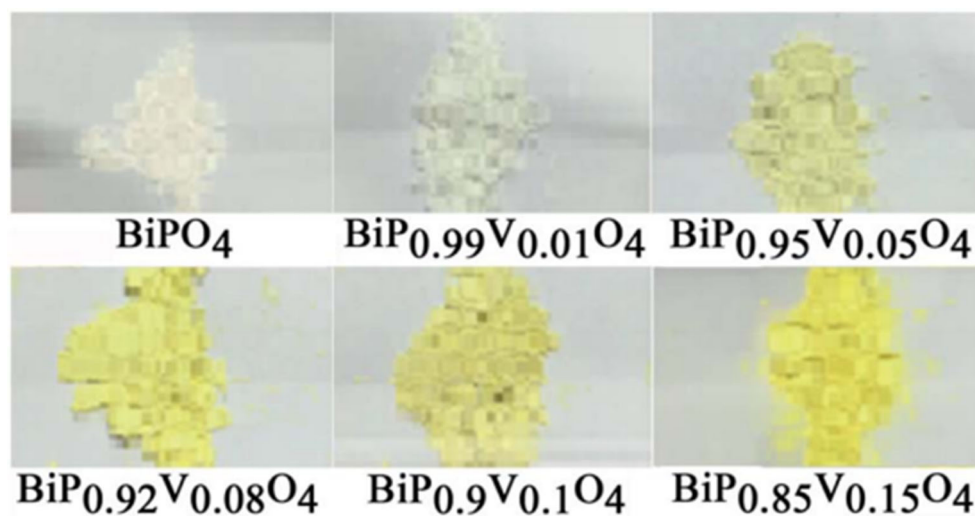


**Figure 39** Photographs of  $\text{BiPO}_4$ -based pigments synthesized by a hydrothermal process. Reproduced with permission from ref. [143], Copyright 2018, Royal Society of Chemistry.

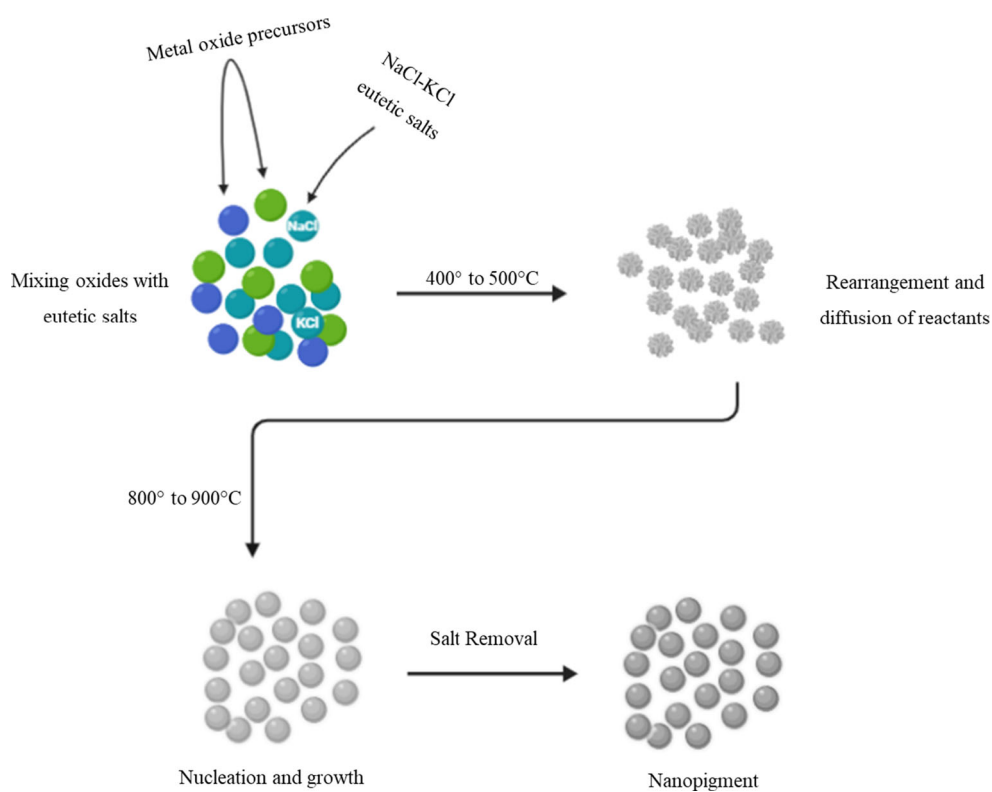


**Figure 40** Schematic representation of a molten salt assisted synthesis reaction.

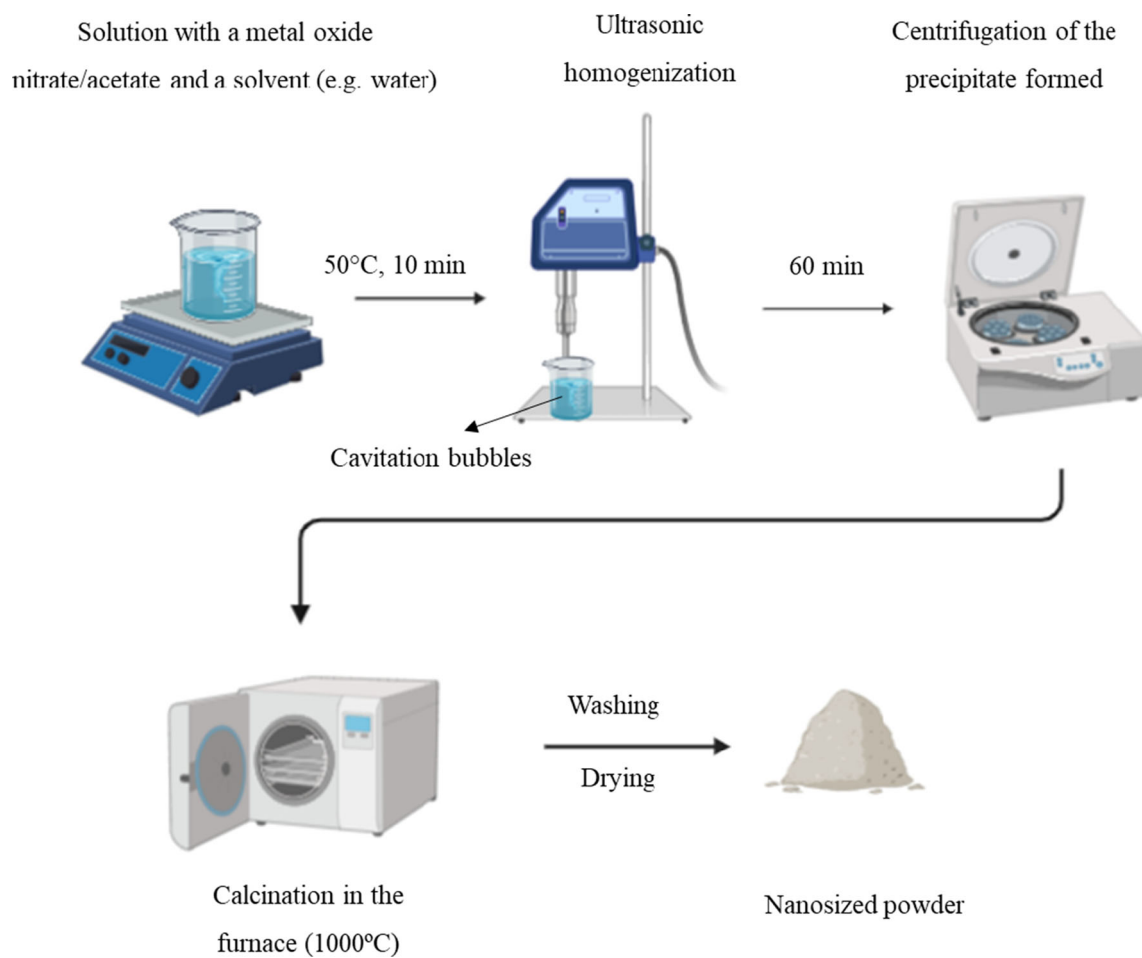


**Figure 41** Schematic representation of green sonochemical synthesis.

## Acknowledgements

This work was financially supported by project Project PTDC/ECI-CON/28766/2017—POCI-01-0145-FEDER-028766—funded by FEDER funds through COMPETE2020—Programa Operacional Competitividade e Internacionalização (POCI) and by national funds (PIDDAC) through FCT/MCTES, project Circular2B - 37\_CALL#2 - Circular Construction in Energy-Efficient Modular Buildings funded by EEA Grants and by Base Funding—UIDB/04708/2020 of the CONSTRUCT—Instituto de I&D em Estruturas e Construções—funded by national funds through the FCT/MCTES (PIDDAC). R. C. Veloso and A. Souza would like to acknowledge the support of FCT—Fundação para a Ciência e Tecnologia for the funding the doctoral grant SFRH/BD/148785/2019 and DFA/BD/8418/2020, respectively.

## Declarations

**Conflict of interest** The authors declare no conflict of interests regarding the publication of this article.

## References

- [1] Kumar S, Bhanjana G, Sharma A et al (2017) Development of nanoformulation approaches for the control of weeds. *Sci Total Environ* 586:1272–1278. <https://doi.org/10.1016/j.scitotenv.2017.02.138>
- [2] Begum P, Fugetsu B (2012) Phytotoxicity of multi-walled carbon nanotubes on red spinach (*Amaranthus tricolor* L) and the role of ascorbic acid as an antioxidant. *J Hazard Mater* 243:212–222. <https://doi.org/10.1016/j.jhazmat.2012.10.025>
- [3] Rico CM, Hong J, Morales MI et al (2013) Effect of cerium oxide nanoparticles on rice: a study involving the antioxidant defense system and in vivo fluorescence imaging. *Environ Sci Technol* 47:5635–5642. <https://doi.org/10.1021/es401032m>
- [4] Li F, Jiang X, Zhao J, Zhang S (2015) Graphene oxide: a promising nanomaterial for energy and environmental applications. *Nano Energy* 16:488–515. <https://doi.org/10.1016/j.nanoen.2015.07.014>
- [5] Ma X, Luo W, Yan M et al (2016) In situ characterization of electrochemical processes in one dimensional nanomaterials for energy storages devices. *Nano Energy* 24:165–188. <https://doi.org/10.1016/j.nanoen.2016.03.023>
- [6] Yu R, Lin Q, Leung S-F, Fan Z (2012) Nanomaterials and nanostructures for efficient light absorption and photovoltaics. *Nano Energy* 1:57–72. <https://doi.org/10.1016/j.nanoen.2011.10.002>
- [7] Mishra YK, Murugan NA, Kotakoski J, Adam J (2017) Progress in electronics and photonics with nanomaterials. *Vacuum* 146:304–307. <https://doi.org/10.1016/j.vacuum.2017.09.035>
- [8] Ede SR, Anantharaj S, Sakthikumar K et al (2018) Investigation of various synthetic protocols for self-assembled nanomaterials and their role in catalysis: progress and perspectives. *Mater Today Chem* 10:31–78. <https://doi.org/10.1016/j.mtchem.2018.07.003>
- [9] Das SK, Bhunia MK, Bhaumik A (2010) Self-assembled TiO<sub>2</sub> nanoparticles: mesoporosity, optical and catalytic properties. *Dalton Trans* 39:4382. <https://doi.org/10.1039/c000317d>
- [10] de Jong (2008) Drug delivery and nanoparticles: applications and hazards. *Int J Nanomed* 3:133. <https://doi.org/10.2147/ijn.s596>
- [11] Jha AK, Prasad K (2019) Nanomaterials from biological and pharmaceutical wastes—a step towards environmental protection. *Mater Today Proc* 18:1465–1471. <https://doi.org/10.1016/j.matpr.2019.06.615>
- [12] Juárez-Moreno K, Pestryakov A, Petranovskii V (2014) Engineering of supported nanomaterials. *Proc Chem* 10:25–30. <https://doi.org/10.1016/j.proche.2014.10.006>
- [13] Tomar R, Abdala AA, Chaudhary RG, Singh NB (2020) Photocatalytic degradation of dyes by nanomaterials. *Mater Today Proc* 29:967–973. <https://doi.org/10.1016/j.matpr.2020.04.144>
- [14] Lewis NS (2016) Developing a scalable artificial photosynthesis technology through nanomaterials by design. *Nat Nanotechnol* 11:1010–1019. <https://doi.org/10.1038/nnano.2016.194>
- [15] Wu S, Xu R, Lu M et al (2015) Graphene-containing nanomaterials for lithium-ion batteries. *Adv Energy Mater* 5:1500400. <https://doi.org/10.1002/aenm.201500400>
- [16] Zeng Y, Zhu Z, Du D, Lin Y (2016) Nanomaterial-based electrochemical biosensors for food safety. *J Electroanal Chem* 781:147–154. <https://doi.org/10.1016/j.jelechem.2016.10.030>
- [17] Lv M, Liu Y, Geng J et al (2018) Engineering nanomaterials-based biosensors for food safety detection. *Biosens Bioelectron* 106:122–128. <https://doi.org/10.1016/j.bios.2018.01.049>
- [18] Louise Liu J, Bashir S (2015) Advanced nanomaterials and their applications in renewable energy. Elsevier, Amsterdam
- [19] Sekoai PT, Ouma CNM, du Preez SP et al (2019) Application of nanoparticles in biofuels: an overview. *Fuel* 237:380–397. <https://doi.org/10.1016/j.fuel.2018.10.030>

- [20] Khin MM, Nair AS, Babu VJ et al (2012) A review on nanomaterials for environmental remediation. *Energy Environ Sci* 5:8075. <https://doi.org/10.1039/c2ee21818f>
- [21] Wegner F (1981) Bounds on the density of states in disordered systems. *Z Phys B Condens Matter* 44:9–15. <https://doi.org/10.1007/bf01292646>
- [22] Ullattil SG, Narendranath SB, Pillai SC, Periyat P (2018) Black TiO<sub>2</sub> nanomaterials: a review of recent advances. *Chem Eng J* 343:708–736. <https://doi.org/10.1016/j.cej.2018.01.069>
- [23] Pacheco-Torgal F, Jalali S (2011) Nanotechnology: advantages and drawbacks in the field of construction and building materials. *Constr Build Mater* 25:582–590. <https://doi.org/10.1016/j.conbuildmat.2010.07.009>
- [24] Commission Communication from the Commission to the European Council, European Economic and Social Committee, Committee of the Regions Energy (2011) Directive 2010/31/EC. European Commission
- [25] Lechtenböhmer S, Schüring A (2010) The potential for large-scale savings from insulating residential buildings in the EU. *Energy Effic* 4:257–270. <https://doi.org/10.1007/s12053-010-9090-6>
- [26] Santamouris M (2007) Heat island research in Europe: the state of the art. *Adv Build Energy Res* 1:123–150. <https://doi.org/10.1080/17512549.2007.9687272>
- [27] Hammad F, Abu-Hijleh B (2010) The energy savings potential of using dynamic external louvers in an office building. *Energy Build* 42:1888–1895. <https://doi.org/10.1016/j.enbuild.2010.05.024>
- [28] Brambilla A, Salvalai G, Imperadori M, Sesana MM (2018) Nearly zero energy building renovation: from energy efficiency to environmental efficiency, a pilot case study. *Energy Build* 166:271–283. <https://doi.org/10.1016/j.enbuild.2018.02.002>
- [29] Cozza ES, Alloisio M, Comite A et al (2015) NIR-reflecting properties of new paints for energy-efficient buildings. *Sol Energy* 116:108–116. <https://doi.org/10.1016/j.solener.2015.04.004>
- [30] Doulos L, Santamouris M, Livada I (2004) Passive cooling of outdoor urban spaces. *Role Mater Solar Energy* 77:231–249. <https://doi.org/10.1016/j.solener.2004.04.005>
- [31] Song Z, Zhang W, Shi Y et al (2013) Optical properties across the solar spectrum and indoor thermal performance of cool white coatings for building energy efficiency. *Energy Build* 63:49–58. <https://doi.org/10.1016/j.enbuild.2013.03.051>
- [32] Wake L (1989) Principles and Formulations of solar reflecting and low IR emitting coatings for defense use. In: Defense technical information center, Washington, DC, USA, AD-A218429
- [33] Santamouris M, Synnefa A, Karlessi T (2011) Using advanced cool materials in the urban built environment to mitigate heat islands and improve thermal comfort conditions. *Sol Energy* 85:3085–3102. <https://doi.org/10.1016/j.solener.2010.12.023>
- [34] Santamouris M, Yun GY (2020) Recent development and research priorities on cool and super cool materials to mitigate urban heat island. *Renew Energy* 161:792–807. <https://doi.org/10.1016/j.renene.2020.07.109>
- [35] Jose S, Joshy D, Narendranath SB, Periyat P (2019) Recent advances in infrared reflective inorganic pigments. *Sol Energy Mater Sol Cells* 194:7–27. <https://doi.org/10.1016/j.solmat.2019.01.037>
- [36] Rawat M, Singh RN (2021) A study on the comparative review of cool roof thermal performance in various regions. *Energy and Built Environment*. <https://doi.org/10.1016/j.enbenv.2021.03.001> (in press)
- [37] Falasca S, Ciancio V, Salata F et al (2019) High albedo materials to counteract heat waves in cities: an assessment of meteorology, buildings energy needs and pedestrian thermal comfort. *Build Environ* 163:106242. <https://doi.org/10.1016/j.buildenv.2019.106242>
- [38] Cheela VRS, John M, Biswas W, Sarker P (2021) Combating urban heat island effect—A review of reflective pavements and tree shading strategies. *Buildings* 11:93. <https://doi.org/10.3390/buildings11030093>
- [39] Hernández-Pérez I, Álvarez G, Xamán J et al (2014) Thermal performance of reflective materials applied to exterior building components—A review. *Energy Build* 80:81–105. <https://doi.org/10.1016/j.enbuild.2014.05.008>
- [40] Wang C, Wang Z-H, Kaloush KE, Shacat J (2021) Cool pavements for urban heat island mitigation: a synthetic review. *Renew Sustain Energy Rev* 146:111171. <https://doi.org/10.1016/j.rser.2021.111171>
- [41] Yenneti K, Ding L, Prasad D et al (2020) Urban overheating and cooling potential in Australia: An evidence-based review. *Climate* 8:126. <https://doi.org/10.3390/cli8110126>
- [42] Jeevanandam P, Mulukutla RS, Phillips M et al (2007) Near infrared reflectance properties of metal oxide nanoparticles. *J Phys Chem C* 111:1912–1918. <https://doi.org/10.1021/jp066363o>
- [43] Papadaki D, Kiriakidis G, Tsoutsos T (2018) Applications of nanotechnology in construction industry. In: Barhoum A, Makhlof A (eds) *Fundamentals of nanoparticles*. Elsevier, Micro and Nano Technologies, pp 343–370
- [44] von Broekhuizen F, von Broekhuizen J (2009) Nanotechnology in the European construction industry- state of the art 2009- executive summary. European federation of



- building and wood workers and european construction industry federation, Amsterdam
- [45] Álvarez-Docio CM, Reinos JJ, del Campo A, Fernández JF (2017) 2D particles forming a nanostructured shell: a step forward cool NIR reflectivity for  $\text{CoAl}_2\text{O}_4$  pigments. *Dyes Pigm* 137:1–11. <https://doi.org/10.1016/j.dyepig.2016.09.061>
- [46] Hincapié I, Künniger T, Hischier R et al (2015) Nanoparticles in facade coatings: a survey of industrial experts on functional and environmental benefits and challenges. *J Nanopart Res*. <https://doi.org/10.1007/s11051-015-3085-3>
- [47] Halawa E, Ghaffarianhoseini A, Ghaffarianhoseini A et al (2018) A review on energy conscious designs of building façades in hot and humid climates: lessons for (and from) Kuala Lumpur and Darwin. *Renew Sustain Energy Rev* 82:2147–2161. <https://doi.org/10.1016/j.rser.2017.08.061>
- [48] Murgia C, Valles D, Ho Park Y, Kuravi S (2019) Effect of high aged albedo cool roofs on commercial buildings energy savings in U.S.A. climates. *Int J Renew Energy Res* 9:65–72
- [49] Synnefa A, Santamouris M, Akbari H (2007) Estimating the effect of using cool coatings on energy loads and thermal comfort in residential buildings in various climatic conditions. *Energy Build* 39:1167–1174. <https://doi.org/10.1016/j.enbuild.2007.01.004>
- [50] Revel GM, Martarelli M, Bengochea MÁ et al (2013) Nanobased coatings with improved NIR reflecting properties for building envelope materials: development and natural aging effect measurement. *Cem Concr Compos* 36:128–135. <https://doi.org/10.1016/j.cemconcomp.2012.10.002>
- [51] Revel GM, Martarelli M, Emiliani M et al (2014) Cool products for building envelope – Part I: development and lab scale testing. *Sol Energy* 105:770–779. <https://doi.org/10.1016/j.solener.2014.03.029>
- [52] Rossi F, Pisello AL, Nicolini A et al (2014) Analysis of retro-reflective surfaces for urban heat island mitigation: a new analytical model. *Appl Energy* 114:621–631. <https://doi.org/10.1016/j.apenergy.2013.10.038>
- [53] Tao Z, Zhang W, Huang Y et al (2014) A novel pyrophosphate  $\text{BaCr}_2(\text{P}_2\text{O}_7)_2$  as green pigment with high NIR solar reflectance and durable chemical stability. *Solid State Sci* 34:78–84. <https://doi.org/10.1016/j.solidstatesciences.2014.05.016>
- [54] Pisello AL (2017) State of the art on the development of cool coatings for buildings and cities. *Sol Energy* 144:660–680. <https://doi.org/10.1016/j.solener.2017.01.068>
- [55] Pisello AL, Castaldo VL, Fabiani C, Cotana F (2016) Investigation on the effect of innovative cool tiles on local indoor thermal conditions: finite element modeling and continuous monitoring. *Build Environ* 97:55–68. <https://doi.org/10.1016/j.buildenv.2015.11.038>
- [56] Malz S, Krenkel W, Steffens O (2020) Infrared reflective wall paint in buildings: energy saving potentials and thermal comfort. *Energy Build* 224:110212. <https://doi.org/10.1016/j.enbuild.2020.110212>
- [57] Gobakis K, Synnefa A, Meier H et al (2016) Cool roofs in the European context. *REHVA J* 04:19–24
- [58] Carnielo E, Zinzi M, Fanchiotti A (2014) On the solar reflectance angular dependence of opaque construction materials and impact on the energy balance of building components. *Energy Proc* 48:1244–1253. <https://doi.org/10.1016/j.egypro.2014.02.141>
- [59] Zinzi M, Carnielo E, Rossi G (2015) Directional and angular response of construction materials solar properties: characterisation and assessment. *Sol Energy* 115:52–67. <https://doi.org/10.1016/j.solener.2015.02.015>
- [60] Takebayashi H (2016) High-reflectance technology on building façades: installation guidelines for pedestrian comfort. *Sustainability* 8:785. <https://doi.org/10.3390/su8080785>
- [61] Taha H, Sailor D, Akbari H (1992) High-albedo materials for reducing building cooling energy use. Lawrence Berkeley National Laboratory, Berkeley, CA
- [62] Uemoto KL, Sato NMN, John VM (2010) Estimating thermal performance of cool colored paints. *Energy Build* 42:17–22. <https://doi.org/10.1016/j.enbuild.2009.07.026>
- [63] Yuan L, Han A, Ye M et al (2018) Synthesis and characterization of environmentally benign inorganic pigments with high NIR reflectance: lanthanum-doped  $\text{BiFeO}_3$ . *Dyes Pigm* 148:137–146. <https://doi.org/10.1016/j.dyepig.2017.09.008>
- [64] Fang F, Kennedy J, Futter J, Manning J (2013) A review of near infrared reflectance properties of metal oxide nanostructures. *GNS Sci Rep* 39:23–43
- [65] Hyde D, Brannon S (2006) Investigation of infrared reflective pigmentation technologies for coatings and composite applications. In: Proceedings of the American composites manufacturers association composites and polycon. St. Louis, USA
- [66] Moezzi A, McDonagh AM, Cortie MB (2012) Zinc oxide particles: synthesis, properties and applications. *Chem Eng J* 185–186:1–22. <https://doi.org/10.1016/j.cej.2012.01.076>
- [67] Levinson R, Berdahl P, Akbari H (2005) Solar spectral optical properties of pigments—Part I: model for deriving scattering and absorption coefficients from transmittance and reflectance measurements. *Sol Energy Mater Sol Cells* 89:319–349. <https://doi.org/10.1016/j.solmat.2004.11.012>
- [68] McNeil LE, French RH (2001) Light scattering from red pigment particles: multiple scattering in a strongly

- absorbing system. *J Appl Phys* 89:283–293. <https://doi.org/10.1063/1.1331344>
- [69] Kolokotsa D, Dimitriou V, Synnefa A (2012) Modelling cool materials' properties. In: *Advances in the development of cool materials for the built environment*. Bentham Science Publishers, pp 195–230
- [70] Gonome H, Baneshi M, Okajima J et al (2014) Control of thermal barrier performance by optimized nanoparticle size and experimental evaluation using a solar simulator. *J Quant Spectrosc Radiat Transf* 149:81–89. <https://doi.org/10.1016/j.jqsrt.2014.07.025>
- [71] Mie G (1908) Beiträge zur Optik trüber Medien, speziell kolloidaler Metallösungen. *Ann Phys* 330:377–445. <http://doi.org/10.1002/andp.19083300302>
- [72] Maradudin AA, Méndez ER (2007) Light scattering from randomly rough surfaces. *Sci Prog* 90:161–221. <https://doi.org/10.3184/003685007x228711>
- [73] Lyu M, Lin J, Krupczak J, Shi D (2020) Light angle dependence of photothermal properties in oxide and porphyrin thin films for energy-efficient window applications. *MRS Commun* 10:439–448. <https://doi.org/10.1557/mrc.2020.39>
- [74] Kubelka P (1948) New contributions to the optics of intensely light-scattering materials part I. *J Opt Soc Am* 38:448. <https://doi.org/10.1364/josa.38.000448>
- [75] Kubelka P, Munk F (1931) Ein beitrag zur optik der farbanstriche. *Z Tech Phys* 12:593–601
- [76] Saunderson JL (1942) Calculation of the color of pigmented plastics\*. *J Opt Soc Am* 32:727. <https://doi.org/10.1364/josa.32.000727>
- [77] Jansen M, Letschert HP (2000) Inorganic yellow-red pigments without toxic metals. *Nature* 404:980–982. <https://doi.org/10.1038/35010082>
- [78] Kiomarsipour N, Shoja Razavi R (2014) Hydrothermal synthesis of ZnO nanopigments with high UV absorption and vis/NIR reflectance. *Ceram Int* 40:11261–11268. <https://doi.org/10.1016/j.ceramint.2014.03.178>
- [79] Kiomarsipour N, Shoja Razavi R, Ghani K, Kioumarsipour M (2013) Evaluation of shape and size effects on optical properties of ZnO pigment. *Appl Surf Sci* 270:33–38. <https://doi.org/10.1016/j.apsusc.2012.11.167>
- [80] Nielsen R, Wilfing G (2005) Zirconium and zirconium compounds. *Ullmann's encyclopedia of industrial chemistry*. Wiley-VCH Verlag GmbH & Co. KGaA, Weinheim, pp 1–27
- [81] Levinson R, Berdahl P, Akbari H (2005) Solar spectral optical properties of pigments—Part II: survey of common colorants. *Sol Energy Mater Sol Cells* 89:351–389. <https://doi.org/10.1016/j.solmat.2004.11.013>
- [82] Liang S, Zhang H, Luo M et al (2015) Preparation of Cr<sub>2</sub>O<sub>3</sub>-based pigments with high NIR reflectance via thermal decomposition of CrOOH. *Trans Nonferrous Metals Soc China* 25:2646–2647. [https://doi.org/10.1016/s1003-6326\(15\)63887-0](https://doi.org/10.1016/s1003-6326(15)63887-0)
- [83] Coser E, Moritz VF, Krenzing A, Ferreira CA (2015) Development of paints with infrared radiation reflective properties. *Polimeros* 25:305–310. <https://doi.org/10.1590/0104-1428.1869>
- [84] Rong X, Jiao L, Kong X, Yuan G (2020) Research on low-brightness and high-reflective coatings suitable for buildings in tropical areas. *Coatings* 10:829. <https://doi.org/10.3390/coatings10090829>
- [85] Soumya S, Mohamed AP, Mohan K, Ananthakumar S (2015) Enhanced near-infrared reflectance and functional characteristics of Al-doped ZnO nano-pigments embedded PMMA coatings. *Sol Energy Mater Sol Cells* 143:335–346. <https://doi.org/10.1016/j.solmat.2015.07.012>
- [86] Zhou A, Yu Z, Chow CL, Lau D (2017) Enhanced solar spectral reflectance of thermal coatings through inorganic additives. *Energy Build* 138:641–647. <https://doi.org/10.1016/j.enbuild.2016.12.027>
- [87] Jameel Z, Haider A, Taha S et al (2016) Evaluation of hybrid sol-gel incorporated with nanoparticles as nano paint. In: *AIP conference proceedings*, p 020001
- [88] Shen L, Zhang Y, Zhang P et al (2016) Effect of TiO<sub>2</sub> pigment gradation on the properties of thermal insulation coatings. *Int J Miner Metall Mater* 23:1466–1474. <https://doi.org/10.1007/s12613-016-1371-4>
- [89] Liu L, Chen X (2014) Titanium dioxide nanomaterials: self-structural modifications. *Chem Rev* 114:9890–9918. <https://doi.org/10.1021/cr400624r>
- [90] Reyes-Coronado D, Rodríguez-Gattorno G, Espinosa-Pesqueira ME et al (2008) Phase-pure TiO<sub>2</sub> nanoparticles: anatase, brookite and rutile. *Nanotechnology* 19:145605. <https://doi.org/10.1088/0957-4484/19/14/145605>
- [91] Chen X, Mao S (2007) Titanium dioxide nanomaterials: synthesis, properties, modifications, and applications. *Chem Rev* 107:2891
- [92] Eppler RA (1987) Effect of antimony oxide on the anatase-rutile transformation in titanium dioxide. *J Am Ceram Soc* 70:C64–C66. <https://doi.org/10.1111/j.1151-2916.1987.tb04985.x>
- [93] Landmann M, Rauls E, Schmidt WG (2012) The electronic structure and optical response of rutile, anatase and brookite TiO<sub>2</sub>. *J Phys Condens Matter* 24:195503. <https://doi.org/10.1088/0953-8984/24/19/195503>
- [94] Yan X, Chen X (2015) Titanium dioxide materials. In: *Encyclopedia of inorganic and bioinorganic chemistry*. John Wiley & Sons Ltd, pp 1–38

- [95] Pelaez M, Nolan NT, Pillai SC et al (2012) A review on the visible light active titanium dioxide photocatalysts for environmental applications. *Appl Catal B* 125:331–349. <https://doi.org/10.1016/j.apcatb.2012.05.036>
- [96] Rahimi N, Pax RA, Gray EMacA, (2016) Review of functional titanium oxides. I: TiO<sub>2</sub> and its modifications. *Prog Solid State Chem* 44:86–105. <https://doi.org/10.1016/j.progsolidstchem.2016.07.002>
- [97] Chen J, Poon C (2009) Photocatalytic construction and building materials: from fundamentals to applications. *Build Environ* 44:1899–1906. <https://doi.org/10.1016/j.buidenv.2009.01.002>
- [98] Popov AP, Priezzhev AV, Lademann J, Myllylä R (2005) TiO<sub>2</sub> nanoparticles as an effective UV-B radiation skin-protective compound in sunscreens. *J Phys D Appl Phys* 38:2564–2570. <https://doi.org/10.1088/0022-3727/38/15/006>
- [99] Godnjavec J, Zabret J, Znoj B et al (2014) Investigation of surface modification of rutile TiO<sub>2</sub> nanoparticles with SiO<sub>2</sub>/Al<sub>2</sub>O<sub>3</sub> on the properties of polyacrylic composite coating. *Prog Org Coat* 77:47–52. <https://doi.org/10.1016/j.porgcoat.2013.08.001>
- [100] Kusior A, Banas J, Trenczek-Zajac A et al (2018) Structural properties of TiO<sub>2</sub> nanomaterials. *J Mol Struct* 1157:327–336
- [101] Song J, Qin J, Qu J et al (2014) The effects of particle size distribution on the optical properties of titanium dioxide rutile pigments and their applications in cool non-white coatings. *Sol Energy Mater Sol Cells* 130:42–50. <https://doi.org/10.1016/j.solmat.2014.06.035>
- [102] Piri N, Shams-nateri A, Mokhtari J (2017) Solar spectral performance of nanopigments. *Sol Energy Mater Sol Cells* 162:72–82. <https://doi.org/10.1016/j.solmat.2016.12.036>
- [103] Allen NS, Edge M, Ortega A et al (2004) Degradation and stabilisation of polymers and coatings: nano versus pigmentary titania particles. *Polym Degrad Stab* 85:927–946. <https://doi.org/10.1016/j.polymdegradstab.2003.09.024>
- [104] Marques J, Gomes TD, Forte MA et al (2019) A new route for the synthesis of highly-active N-doped TiO<sub>2</sub> nanoparticles for visible light photocatalysis using urea as nitrogen precursor. *Catal Today* 326:36–45. <https://doi.org/10.1016/j.cattod.2018.09.002>
- [105] Kumar S, Verma NK, Singla ML (2012) Study on reflectivity and photostability of Al-doped TiO<sub>2</sub> nanoparticles and their reflectors. *J Mater Res* 28:521–528. <https://doi.org/10.1557/jmr.2012.361>
- [106] Islam MM, Bredow T, Gerson A (2007) Electronic properties of oxygen-deficient and aluminum-doped rutile TiO<sub>2</sub> from first principles. *Phys Rev B*. <https://doi.org/10.1103/physrevb.76.045217>
- [107] Grabstanowicz LR, Gao S, Li T et al (2013) Facile oxidative conversion of TiH<sub>2</sub> to high-concentration Ti<sup>3+</sup>-self-doped rutile TiO<sub>2</sub> with visible-light photoactivity. *Inorg Chem* 52:3884–3890. <https://doi.org/10.1021/ic3026182>
- [108] Zaleska A (2008) Doped-TiO<sub>2</sub>: a review. *Recent Pat Eng* 2:157–164. <https://doi.org/10.2174/187221208786306289>
- [109] Mohan AC, Renjanadevi B (2016) Preparation of zinc oxide nanoparticles and its characterization using scanning electron microscopy (SEM) and X-ray diffraction (XRD). *Proc Technol* 24:761–766. <https://doi.org/10.1016/j.protcy.2016.05.078>
- [110] Dimapilis EAS, Hsu C-S, Mendoza RMO, Lu M-C (2018) Zinc oxide nanoparticles for water disinfection. *Sustain Environ Res* 28:47–56. <https://doi.org/10.1016/j.serj.2017.10.001>
- [111] Wei ZP, Lu YM, Shen DZ et al (2007) Room temperature p-n ZnO blue-violet light-emitting diodes. *Appl Phys Lett* 90:042113. <https://doi.org/10.1063/1.2435699>
- [112] Osmond G (2012) Zinc white: a review of zinc oxide pigment properties and implications for stability in oil-based paintings. *AICCM Bull* 33:20–29. <https://doi.org/10.1179/bac.2012.33.1.004>
- [113] N. Jones F, E. Nichols M, Pappas SP (2017) Pigments. In: *Organic coatings: science and technology*, 4th edn. John Wiley & Sons, Inc., pp 417–434
- [114] Clementi C, Rosi F, Romani A et al (2012) Photoluminescence properties of zinc oxide in paints: a study of the effect of self-absorption and passivation. *Appl Spectrosc* 66:1233–1241. <https://doi.org/10.1366/12-06643>
- [115] de Liedekerke M (2006) Zinc Oxide (Zinc White): pigments, inorganic. *Ullmann's encyclopedia of industrial chemistry*. Wiley-VCH Verlag GmbH & Co. KGaA, Weinheim, pp 56–60
- [116] Lv J, Tang M, Quan R, Chai Z (2019) Synthesis of solar heat-reflective ZnTiO<sub>3</sub> pigments with novel roof cooling effect. *Ceram Int* 45:15768–15771. <https://doi.org/10.1016/j.ceramint.2019.05.081>
- [117] Terki R, Bertrand G, Aourag H, Coddet C (2006) Structural and electronic properties of zirconia phases: a FP-LAPW investigations. *Mater Sci Semicond Process* 9:1006–1013. <https://doi.org/10.1016/j.mssp.2006.10.033>
- [118] Han Y, Zhu J (2013) Surface science studies on the zirconia-based model. *Topics Catal* 56:1525–1541. <https://doi.org/10.1002/chin.201349222>
- [119] Moles P (2017) The use of zirconium in surface coatings. In: *Luxfer MEL technologies*. <http://www.zrchem.com/>. Accessed 17 Jun 2021
- [120] George G, Vishnu VS, Reddy MLP (2011) The synthesis, characterization and optical properties of silicon and praseodymium doped Y<sub>6</sub>MoO<sub>12</sub> compounds: environmentally

- benign inorganic pigments with high NIR reflectance. *Dyes Pigm* 88:109–115. <https://doi.org/10.1016/j.dyepig.2010.05.010>
- [121] Makhlof SA, Bakr ZH, Al-Attar H, Moustafa MS (2013) Structural, morphological and electrical properties of  $\text{Cr}_2\text{O}_3$  nanoparticles. *Mater Sci Eng B* 178:337–343. <https://doi.org/10.1016/j.mseb.2013.01.012>
- [122] Zhao P, Zhao H, Yu J et al (2018) Crystal structure and properties of  $\text{Al}_2\text{O}_3$ – $\text{Cr}_2\text{O}_3$  solid solutions with different  $\text{Cr}_2\text{O}_3$  contents. *Ceram Int* 44:1356–1361. <https://doi.org/10.1016/j.ceramint.2017.08.195>
- [123] Newnham R, Hann Y (1962) Refinement of the  $\alpha$ - $\text{Al}_2\text{O}_3$ ,  $\text{Ti}_2\text{O}_3$ ,  $\text{V}_2\text{O}_3$  and  $\text{Cr}_2\text{O}_3$  structures. *Z Kristallogr* 117:235–237
- [124] Santulli A, Feygenson M, Camino F et al (2011) Synthesis and characterization of one-dimensional  $\text{Cr}_2\text{O}_3$  nanostructures. *Chem Mater* 23:1000–1008
- [125] Thongkanluang T, Wutisatwongkul J, Chirakanphaisarn N, Pokaipisit A (2013) Performance of near-infrared reflective tile roofs. *Adv Mater Res* 770:30–33
- [126] Deepak HN, Choudhari KS, Shivashankar SA et al (2019) Facile microwave-assisted synthesis of  $\text{Cr}_2\text{O}_3$  nanoparticles with high near-infrared reflection for roof-top cooling applications. *J Alloy Compd* 785:747–753. <https://doi.org/10.1016/j.jallcom.2019.01.254>
- [127] Thongkanluang T, Limsuwan P, Rakkwamsuk P (2011) Preparation and application of high near-infrared reflective green pigment for ceramic tile roofs. *Int J Appl Ceram Technol* 8:1451–1458. <https://doi.org/10.1111/j.1744-7402.2010.02599.x>
- [128] Singh J, Verma V, Kumar R (2019) Preparation and structural, optical studies of Al substituted chromium oxide ( $\text{Cr}_2\text{O}_3$ ) nanoparticles. *Vacuum* 159:282–286. <https://doi.org/10.1016/j.vacuum.2018.09.033>
- [129] Li P, Xu H, Zhang Y et al (2009) The effects of Al and Ba on the colour performance of chromic oxide green pigment. *Dyes Pigm* 80:287–291. <https://doi.org/10.1016/j.dyepig.2008.07.016>
- [130] Sangeetha S, Basha R, Sreeram KJ et al (2012) Functional pigments from chromium (III) oxide nanoparticles. *Dyes Pigm* 94:548–552. <https://doi.org/10.1016/j.dyepig.2012.03.019>
- [131] Muñoz R, Masó N, Julián B et al (2004) Environmental study of  $\text{Cr}_2\text{O}_3$ – $\text{Al}_2\text{O}_3$  green ceramic pigment synthesis. *J Eur Ceram Soc* 24:2087–2094. [https://doi.org/10.1016/S0955-2219\(03\)00360-1](https://doi.org/10.1016/S0955-2219(03)00360-1)
- [132] Elakkiya V, Abhishekram R, Sumathi S (2019) Copper doped nickel aluminate: synthesis, characterisation, optical and colour properties. *Chin J Chem Eng* 27:2596–2605. <https://doi.org/10.1016/j.cjche.2019.01.008>
- [133] Karmaoui M, Silva NJO, Amaral VS et al (2013) Synthesis of cobalt aluminate nanopigments by a non-aqueous sol–gel route. *Nanoscale* 5:4277. <https://doi.org/10.1039/c3nr34229h>
- [134] Dey S, Dhal GC (2019) Catalytic conversion of carbon monoxide into carbon dioxide over spinel catalysts: an overview. *Mater Sci Energy Technol* 2:575–588. <https://doi.org/10.1016/j.mset.2019.06.003>
- [135] Paudel TR, Zakutayev A, Lany S et al (2011) Doping rules and doping prototypes in  $\text{A}_2\text{BO}_4$  spinel oxides. *Adv Funct Mater* 21:4493–4501. <https://doi.org/10.1002/adfm.201101469>
- [136] Ali AA, El Fadaly E, Ahmed IS (2018) Near-infrared reflecting blue inorganic nano-pigment based on cobalt aluminate spinel via combustion synthesis method. *Dyes Pigm* 158:451–462. <https://doi.org/10.1016/j.dyepig.2018.05.058>
- [137] Tong Y, Zhang H, Wang S et al (2016) Highly dispersed red-doped  $\text{CoAl}_2\text{O}_4$  nanopigments: synthesis and chromatic properties. *J Nanomater* 2016:1–7. <https://doi.org/10.1155/2016/4169673>
- [138] Yang R, Han A, Ye M et al (2017) The influence of Mn/N-codoping on the thermal performance of  $\text{ZnAl}_2\text{O}_4$  as high near-infrared reflective inorganic pigment. *J Alloy Compd* 696:1329–1341. <https://doi.org/10.1016/j.jallcom.2016.12.100>
- [139] Hedayati HR, Sabbagh Alvani AA, Sameie H et al (2015) Synthesis and characterization of  $\text{Co}_{1-x}\text{Zn}_x\text{Cr}_2-y\text{Al}_y\text{O}_4$  as a near-infrared reflective color tunable nano-pigment. *Dyes Pigm* 113:588–595. <https://doi.org/10.1016/j.dyepig.2014.09.030>
- [140] Menon SG, Swart HC (2020) Microwave-assisted synthesis of blue-green  $\text{NiAl}_2\text{O}_4$  nanoparticle pigments with high near-infrared reflectance for indoor cooling. *J Alloy Compd* 819:152991. <https://doi.org/10.1016/j.jallcom.2019.152991>
- [141] Thejus PK, Krishnapriya KV, Nishanth KG (2021) A cost-effective intense blue colour inorganic pigment for multi-functional cool roof and anticorrosive coatings. *Sol Energy Mater Sol Cells* 219:110778. <https://doi.org/10.1016/j.solmat.2020.110778>
- [142] Wendusu T, Honda T, Masui T, Imanaka N (2013) Novel environmentally friendly (Bi, Ca, Zn, La)  $\text{VO}_4$  inorganic yellow pigments. *RSC Adv* 3:24941. <https://doi.org/10.1039/c3ra43978j>
- [143] Ding C, Han A, Ye M et al (2018) Hydrothermal synthesis and characterization of novel yellow pigments based on  $\text{V}^{5+}$  doped  $\text{BiPO}_4$  with high near-infrared reflectance. *RSC Adv* 8:19690–19700. <https://doi.org/10.1039/c8ra02406e>



- [144] Sandhya Kumari L, Prabhakar Rao P, Narayana Pillai Radhakrishnan A et al (2013) Brilliant yellow color and enhanced NIR reflectance of monoclinic BiVO<sub>4</sub> through distortion in VO<sub>4</sub><sup>3-</sup> tetrahedra. *Sol Energy Mater Sol Cells* 112:134–143. <https://doi.org/10.1016/j.solmat.2013.01.022>
- [145] Ianoş R, Muntean E, Păcurariu C et al (2017) Combustion synthesis of a blue Co-doped zinc aluminate near-infrared reflective pigment. *Dyes Pigm* 142:24–31. <https://doi.org/10.1016/j.dyepig.2017.03.016>
- [146] Bao W, Ma F, Zhang Y et al (2016) Synthesis and characterization of Fe<sup>3+</sup> doped Co<sub>0.5</sub>Mg<sub>0.5</sub>Al<sub>2</sub>O<sub>4</sub> inorganic pigments with high near-infrared reflectance. *Powder Technol* 292:7–13. <https://doi.org/10.1016/j.powtec.2016.01.013>
- [147] Elakkiya V, Sumathi S (2020) Ce and Fe doped gahnite: cost effective solar reflective pigment for cool coating applications. *J Alloy Compd* 820:153174. <https://doi.org/10.1016/j.jallcom.2019.153174>
- [148] Merikhi J, Jungk H-O, Feldmann C (2000) Sub-micrometer CoAl<sub>2</sub>O<sub>4</sub> pigment particles—synthesis and preparation of coatings. *J Mater Chem* 10:1311–1314. <https://doi.org/10.1039/a910201i>
- [149] Eliziário SA, de Andrade JM, Lima SJG et al (2011) Black and green pigments based on chromium–cobalt spinels. *Mater Chem Phys* 129:619–624. <https://doi.org/10.1016/j.matchemphys.2011.05.001>
- [150] Yuvaraj S, Nithya VD, Fathima KS et al (2013) Investigations on the temperature dependent electrical and magnetic properties of NiTiO<sub>3</sub> by molten salt synthesis. *Mater Res Bull* 48:1110–1116. <https://doi.org/10.1016/j.materresbull.2012.12.001>
- [151] Du Y, Zhang M, Wu J et al (2003) Optical properties of SrTiO<sub>3</sub> thin films by pulsed laser deposition. *Appl Phys A* 76:1105–1108
- [152] Ramadass N (1978) ABO<sub>3</sub>-type oxides—Their structure and properties—A bird's eye view. *Mater Sci Eng* 36:231–239. [https://doi.org/10.1016/0025-5416\(78\)90076-9](https://doi.org/10.1016/0025-5416(78)90076-9)
- [153] Cousin P, Ross RA (1990) Preparation of mixed oxides: a review. *Mater Sci Eng A* 130:119–125. [https://doi.org/10.1016/0921-5093\(90\)90087-j](https://doi.org/10.1016/0921-5093(90)90087-j)
- [154] Singh L, Rai US, Mandal KD, Singh NB (2014) Progress in the growth of CaCu<sub>3</sub>Ti<sub>4</sub>O<sub>12</sub> and related functional dielectric perovskites. *Prog Cryst Growth Charact Mater* 60:15–62. <https://doi.org/10.1016/j.pcrysgrow.2014.04.001>
- [155] Meenakshi P, Selvaraj M (2018) Bismuth titanate as an infrared reflective pigment for cool roof coating. *Sol Energy Mater Sol Cells* 174:530–537. <https://doi.org/10.1016/j.solmat.2017.09.048>
- [156] Yang R, Han A, Ye M et al (2017) Synthesis, characterization and thermal performance of Fe/N co-doped MgTiO<sub>3</sub> as a novel high near-infrared reflective pigment. *Sol Energy Mater Sol Cells* 160:307–318. <https://doi.org/10.1016/j.solmat.2016.10.045>
- [157] Sun H, Tao Y, Zhang J (2020) Magnesium titanate as a new high solar reflectance pigment to fabricate cooling engineering composites for energy saving areas. *J Alloy Compd* 847:156527. <https://doi.org/10.1016/j.jallcom.2020.156527>
- [158] Moghtada A, Shahrouzianfar A, Ashiri R (2017) Facile synthesis of NiTiO<sub>3</sub> yellow nano-pigments with enhanced solar radiation reflection efficiency by an innovative one-step method at low temperature. *Dyes Pigm* 139:388–396. <https://doi.org/10.1016/j.dyepig.2016.12.044>
- [159] Wang J-L, Li Y-Q, Byon Y-J et al (2013) Synthesis and characterization of NiTiO<sub>3</sub> yellow nano pigment with high solar radiation reflection efficiency. *Powder Technol* 235:303–306. <https://doi.org/10.1016/j.powtec.2012.10.044>
- [160] Zou J, Zheng W (2016) TiO<sub>2</sub>@CoTiO<sub>3</sub> complex green pigments with low cobalt content and tunable color properties. *Ceram Int* 42:8198–8205. <https://doi.org/10.1016/j.ceramint.2016.02.029>
- [161] Mao Z, Yang Z, Zhang J (2019) SrTiO<sub>3</sub> as a new solar reflective pigment on the cooling property of PMMA-ceramic composites. *Ceram Int* 45:16078–16087. <https://doi.org/10.1016/j.ceramint.2019.05.124>
- [162] Viruthagiri G, Praveen P, Mugundan S, Gopinathan E (2013) Synthesis and characterization of pure and nickel doped SrTiO<sub>3</sub> nanoparticles via solid state reaction route. *Indian J Adv Chem Sci* 1:132–138
- [163] Zou J, Zhang T, He X (2019) Dark brown Cr doped CaTiO<sub>3</sub> pigments with high NIR reflectance. *Mater Lett* 248:173–176. <https://doi.org/10.1016/j.matlet.2019.04.031>
- [164] Chen Y, Ma Y, Wang Z et al (2018) Molten salt synthesis of YMnO<sub>3</sub> powder with high near-infrared reflectivity. *Mater Lett* 229:171–173. <https://doi.org/10.1016/j.matlet.2018.07.002>
- [165] Han A, Zhao M, Ye M et al (2013) Crystal structure and optical properties of YMnO<sub>3</sub> compound with high near-infrared reflectance. *Sol Energy* 91:32–36. <https://doi.org/10.1016/j.solener.2013.01.011>
- [166] Xu Z, Wang D, Zhong M, Zhang Z (2020) Preparation and characterization of Mg<sup>2+</sup>-doped CaCu<sub>3</sub>Ti<sub>4</sub>O<sub>12</sub> pigment with high NIR reflectance. *Ceram Int* 46:25306–25312. <https://doi.org/10.1016/j.ceramint.2020.06.324>
- [167] Oka R, Masui T (2016) Synthesis and characterization of black pigments based on calcium manganese oxides for high near-infrared (NIR) reflectance. *RSC Adv* 6:90952–90957. <https://doi.org/10.1039/c6ra21443f>

- [168] Dohnalová Ž, Šulcová P, Bělina P (2019) Pink NIR pigment based on Cr-doped  $\text{SrSnO}_3$ . *J Therm Anal Calorim* 138:4475–4484. <https://doi.org/10.1007/s10973-019-08522-z>
- [169] Tian M, Han A, Ma S et al (2021) Preparation of Cr-doped  $\text{BaTiO}_3$  near infrared reflection pigment powder and its anti-aging performance for acrylonitrile-styrene-acrylate. *Powder Technol* 378:182–190. <https://doi.org/10.1016/j.powtec.2020.09.072>
- [170] Li J, Lorgier S, Stalick JK et al (2016) From serendipity to rational design: tuning the blue trigonal bipyramidal  $\text{Mn}^{3+}$ -chromophore to violet and purple through application of chemical pressure. *Inorg Chem* 55:9798–9804. <https://doi.org/10.1021/acs.inorgchem.6b01639>
- [171] Smith AE, Comstock MC, Subramanian MA (2016) Spectral properties of the UV absorbing and near-IR reflecting blue pigment,  $\text{YIn}_{1-x}\text{Mn}_x\text{O}_3$ . *Dyes Pigm* 133:214–221. <https://doi.org/10.1016/j.dyepig.2016.05.029>
- [172] Rosati A, Fedel M, Rossi S (2021)  $\text{YIn}_{0.9}\text{Mn}_{0.1}\text{O}_3\text{--ZnO}$  NIR reflective nano-pigment exhibiting three different colors: ochre, cyan blue, and deep blue. *J Solid State Chem* 299:122176. <https://doi.org/10.1016/j.jssc.2021.122176>
- [173] Ma Y, Chen Y, Wang Z et al (2020) Controllable near-infrared reflectivity and infrared emissivity with substitutional iron-doped orthorhombic  $\text{YMnO}_3$  coatings. *Sol Energy* 206:778–786. <https://doi.org/10.1016/j.solener.2020.06.063>
- [174] Sreeram KJ, Aby CP, Nair BU, Ramasami T (2008) Colored cool colorants based on rare earth metal ions. *Sol Energy Mater Sol Cells* 92:1462–1467. <https://doi.org/10.1016/j.solmat.2008.06.008>
- [175] Jovaní M, Sanz A, Beltrán-Mir H, Cordoncillo E (2016) New red-shade environmental-friendly multifunctional pigment based on Tb and Fe doped  $\text{Y}_2\text{Zr}_2\text{O}_7$  for ceramic applications and cool roof coatings. *Dyes Pigm* 133:33–40. <https://doi.org/10.1016/j.dyepig.2016.05.042>
- [176] Raj AKV, Rao P, Sreena TS, Thara T (2019) Pigmentary colors from yellow to red in  $\text{Bi}_2\text{Ce}_2\text{O}_7$  by rare earth ion substitutions as possible high NIR reflecting pigments. *Dyes Pigm* 160:177–187. <https://doi.org/10.1016/j.dyepig.2018.08.010>
- [177] Olegário RC, Ferreira de Souza EC, Marcelino Borges JF et al (2013) Synthesis and characterization of  $\text{Fe}^{3+}$ -doped cerium–praseodymium oxide pigments. *Dyes Pigm* 97:113–117. <https://doi.org/10.1016/j.dyepig.2012.12.011>
- [178] Jose S, Narendranath SB, Joshy D et al (2018) Low temperature synthesis of NIR reflecting bismuth doped cerium oxide yellow nano-pigments. *Mater Lett* 233:82–85. <https://doi.org/10.1016/j.matlet.2018.08.136>
- [179] Farbod M, Rafati Z (2016) Color parameters of  $\text{Y}_2\text{Cu}_2\text{O}_5$  green-blue nanopigments fabricated by the sol-gel combustion method and their efficiency for coloring the glazed tiles. *Ceram Int* 42:15732–15738. <https://doi.org/10.1016/j.ceramint.2016.07.033>
- [180] Jose S, Prakash A, Laha S et al (2014) Green colored nanopigments derived from  $\text{Y}_2\text{BaCuO}_5$ : NIR reflective coatings. *Dyes Pigm* 107:118–126. <https://doi.org/10.1016/j.dyepig.2014.03.025>
- [181] Těšitelová K, Šulcová P (2016) Synthesis and study of  $\text{Bi}_2\text{Ce}_2\text{O}_7$  as inorganic pigment. *J Therm Anal Calorim* 125:1047–1052. <https://doi.org/10.1007/s10973-016-5322-0>
- [182] Xiao Y, Huang B, Chen J, Sun X (2018) Novel  $\text{Bi}^{3+}$ -doped and  $\text{Bi}^{3+}/\text{Tb}^{3+}$ -co-doped  $\text{LaYO}_3$  pigments with high near-infrared reflectances. *J Alloy Compd* 762:873–880. <https://doi.org/10.1016/j.jallcom.2018.05.233>
- [183] Liu L, Han A, Ye M, Zhao M (2015) Synthesis and characterization of  $\text{Al}^{3+}$ -doped  $\text{LaFeO}_3$  compounds: a novel inorganic pigments with high near-infrared reflectance. *Sol Energy Mater Sol Cells* 132:377–384. <https://doi.org/10.1016/j.solmat.2014.08.048>
- [184] Zhao M, Han A, Ye M, Wu T (2013) Preparation and characterization of  $\text{Fe}^{3+}$ -doped  $\text{Y}_2\text{Ce}_2\text{O}_7$  pigments with high near-infrared reflectance. *Sol Energy* 97:350–355. <https://doi.org/10.1016/j.solener.2013.08.007>
- [185] Sarasamma Vishnu V, Lakshmiipathi Reddy M (2011) Near-infrared reflecting inorganic pigments based on molybdenum and praseodymium doped yttrium cerate: synthesis, characterization and optical properties. *Sol Energy Mater Sol Cells* 95:2685–2692. <https://doi.org/10.1016/j.solmat.2011.05.042>
- [186] Huang B, Xiao Y, Huang C et al (2017) Environment-friendly pigments based on praseodymium and terbium doped  $\text{La}_2\text{Ce}_2\text{O}_7$  with high near-infrared reflectance: synthesis and characterization. *Dyes Pigm* 147:225–233. <https://doi.org/10.1016/j.dyepig.2017.08.004>
- [187] Vishnu VS, George G, Reddy MLP (2010) Effect of molybdenum and praseodymium dopants on the optical properties of  $\text{Sm}_2\text{Ce}_2\text{O}_7$ : tuning of band gaps to realize various color hues. *Dyes Pigm* 85:117–123. <https://doi.org/10.1016/j.dyepig.2009.10.012>
- [188] Radhika SP, Sreeram KJ, Unni Nair B (2014) Mo-doped cerium gadolinium oxide as environmentally sustainable yellow pigments. *ACS Sustain Chem Eng* 2:1251–1256. <https://doi.org/10.1021/sc500085m>
- [189] Raj AKV, Prabhakar Rao P, Sameera S, Divya S (2015) Pigments based on terbium-doped yttrium cerate with high NIR reflectance for cool roof and surface coating

- applications. *Dyes Pigm* 122:116–125. <https://doi.org/10.1016/j.dyepig.2015.06.021>
- [190] Chen J, Xiao Y, Huang B, Sun X (2018) Sustainable cool pigments based on iron and tungsten co-doped lanthanum cerium oxide with high NIR reflectance for energy saving. *Dyes Pigm* 154:1–7. <https://doi.org/10.1016/j.dyepig.2018.02.032>
- [191] Chen J, Xie W, Guo X et al (2020) Near infrared reflective pigments based on  $\text{Bi}_3\text{YO}_6$  for heat insulation. *Ceram Int* 46:24575–24584. <https://doi.org/10.1016/j.ceramint.2020.06.245>
- [192] Ding C, Tian M, Han A et al (2020) V-doped  $\text{LaPO}_4$  new solar heat-reflective pigments and its improvement on the aging resistance of poly-methyl methacrylate. *Sol Energy* 195:660–669. <https://doi.org/10.1016/j.solener.2019.12.002>
- [193] Fortuño-Morte M, Beltrán-Mir H, Cordoncillo E (2020) Study of the role of praseodymium and iron in an environment-friendly reddish orange pigment based on Fe doped  $\text{Pr}_2\text{Zr}_2\text{O}_7$ : a multifunctional material. *J Alloy Compd* 845:155841. <https://doi.org/10.1016/j.jallcom.2020.155841>
- [194] Vishnu VS, George G, Divya V, Reddy MLP (2009) Synthesis and characterization of new environmentally benign tantalum-doped  $\text{Ce}_{0.8}\text{Zr}_{0.2}\text{O}_2$  yellow pigments: applications in coloring of plastics. *Dyes Pigm* 82:53–57. <https://doi.org/10.1016/j.dyepig.2008.11.001>
- [195] Yao B, Geng S, Wang J, Wang L (2018) Synthesis, characterization, and optical properties of near-infrared reflecting composite inorganic pigments composed of  $\text{TiO}_2/\text{CuO}$  core-shell particles. *Aust J Chem* 71:373. <https://doi.org/10.1071/ch17626>
- [196] He X, Wang F, Liu H et al (2017) Fabrication of highly dispersed  $\text{NiTiO}_3/\text{TiO}_2$  yellow pigments with enhanced NIR reflectance. *Mater Lett* 208:82–85. <https://doi.org/10.1016/j.matlet.2017.05.047>
- [197] He X, Wang F, Liu H et al (2017) Synthesis and coloration of highly dispersed  $\text{NiTiO}_3/\text{TiO}_2$  yellow pigments with core-shell structure. *J Eur Ceram Soc* 37:2965–2972. <https://doi.org/10.1016/j.jeurceramsoc.2017.03.020>
- [198] Zou J, Chen Y, Zhang P (2021) Influence of crystallite size on color properties and NIR reflectance of  $\text{TiO}_2/\text{NiTiO}_3$  inorganic pigments. *Ceram Int* 47:12661–12666. <https://doi.org/10.1016/j.ceramint.2021.01.126>
- [199] Sadeghi-Niaraki S, Ghasemi B, Adeb AH, et al (2019) Preparation of  $(\text{Fe}, \text{Cr})_2\text{O}_3/\text{TiO}_2$  cool pigments for energy saving applications. *J Alloy Compd* 779:367–379. <https://doi.org/10.1016/j.jallcom.2018.11.114>
- [200] Sadeghi-Niaraki S, Ghasemi B, Habibolahzadeh A et al (2020) Cool and photocatalytic reddish-brown nanostructured  $\text{Fe}_2\text{O}_3/\text{SiO}_2/\text{TiO}_2$  pigments. *Mater Sci Eng, B* 262:114752. <https://doi.org/10.1016/j.mseb.2020.114752>
- [201] Soranakom P, Vittayakorn N, Rakkwamsuk P et al (2021) Effect of surfactant concentration on the formation of  $\text{Fe}_2\text{O}_3/\text{SiO}_2$  NIR-reflective red pigments. *Ceram Int* 47:13147–13155. <https://doi.org/10.1016/j.ceramint.2021.01.179>
- [202] Zhang T, Wang Y, Pan Z (2019) Preparation of hollow glass microspheres@ $\text{ZnS SeI}$ —or copper-/indium-co-doped  $\text{ZnS SeI}$ — composite color pigments with enhanced near-infrared reflectance. *Sol Energy* 184:570–583. <https://doi.org/10.1016/j.solener.2019.04.038>
- [203] Lu D, Gao Q, Wu X, Fan Y (2017)  $\text{ZnO}$  nanostructures decorated hollow glass microspheres as near infrared reflective pigment. *Ceram Int* 43:9164–9170. <https://doi.org/10.1016/j.ceramint.2017.04.067>
- [204] Gao Q, Wu X, Fan Y, Meng Q (2018) Novel near infrared reflective pigments based on hollow glass microsphere/ $\text{BiOCl}$ -xI<sub>x</sub> composites: optical property and superhydrophobicity. *Sol Energy Mater Sol Cells* 180:138–147. <https://doi.org/10.1016/j.solmat.2018.02.033>
- [205] Gao Q, Wu X, Fan Y (2014) Solar spectral optical properties of rutile  $\text{TiO}_2$  coated mica–titania pigments. *Dyes Pigm* 109:90–95. <https://doi.org/10.1016/j.dyepig.2014.04.028>
- [206] Yuan L, Han A, Ye M et al (2017) Synthesis and characterization of novel nontoxic  $\text{BiFe}_{1-x}\text{Al}_x\text{O}_3/\text{mica-titania}$  pigments with high NIR reflectance. *Ceram Int* 43:16488–16494. <https://doi.org/10.1016/j.ceramint.2017.09.032>
- [207] Bedon C, Honfi D, Machalická KV et al (2019) Structural characterisation of adaptive facades in Europe—Part I: insight on classification rules, performance metrics and design
- [208] Ascione F, Bianco N, Iovane T et al (2021) The evolution of building energy retrofit via double-skin and responsive façades: a review. *Sol Energy* 224:703–717. <https://doi.org/10.1016/j.solener.2021.06.035>
- [209] Balali A, Valipour A (2020) Identification and selection of building façade's smart materials according to sustainable development goals. *Sustain Mater Technol* 26:e00213. <https://doi.org/10.1016/j.susmat.2020.e00213>
- [210] Karlessi T, Santamouris M, Apostolakis K et al (2009) Development and testing of thermochromic coatings for buildings and urban structures. *Sol Energy* 83:538–551. <https://doi.org/10.1016/j.solener.2008.10.005>
- [211] Berardi U, Garai M, Morselli T (2020) Preparation and assessment of the potential energy savings of thermochromic and cool coatings considering inter-building effects. *Sol Energy* 209:493–504. <https://doi.org/10.1016/j.solener.2020.09.015>

- [212] Granadeiro V, Almeida M, Souto T et al (2020) Thermochromic paints on external surfaces: impact assessment for a residential building through thermal and energy simulation. *Energies* 13:1912. <https://doi.org/10.3390/en13081912>
- [213] Chang T-C, Cao X, Bao S-H et al (2018) Review on thermochromic vanadium dioxide based smart coatings: from lab to commercial application. *Adv Manuf* 6:1–19. <https://doi.org/10.1007/s40436-017-0209-2>
- [214] Luceño-Sánchez J, Díez-Pascual A, Peña Capilla R (2019) Materials for photovoltaics: state of art and recent developments. *Int J Mol Sci* 20:976. <https://doi.org/10.3390/ijms20040976>
- [215] Joost U, Šutka A, Oja M et al (2018) Reversible photodoping of TiO<sub>2</sub> nanoparticles for photochromic applications. *Chem Mater* 30:8968–8974. <https://doi.org/10.1021/acs.chemmater.8b04813>
- [216] Wang S, Fan W, Liu Z et al (2018) Advances on tungsten oxide based photochromic materials: strategies to improve their photochromic properties. *J Mater Chem C* 6:191–212. <https://doi.org/10.1039/c7tc04189f>
- [217] Moreira MANS, Heitmann AP, Bezerra ACS et al (2020) Photocatalytic performance of cementitious materials with addition of red mud and Nb<sub>2</sub>O<sub>5</sub> particles. *Constr Build Mater* 259:119851. <https://doi.org/10.1016/j.conbuildmat.2020.119851>
- [218] Kousis I, Fabiani C, Gobbi L, Pisello AL (2020) Phosphorescent-based pavements for counteracting urban overheating – A proof of concept. *Sol Energy* 202:540–552. <https://doi.org/10.1016/j.solener.2020.03.092>
- [219] Lu X, Guo S, Tong X et al (2017) Tunable photocontrolled motions using stored strain energy in malleable azobenzene liquid crystalline polymer actuators. *Adv Mater* 29:1606467. <https://doi.org/10.1002/adma.201606467>
- [220] Fabiani C, Chiatti C, Pisello AL (2021) Development of photoluminescent composites for energy efficiency in smart outdoor lighting applications: an experimental and numerical investigation. *Renew Energy* 172:1–15. <https://doi.org/10.1016/j.renene.2021.02.071>
- [221] Chiatti C, Fabiani C, Cotana F, Pisello AL (2021) Exploring the potential of photoluminescence for urban passive cooling and lighting applications: a new approach towards materials optimization. *Energy* 231:120815. <https://doi.org/10.1016/j.energy.2021.120815>
- [222] Wang J, (Jialiang), Shi D, (2017) Spectral selective and photothermal nano structured thin films for energy efficient windows. *Appl Energy* 208:83–96. <https://doi.org/10.1016/j.apenergy.2017.10.066>
- [223] Kulczyk-Malecka J, Kelly PJ, West G et al (2014) Investigation of silver diffusion in TiO<sub>2</sub>/Ag/TiO<sub>2</sub> coatings. *Acta Mater* 66:396–404. <https://doi.org/10.1016/j.actamat.2013.11.030>
- [224] Sahu DR, Lin S-Y, Huang J-L (2006) ZnO/Ag/ZnO multilayer films for the application of a very low resistance transparent electrode. *Appl Surf Sci* 252:7509–7514. <http://doi.org/10.1016/j.apsusc.2005.09.021>
- [225] White JR, de Poumeyrol B, Hale JM, Stephenson R (2004) Piezoelectric paint: ceramic-polymer composites for vibration sensors. *J Mater Sci* 39:3105–3114. <https://doi.org/10.1023/b:jmsc.0000025839.98785.b9>
- [226] Ahmed R, Mir F, Banerjee S (2017) A review on energy harvesting approaches for renewable energies from ambient vibrations and acoustic waves using piezoelectricity. *Smart Mater Struct* 26:085031. <https://doi.org/10.1088/1361-665x/aa7bfb>
- [227] Gu L, Zhou D, Cao J (2016) Piezoelectric active humidity sensors based on lead-free NaNbO<sub>3</sub> piezoelectric nanofibers. *Sensors* 16:833. <https://doi.org/10.3390/s16060833>
- [228] Rodrigues C, Nunes D, Clemente D et al (2020) Emerging triboelectric nanogenerators for ocean wave energy harvesting: state of the art and future perspectives. *Energy Environ Sci* 13:2657–2683. <https://doi.org/10.1039/d0ee01258k>
- [229] Chen J, Guo H, Ding P et al (2016) Transparent triboelectric generators based on glass and polydimethylsiloxane. *Nano Energy* 30:235–241. <https://doi.org/10.1016/j.nanoen.2016.10.005>
- [230] Wang J, Meng C, Gu Q et al (2020) Normally transparent tribo-induced smart window. *ACS Nano* 14:3630–3639. <https://doi.org/10.1021/acsnano.0c00107>
- [231] Akeiber H, Nejat P, Majid MZAbd, et al (2016) A review on phase change material (PCM) for sustainable passive cooling in building envelopes. *Renew Sustain Energy Rev* 60:1470–1497. <https://doi.org/10.1016/j.rser.2016.03.036>
- [232] Cheng X, Zhai X, Wang R (2016) Thermal performance analysis of a packed bed cold storage unit using composite PCM capsules for high temperature solar cooling application. *Appl Therm Eng* 100:247–255. <https://doi.org/10.1016/j.applthermaleng.2016.02.036>
- [233] Chung MH, Park JC (2016) Development of PCM cool roof system to control urban heat island considering temperate climatic conditions. *Energy Build* 116:341–348. <https://doi.org/10.1016/j.enbuild.2015.12.056>
- [234] Lei J, Kumarasamy K, Zingre KT et al (2017) Cool colored coating and phase change materials as complementary cooling strategies for building cooling load reduction in tropics. *Appl Energy* 190:57–63. <https://doi.org/10.1016/j.apenergy.2016.12.114>
- [235] Cannavale A, Ayr U, Fiorito F, Martellotta F (2020) Smart electrochromic windows to enhance building energy



- efficiency and visual comfort. *Energies* 13:1449. <https://doi.org/10.3390/en13061449>
- [236] Tavares PF, Gaspar AR, Martins AG, Frontini F (2014) Evaluation of electrochromic windows impact in the energy performance of buildings in Mediterranean climates. *Energy Policy* 67:68–81. <https://doi.org/10.1016/j.enpol.2013.07.038>
- [237] Jelle BP, Gao T (2015) The utilization of electrochromic materials for smart window applications in energy-efficient buildings. In: *Proceedings of Techconnect world innovation*
- [238] Nishizawa K, Yamada Y, Yoshimura K (2017) Low-temperature chemical fabrication of Pt-WO<sub>3</sub> gasochromic switchable films using UV irradiation. *Sol Energy Mater Sol Cells* 170:21–26. <https://doi.org/10.1016/j.solmat.2017.05.058>
- [239] Zahir MdH, Mohamed SA, Saidur R, Al-Sulaiman FA (2019) Supercooling of phase-change materials and the techniques used to mitigate the phenomenon. *Appl Energy* 240:793–817. <https://doi.org/10.1016/j.apenergy.2019.02.045>
- [240] Cannavale A (2020) Chromogenic technologies for energy saving. *Clean Technol* 2:462–475. <https://doi.org/10.3390/cleantechnol2040029>
- [241] Piccolo A, Marino C, Nucara A, Pietrafesa M (2018) Energy performance of an electrochromic switchable glazing: experimental and computational assessments. *Energy Build* 165:390–398. <https://doi.org/10.1016/j.enbui.2017.12.049>
- [242] Lin Y-J, Chang Y-H, Yang W-D, Tsai B-S (2006) Synthesis and characterization of ilmenite NiTiO<sub>3</sub> and CoTiO<sub>3</sub> prepared by a modified Pechini method. *J Non Cryst Solids* 352:789–794. <https://doi.org/10.1016/j.jnoncrysol.2006.02.001>
- [243] Sakka S (2013) Sol–gel process and applications. In: *Handbook of advanced ceramics*, 2nd edn. Academic Press, pp 883–910
- [244] Yu Y-H, Xia M (2012) Preparation and characterization of ZnTiO<sub>3</sub> powders by sol–gel process. *Mater Lett* 77:10–12. <https://doi.org/10.1016/j.matlet.2012.02.113>
- [245] Brinker C (1990) Sol-gel science. The physics and chemistry of sol-gel processing. Academic Press, USA, pp xvi–18
- [246] Spooren J, Walton RI (2005) Hydrothermal synthesis of the perovskite manganites Pr<sub>0.5</sub>Sr<sub>0.5</sub>MnO<sub>3</sub> and Nd<sub>0.5</sub>Sr<sub>0.5</sub>MnO<sub>3</sub> and alkali-earth manganese oxides CaMn<sub>2</sub>O<sub>4</sub>, 4H-SrMnO<sub>3</sub>, and 2H-BaMnO<sub>3</sub>. *J Solid State Chem* 178:1683–1691. <https://doi.org/10.1016/j.jssc.2005.03.006>
- [247] Xia C-T, Shi E-W, Zhong W-Z, Guo J-K (1996) Hydrothermal synthesis of BaTiO<sub>3</sub> nano/microcrystals. *J Cryst Growth* 166:961–966. [https://doi.org/10.1016/0022-0248\(95\)00521-8](https://doi.org/10.1016/0022-0248(95)00521-8)
- [248] Xue P, Hu Y, Xia W et al (2017) Molten-salt synthesis of BaTiO<sub>3</sub> powders and their atomic-scale structural characterization. *J Alloy Compd* 695:2870–2877. <https://doi.org/10.1016/j.jallcom.2016.11.395>
- [249] Xing X, Zhang C, Qiao L et al (2006) Facile preparation of ZnTiO<sub>3</sub> ceramic powders in sodium/potassium chloride melts. *J Am Ceram Soc* 89:1150–1152. <https://doi.org/10.1111/j.1551-2916.2005.00853.x>
- [250] Pholnak C, Sirisathitkul C, Danworaphong S, Harding DJ (2013) Sonochemical synthesis of zinc oxide nanoparticles using an ultrasonic homogenizer. *Ferroelectrics* 455:15–20. <https://doi.org/10.1080/00150193.2013.843405>
- [251] Hassanjani-Roshan A, Vaezi MR, Shokuhfar A, Rajabali Z (2011) Synthesis of iron oxide nanoparticles via sonochemical method and their characterization. *Particuology* 9:95–99. <https://doi.org/10.1016/j.partic.2010.05.013>
- [252] Mason TJ, Lorimer JP (2002) Introduction to applied ultrasonics. *Applied sonochemistry: uses of power ultrasound in chemistry and processing*. Wiley-VCH Verlag GmbH & Co. KGaA, UK, pp 20–21

**Publisher's Note** Springer Nature remains neutral with regard to jurisdictional claims in published maps and institutional affiliations.